Universidad Rey Juan Carlos

DOCTORAL THESIS

HIGH PERFORMANCE BIOBASED EPOXY VITRIMER AND FIBER REINFORCED EPOXY COMPOSITES: PREPARATION, CHARACTERIZATION, AND PROPERTIES

Author:

Meihui Zhou

Supervisors:

De-Yi Wang
Silvia Gonzáles Prolongo

Doctoral Program in Industrial Technologies: Chemical, Environmental, Energy, Electronics, Mechanics, and Materials

International Doctoral School

2025

©2025 Meihui Zhou

Algunos derechos reservados
Este documento se distribuye bajo la licencia
“Atribución 4.0 Internacional” de Creative Commons,
disponible en https://creativecommons.org/licenses/by/4.0/deed.es

Acknowledgements

In the blink of an eye, I am approaching the end of my fifth year as a PhD student. Over these years, I have studied in many places and experienced a great deal: there have been losses, but even more gains. Still, I have always walked a path I do not regret. Throughout this journey, I have been fortunate to meet many people, both mentors and friends, who have taught me not only how to conduct research but also how to live a meaningful life.

First and foremost, I would like to express my heartfelt gratitude to my PhD supervisors, Professor De-Yi Wang and Professor Silvia González Prolongo. Professor Wang gave me the opportunity to pursue a PhD, which marked an important turning point in my life and helped me avoid several major risks along the way. He has provided me with patient guidance and unwavering support in my research, as well as great care and encouragement in life — a teacher I hold in the highest regard. Over the past four years, Professor Silvia has supervised my research with rigorous academic standards, efficiency, openness, and sincerity. She leads by example, holding me to high standards while offering genuine care and support both professionally and personally. As a female researcher, I deeply admire her; she is a role model whom I aspire to emulate in the future. I am also grateful to Professor Na Wang, whose warm encouragement has been a source of comfort and strength whenever I needed it.

I would also like to sincerely thank all the friends and colleagues who have accompanied me on this journey: Alberto Jiménez Suárez, Xiaolu Li, Jimena de la Vega, Juncheng Xiao, Xiang Ao, Javier Gomez Sanchez, Alejandro Cortés Fernández, Emma Espeute, Isaac Lorero Gómez, Ignacio Collado Ropero, Mingyang Zhang, Qi Chen, Wei Tang, Jie Xu, Yunhuan Liu, Sunan Tian, Wei Cai, Ruofan Yang, Zongquan Zhao, Jalal Ahmad, Arnab Ghosh, Guangzhong Yin, Jose Hobson, Monsur Islam, Juan León, Burcu Özdemir, Sreelakshmi Vinod, and Xiaomei Yang. Your friendship and support have made my PhD life colorful and fulfilling, helping me find joy and balance between research and life.

Finally, I want to express my deepest gratitude to my parents. Their unwavering support and love have been my strongest source of strength and the courage behind every step I take forward.

Meihui Zhou (周美慧) En Madrid

17 June 2025

“NO ONE IS COMING, BUT YOU CAN ALWAYS BE THERE FOR YOURSELF.”

Resumen

Las resinas epoxi han sido ampliamente reconocidas como materiales termoestables clave en ingeniería avanzada, debido a su excelente comportamiento térmico y mecánico, su facilidad de procesamiento y su fuerte adhesión a distintos sustratos. Estas cualidades han favorecido su incorporación en sectores exigentes como la aeronáutica, la electrónica, la automoción, la ingeniería civil y los sistemas eléctricos, así como en la fabricación de materiales compuestos de alto rendimiento. No obstante, más allá de sus ventajas técnicas, estas resinas presentan limitaciones estructurales y medioambientales que han motivado una búsqueda activa de alternativas más sostenibles.

La mayoría de las formulaciones comerciales de resina epoxi se basan en monómeros derivados de recursos fósiles, en particular el diglicidil éter de bisfenol A (DGEBA), una molécula no renovable asociada a riesgos para la salud humana, como alteraciones endocrinas y efectos tóxicos en la reproducción. Además, las redes poliméricas resultantes del curado son altamente entrecruzadas y químicamente irreversibles, lo que imposibilita su reciclaje o reprocesamiento posterior. Esta falta de circularidad contribuye a la acumulación de residuos termoestables de difícil gestión. A ello se suma la inflamabilidad intrínseca de estos materiales, que al arder liberan calor intensamente y emiten gases tóxicos, lo que compromete la seguridad en aplicaciones críticas. Estas limitaciones no solo afectan al rendimiento técnico del material, sino que también tienen implicaciones directas en el cumplimiento de las nuevas regulaciones ambientales, como las políticas de la Unión Europea sobre el uso de productos químicos y la gestión de residuos.

Los compuestos reforzados con fibra de carbono (CFRP) destacan por su ligereza, rigidez y durabilidad, lo que los hace indispensables en industrias como la aeroespacial, el transporte ferroviario, la energía eólica y la defensa. Sin embargo, la mayoría de los CFRP actuales emplean matrices termoestables convencionales, que heredan las mismas carencias de reciclabilidad, ignifugación y sostenibilidad. Esto limita su evolución hacia soluciones verdaderamente respetuosas con el medio ambiente y plantea importantes retos en términos de regulación y circularidad. A medida que aumentan las exigencias de sostenibilidad en los sectores industriales, la necesidad de alternativas funcionales y responsables se vuelve más urgente.

En respuesta a este contexto, la presente tesis se orienta al desarrollo de nuevas matrices epoxi vitrimer, reciclables, retardantes a la llama y de base biológica, específicamente diseñadas para su

uso en CFRP. El enfoque de diseño se basa en introducir enlaces dinámicos tipo imina dentro de la red epoxi. Estos enlaces permiten reacciones reversibles como la transiminación y la hidrólisis-reformación, otorgando al material capacidades de reconfiguración térmica, auto-reparación y reciclado químico. Al mismo tiempo, la incorporación de grupos fosforados y estructuras aromáticas favorece la formación de residuos carbonosos durante la combustión, contribuyendo a una mayor estabilidad térmica y a un comportamiento ignífugo mejorado. Estas funcionalidades no sólo responden a demandas técnicas, sino que también abren nuevas posibilidades de gestión de fin de vida útil de materiales compuestos.

La elección de los enlaces imina como unidad dinámica en esta investigación no fue aleatoria. Los enlaces imina, formados por la condensación entre un grupo carbonilo y un grupo amino, poseen una estructura relativamente estable en condiciones ambientales, pero presentan una capacidad única de romperse y reformarse bajo estímulos suaves, como calor o presencia de nucleófilos. Esta característica los convierte en una herramienta especialmente atractiva para introducir reversibilidad en sistemas termoestables, sin comprometer la integridad estructural del material durante su vida útil. A diferencia de otros enlaces dinámicos como los ésteres o las urethane-disulfuros, los enlaces imina ofrecen una velocidad de intercambio ajustable y una compatibilidad sintética con una amplia gama de compuestos bio-basados. Además, su introducción en redes epoxi no requiere el uso de catalizadores externos, lo que simplifica los procesos de formulación y reduce los costes asociados. Desde una perspectiva ambiental, muchos precursores de enlaces imina, como las aminas aromáticas o los aldehídos naturales (por ejemplo, la vainillina), pueden obtenerse de fuentes renovables, alineando esta elección con los principios de la química verde. Asimismo, se ha demostrado que los vitrímeros basados en enlaces imina mantienen sus propiedades funcionales incluso después de varios ciclos de reciclado, lo que garantiza la estabilidad a largo plazo del material sin pérdida significativa de rendimiento. Por estas razones, la imina se posiciona como una de las estrategias más prometedoras para el diseño de termofijos reversibles de alto rendimiento.

Como resina base se eligió el triglicidil éter de glicerol (Gte), un epoxi biobasado que no contiene estructuras de bisfenol A. A partir de este monómero se diseñaron y estudiaron tres sistemas vitrimer distintos, abarcando desde la síntesis de los componentes hasta su procesamiento, caracterización y evaluación final en forma de compuestos reforzados con fibra de carbono. La selección del Gte no fue arbitraria, ya que su bajo peso molecular, elevada funcionalidad y origen

renovable lo convierten en una plataforma atractiva para formulaciones sostenibles con buenas propiedades mecánicas.

En el Capítulo 4 se describe el desarrollo del sistema GVD, formulado a partir de Gte, un agente de curado imínico derivado de vainillina y p-aminofenol (VA), y el aditivo fosforado DOPO. Con el fin de evitar reacciones secundarias entre el DOPO y los grupos funcionales del curado, este aditivo fue previamente incorporado a la cadena epoxi. El sistema GVD presentó un rendimiento ignífugo notable, alcanzando clasificación UL-94 V-0 y un índice LOI del 31%. Las pruebas de calorimetría cónica mostraron reducciones significativas del 38,2% en el valor máximo de liberación de calor (pHRR) y del 26,3% en el calor total liberado (THR). Además, demostró propiedades funcionales como moldeado térmico, memoria de forma y reciclabilidad, confirmando el éxito del entrecruzamiento dinámico mediante enlaces imina. Los resultados obtenidos en esta etapa sentaron una base sólida para explorar formulaciones más complejas y robustas.

En el Capítulo 5 se abordó una de las debilidades observadas en el sistema Gte-VA: su limitada densidad de reticulación bajo procesamiento por fusión. Para solucionarlo, se incorporó un comonómero aromático rígido, el tris(trihidroxifenil)metano triglicidil éter (Tmte), que permitió aumentar la rigidez y mejorar las propiedades mecánicas. El sistema híbrido resultante, denominado GTV, mostró un comportamiento balanceado entre flexibilidad y resistencia. La formulación óptima (GTV-4) alcanzó una T_g de 91,1 °C, una resistencia a tracción de 73,4 MPa y un módulo de Young de 1069 MPa. Conservó además propiedades vitrimer como la auto-reparación, el remodelado térmico y la memoria de forma. Este sistema se procesó con éxito en forma de preimpregnados sin disolvente y se utilizó para fabricar CFRP. Las muestras laminadas pudieron degradarse selectivamente en una solución de etilendiamina a 60 °C, recuperando completamente las fibras sin dañarlas. Este procedimiento, que no requiere el uso de disolventes tóxicos ni condiciones extremas, representa una contribución significativa hacia tecnologías de reciclado más accesibles.

El Capítulo 6 se centró en resolver los problemas prácticos asociados a la alta reactividad y estrecho margen de procesamiento de los sistemas anteriores cuando se aplicaban en líneas de producción continua de preimpregnados por fusión. Para ello se diseñó y sintetizó un nuevo agente de curado con enlaces imina, grupos fosforados y funciones hidroxilo: FROH. Este agente trifuncional se obtuvo mediante una ruta en dos etapas: condensación de $POCl_3$ con vainillina,

seguida de reacción con p-aminofenol. El sistema Gte-FROH presentó un comportamiento reológico estable y una cinética de curado compatible con equipos industriales. A partir de esta formulación, se construyó un sistema semiautomatizado de producción continua de preimpregnados por fusión, logrando una impregnación homogénea y una manipulación estable. El compuesto final reforzado con fibra de carbono (Gte-FROH-CF) alcanzó una resistencia a flexión de 1024,5 MPa y clasificación UL-94 V-0. Lo más relevante fue que el sistema permitió recuperar completamente las fibras bajo condiciones suaves, consolidando su potencial como alternativa reciclable y segura en procesos industriales. Además, esta metodología demuestra la viabilidad de integrar estos sistemas en procesos productivos de escala real, algo fundamental para su transferencia tecnológica.

En conjunto, esta tesis establece una estrategia integral de diseño y validación para el desarrollo de sistemas vitrimer epoxi de alto rendimiento, sostenibles y funcionales, adecuados para aplicaciones estructurales avanzadas. La introducción de enlaces dinámicos, combinada con elementos ignífugos y enfoques de copolimerización, permitió superar varias limitaciones críticas de las resinas epoxi tradicionales. Desde una perspectiva científica, los resultados permiten comprender mejor cómo la estructura química influye en propiedades como la reprocesabilidad, el comportamiento térmico y la resistencia mecánica. Desde el punto de vista tecnológico, el trabajo demuestra la viabilidad de fabricar preimpregnados mediante técnicas sostenibles, sin comprometer la calidad del producto final.

Cabe destacar que las metodologías propuestas pueden extenderse a otros polímeros termoestables, abriendo nuevas oportunidades para implementar soluciones circulares en campos donde el reciclado aún representa un reto. El diseño molecular adaptativo, basado en enlaces dinámicos e incorporaciones funcionales estratégicas, constituye una vía prometedora hacia materiales inteligentes, capaces de combinar durabilidad, seguridad y respeto ambiental. En un contexto industrial marcado por regulaciones estrictas y exigencias funcionales crecientes, los sistemas vitrimer desarrollados ofrecen una plataforma versátil y robusta con potencial para transformar el panorama de los materiales compuestos en un entorno tecnológico cada vez más orientado hacia la sostenibilidad y la circularidad. Además, su adaptabilidad a procesos industriales y su compatibilidad con técnicas de fabricación de compuestos existentes los posiciona como una alternativa realista y escalable para una nueva generación de materiales estructurales sostenibles. En definitiva, esta investigación sienta las bases para una transición hacia modelos de producción

más responsables, con menor impacto ambiental y mayores beneficios a largo plazo tanto para la industria como para la sociedad.

Abstract

Epoxy resins have long been recognized as key thermosetting materials in advanced engineering, due to their excellent thermal and mechanical properties, ease of processing, and strong adhesion to a wide range of substrates. These features have facilitated their widespread application in demanding sectors such as aerospace, electronics, automotive, civil engineering, and electrical systems, as well as in the production of high-performance composite materials. However, beyond their technical advantages, these resins present structural and environmental limitations that have motivated an active search for more sustainable alternatives.

Most commercial epoxy resin formulations are based on monomers derived from fossil resources, particularly bisphenol A diglycidyl ether (DGEBA), a non-renewable compound associated with health risks such as endocrine disruption and reproductive toxicity. In addition, the polymer networks formed upon curing are highly crosslinked and chemically irreversible, which prevents their recycling or subsequent reprocessing. This lack of circularity contributes to the accumulation of thermoset waste that is difficult to manage. Moreover, these materials are inherently flammable and release large amounts of heat and toxic gases during combustion, compromising safety in critical applications. These limitations not only affect the technical performance of the material but also have direct implications for compliance with emerging environmental regulations, such as EU policies on chemical usage and waste management.

Carbon fiber reinforced polymers (CFRP) stand out for their lightweight, rigidity, and durability, making them indispensable in industries such as aerospace, high-speed rail, wind energy, and defense. However, most current CFRP employ conventional thermoset matrices, which inherit the same shortcomings of non-recyclability, flammability, and lack of sustainability. This hinders their transition to truly environmentally friendly solutions and presents major challenges in terms of regulatory compliance and circularity. As sustainability demands increase across industrial sectors, the need for functional and responsible alternatives becomes more urgent.

In response to this scenario, the present thesis focuses on the development of new bio-based vitrimer epoxy matrices that are recyclable, flame-retardant, and specifically designed for applications in CFRP. The design strategy involves the incorporation of dynamic imine bonds into the epoxy network. These bonds undergo reversible reactions such as transimination and hydrolysis-reformation, enabling thermal reconfiguration, self-healing, and chemical recycling

capabilities. At the same time, the introduction of phosphorus-containing groups and aromatic structures promotes the formation of char residues during combustion, contributing to enhanced thermal stability and synergistic flame-retardant performance. These functionalities not only meet technical demands but also enable more effective end-of-life management of composite materials.

The selection of imine bonds as the dynamic motif in this study was deliberate. Formed through the condensation of carbonyl and amine groups, imines exhibit a stable structure under ambient conditions yet possess a unique ability to reversibly break and reform under mild stimuli such as heat or nucleophilic attack. This makes them particularly attractive for introducing reprocessability into thermoset systems without compromising the structural integrity during service. Compared to other dynamic bonds like esters or disulfide-urethanes, imines offer tunable exchange rates and synthetic compatibility with a broad range of bio-based compounds. Moreover, their integration into epoxy networks does not require external catalysts, simplifying formulation processes and reducing associated costs. Environmentally, many imine precursors, including aromatic amines and natural aldehydes (e.g., vanillin), can be sourced from renewable feedstocks, aligning with the principles of green chemistry. Furthermore, imine-based vitrimers have been shown to retain their functional properties after multiple recycling cycles, ensuring long-term material stability without significant performance loss. For these reasons, imines are positioned as one of the most promising strategies for designing high-performance reversible thermosets.

As the epoxy base resin, glycerol triglycidyl ether (Gte) was selected. This bio-based epoxy contains no bisphenol A structures and offers low molecular weight, high functionality, and renewable origin. Three distinct vitrimer systems were designed and evaluated based on Gte, encompassing the synthesis of key components, processing, characterization, and final performance evaluation in carbon fiber composites.

Chapter 4 presents the development of the GVD system, formulated from Gte, an imine curing agent derived from vanillin and p-aminophenol (VA), and the phosphorus-based flame retardant DOPO. To prevent undesirable side reactions between DOPO and the curing functionalities, the DOPO was first grafted onto the epoxy backbone. The resulting GVD system exhibited excellent flame resistance, achieving UL-94 V-0 classification and a limiting oxygen index (LOI) of 31%. Cone calorimetry showed significant reductions of 38.2% in peak heat release rate (pHRR) and 26.3% in total heat release (THR). Moreover, the system demonstrated thermal reprocessability,

shape memory, and recyclability, validating the effectiveness of dynamic imine crosslinking. These findings established a solid foundation for more complex vitrimer designs.

Chapter 5 addressed the relatively low crosslink density of the Gte-VA system under melt-processing conditions. To improve this, the rigid aromatic epoxy monomer tris(4-hydroxyphenyl) methane triglycidyl ether (Tmte) was introduced, leading to the hybrid GTV system with enhanced rigidity and mechanical strength. The optimized GTV-4 formulation exhibited a glass transition temperature of 91.1°C, tensile strength of 73.4 MPa, and Young's modulus of 1069 MPa. It maintained vitrimer properties such as self-healing, thermal reshaping, and shape memory. Solvent-free prepregs were successfully fabricated and laminated into CFRP. The resulting composites were chemically degraded in an ethylenediamine solution at 60 °C, enabling non-destructive fiber recovery. This solvent-free and mild degradation process represents a significant advance toward more accessible recycling technologies.

Chapter 6 tackled the challenges associated with high reactivity and narrow processing windows observed during continuous melt-prepreg fabrication. To overcome these limitations, a new imine-based curing agent with phosphorus content and hydroxyl functionality, termed FROH, was designed and synthesized. This trifunctional agent was produced via a two-step route: condensation of $POCl_3$ with vanillin, followed by reaction with p-aminophenol. The Gte-FROH system displayed favorable rheological behavior and a curing profile compatible with industrial equipment. Based on this formulation, a semi-automated continuous production system for melt-prepregs was developed, achieving uniform fiber impregnation and stable operation. The final carbon fiber composite (Gte-FROH-CF) exhibited a flexural strength of 1024.5 MPa and UL-94 V-0 classification. Most importantly, the vitrimer matrix allowed for full fiber recovery under mild degradation conditions, confirming its suitability for sustainable manufacturing and recycling processes. This also demonstrated the system's feasibility for integration into real-scale production lines.

Overall, this thesis establishes an integrated strategy for the design and validation of high-performance, sustainable, and functional vitrimer epoxy systems for advanced structural applications. The introduction of dynamic bonds, combined with flame-retardant elements and copolymerization strategies, effectively overcame the critical limitations of traditional epoxy systems. Scientifically, the findings offer deeper insights into the structure-property relationships

governing vitrimer performance. Technologically, the work proves the feasibility of fabricating prepregs using solvent-free and scalable methods without compromising final product quality.

Notably, the methodologies developed here can be extended to other thermosetting polymers, opening new opportunities for implementing circular solutions in materials where recyclability remains a challenge. The adaptive molecular design based on dynamic bonds and strategic functional group incorporation presents a promising path toward intelligent materials that combine durability, safety, and environmental responsibility. In an industrial context increasingly defined by strict regulations and rising functional demands, the vitrimer systems developed herein provide a versatile and robust platform with the potential to reshape the landscape of composite materials in a technological environment progressively geared toward sustainability and circularity. Ultimately, this research lays the groundwork for a transition toward more responsible production models with reduced environmental impact and long-term benefits for both industry and society.

Contents

CHAPTER 1
Introduction

1.1 Background: epoxy resin

Epoxy resin (EP) is a class of important thermosetting polymers that have been widely used in various industrial fields since their first discovery by Prileschajew in 1909 [1, 2]. Characterized by the presence of two or more reactive epoxide groups in their molecular structure (**Figure 1-1**), EP is typically low molecular weight prepolymers. Under thermal or catalytic conditions, these epoxide groups undergo addition or ring-opening polymerization reactions with curing agents, leading to the formation of highly crosslinked three-dimensional (3D) networks [3]. Thanks to their excellent mechanical properties, dimensional stability, electrical insulation, chemical resistance, and strong adhesion to diverse substrates, EP are extensively applied in coatings, adhesives, electronic encapsulants, structural composites, and insulating materials, particularly in automotive, aerospace, construction, and electronics industries [4].

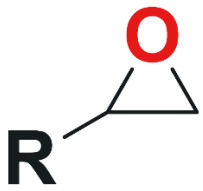

Figure 1-1 The structure of epoxy group.

Among commercial epoxy systems, diglycidyl ether of bisphenol A (DGEBA) is the most widely used epoxy monomer (**Figure 1-2**). Its rigid aromatic backbone and π–π stacking interactions contribute to the outstanding thermal and mechanical performance of the cured materials [5]. It is estimated that approximately 85% of commercial epoxy formulations are based on DGEBA [6]. This monomer is synthesized via the reaction of epichlorohydrin with bisphenol A (BPA) in the presence of a base catalyst and features a well-established synthetic process and favorable processability. However, BPA is derived from petrochemical sources and has been classified by the European Chemicals Agency (ECHA) in 2018 as a category 1B endocrine disruptor, posing risks to both human health and the environment [7].

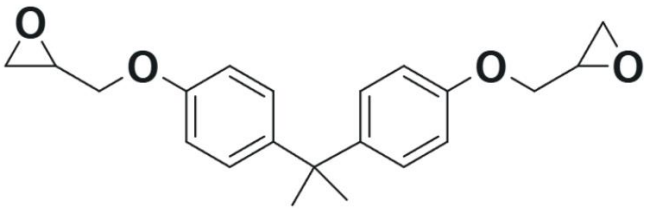

Figure 1-2 Chemical structure of diglycidyl ether of bisphenol A (DGEBA).

In recent years, bio-based epoxy resins have attracted increasing attention as sustainable alternatives. Researchers have been developing new epoxy monomers from renewable sources such as vegetable oils, lignin, and natural phenolics to reduce dependency on fossil-based chemicals [8-11]. Auvergne et al [12] reported the synthesis and polymerization behavior of an aromatic bio-based epoxy monomer derived from eugenol. Jablonskis et al [13] partially replaced commercial DGEBA-based epoxy resin (Araldite LY1564) with glycidylated lignin and observed improvements in tensile strength, strain, and rigidity with increased lignin content. Additionally, Resoltech Advanced Technology Resins Company has developed an ECO epoxy series based on BPA and bisphenol F (BPF), optimizing the bio-based carbon content and reactive diluent ratios to reduce petroleum usage. Among various candidates, glycerol triglycidyl ether (Gte) is a commercially available aliphatic bio-based epoxy monomer (**Figure 1-3**) [14, 15]. With three reactive epoxide groups, Gte exhibits high functionality and readily forms dense 3D crosslinked networks with various curing agents.

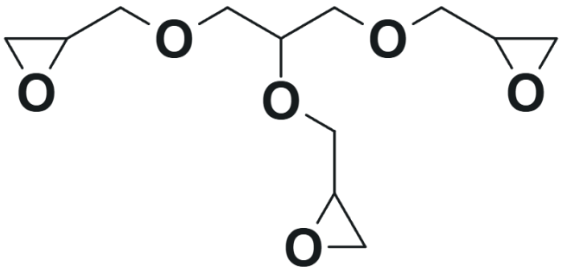

Figure 1-3 Chemical structure of glycerol triglycidyl ether (Gte) [15].

The curing behavior of EP is closely related to the type of curing agent used. Common curing agents include amines, hydroxyl, and carboxyl group etc [16], each reacting with epoxy groups through distinct mechanisms to form crosslinked networks with different structures and properties (**Figure 1-4)**. Among these, phenolic hydroxyl-based curing agents can undergo condensation

reactions with epoxy groups under elevated temperatures or catalytic conditions, forming stable ether linkages [17]. The resulting networks typically exhibit high crosslink density, thermal stability, and mechanical strength, making them especially suitable for the fabrication of high glass transition temperature (T_g) thermoset materials.

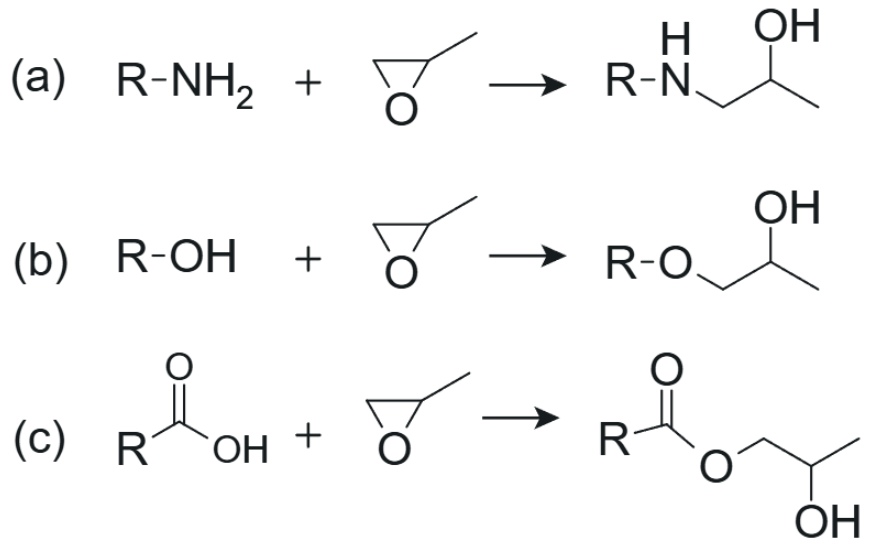

Figure 1-4 Reaction mechanisms of epoxy group ring-opening with different nucleophiles [3]: (a) amine group; (b) hydroxyl group; (c) carboxyl group.

According to recent market forecasts, the global EP market is valued at approximately USD 11.58 billion in 2024, expected to grow to USD 12.33 billion in 2025, and reach USD 20.31 billion by 2034, with a compound annual growth rate (CAGR) of 5.71% from 2025 to 2034 (**Figure 1-5**). The Asia-Pacific region remains the largest consumer, with major applications in construction, electronics, automotive, and wind energy. With the continued advancement of renewable energy, lightweight design, and sustainable materials, the demand for EP in emerging industries continues to rise. However, conventional thermoset epoxy resins are difficult to recycle or degrade after curing and are inherently flammable, leading to issues such as resource waste, environmental pollution, and fire hazards. As a result, the development of bio-based epoxy systems that combine excellent mechanical performance, sustainability and flame retardancy has become a major focus in polymer materials research.

Figure 1-5 The prediction of the value of global EP market size [18].

In this context, the present study investigates the curing behavior and structure–property relationships of a phenolic hydroxyl-based curing agent containing dynamic covalent bonds (imine bonds) in reaction with the commercially bio-based epoxy monomer Gte. The aim is to construct a novel sustainable epoxy vitrimer network with environmental friendliness, high performance, flame retardancy, and recyclability, thus providing theoretical support and technical strategies for the development of next-generation green epoxy materials.

1.2 Sustainability challenges of epoxy resins

In many practical applications, EP-based materials are subjected to complex service conditions such as high mechanical loads, pressure, temperature, friction, and vibration. These factors often lead to creep, cracking, and fracture, significantly shortening the service life of the material and increasing the risk of failure. Like other conventional thermosetting polymers, EP form an irreversible 3D covalent network upon curing, exhibiting thermoset characteristics such as insolubility and infusibility. As a result, they cannot be remelted, reshaped, or reprocessed after use. Consequently, a large amount of aged, damaged, or discarded epoxy-based waste is ultimately disposed of via incineration or landfilling, causing severe environmental pollution and resource depletion [19].

To address these limitations, various strategies have been proposed in recent years to enhance the sustainability of crosslinked polymer systems. One traditional approach involves the

introduction of supramolecular interactions [20] such as hydrogen bonding [21], metal coordination [22], or ionic interactions [23] as reversible physical crosslinks. While this can impart limited self-healing or recyclability, the relatively weak strength of supramolecular bonds compromises the thermal and mechanical performance compared to covalently crosslinked systems [24].

A more promising strategy is the incorporation of dynamic covalent bonds, which can reversibly break and reform under specific external stimuli such as heat, light, pH, or catalysts. These networks, known as Covalent Adaptable Networks (CANs), enable topological rearrangement without compromising the covalent nature of the network, thereby combining functionality such as reprocessability and recyclability with structural integrity under normal conditions [25, 26].

Based on their rearrangement mechanism, CANs can be categorized into dissociative CANs and associative CANs (**Figure 1-6**). Dissociative CANs rely on reversible bond cleavage and reformation, as exemplified by the Diels–Alder reaction. However, the temporary loss of crosslink density during bond dissociation may lead to undesirable effects such as sharp viscosity drops and dimensional instability. In contrast, associative CANs maintain a constant crosslink density through bond exchange mechanisms, providing better dimensional control and structural stability[27].

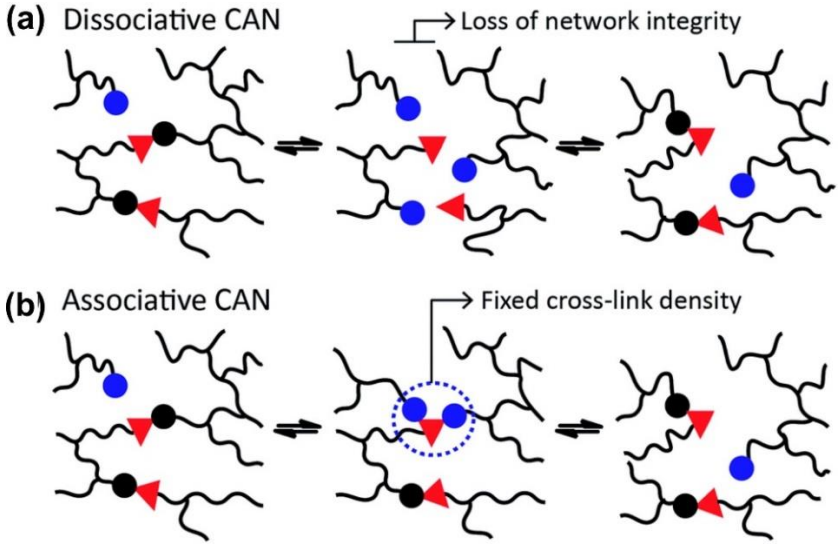

Figure 1-6 Dissociative CAN and associative CAN based on the exchange reactions that proceed respectively with or without a temporary loss of cross-link density [27].

Vitrimers, a subclass of associative CANs, incorporate dynamic covalent exchange bonds into a thermoset network. At typical service temperatures, vitrimer materials exhibit mechanical and thermal behavior like traditional thermosets. When heated above the topology freezing transition temperature (T_v), the dynamic bonds begin to exchange, enabling topological rearrangement of the network [28]. As a result, vitrimers demonstrate intelligent functions such as reprocessability, weldability, self-healing, and recyclability. Owing to their ability to bridge high performance with sustainability, vitrimers are considered a promising solution for recyclable thermosets, with potential applications in aerospace, electronics, and wind energy sectors.

1.3 State of the art of epoxy vitrimer

This section reviews the latest progress in epoxy vitrimer research, including the fundamental concepts, representative types of dynamic covalent bonds such as transesterification, disulfide exchange, and imine metathesis, as well as strategies for designing sustainable bio-based vitrimer systems. It also highlights the diverse functional properties of these materials, including reshaping, welding, self-healing, shape memory and recyclability. Through an in-depth discussion of network design and exchange mechanisms, this section highlights the unique capability of epoxy vitrimers to integrate high performance with environmental sustainability.

1.3.1 Basic concept of epoxy vitrimer

Since the pioneering work of Leibler et al [29] vitrimers have gained significant attention for their ability to combine the high performance of thermosets with the processability of thermoplastics. At the core of vitrimer technology lies the incorporation of dynamic covalent bonds (DCBs), which enable the rearrangement of the network topology under specific stimuli, such as heat, while maintaining the integrity of the covalent network under ambient conditions [30].

A typical vitrimer is composed of a highly crosslinked polymer network formed through covalent bonding. When exposed to elevated temperatures, the dynamic bonds within the network undergo associative exchange reactions, in which new covalent bonds are formed simultaneously as existing ones are broken. This enables continuous topological rearrangement of the network without reducing the overall crosslink density. In contrast to dissociative mechanisms that

temporarily depolymerize the material, the associative mechanism allows the vitrimer to retain its structural integrity during processing [31]. As a result, the material exhibits viscoelastic flow at high temperatures, while maintaining solid-like mechanical stability under service conditions.

The viscoelastic behavior of vitrimers is governed by two critical temperatures: the T_g and the T_v. T_g marks the transition from a glassy to a rubbery state, driven by segmental mobility of polymer chains. T_v defines the threshold above which the exchange of dynamic covalent bonds becomes sufficiently fast to induce network rearrangement. When the material is heated above T_v, topological changes dominate and the network flows, following Arrhenius-type viscosity behavior [32].

The thermal response of vitrimers varies depending on the relative positions of T_g and T_v. If $T_g < T_v$, the material transitions from a glassy state to a rubbery state ($T_g < T < T_v$) where the network remains topologically frozen despite chain mobility. Further heating beyond Tv activates bond exchange reactions, transforming the material into a viscoelastic liquid (**Figure 1-7 (a)**). Conversely, if $T_v < T_g$, even though the exchange reaction is inherently fast, the network remains immobilized due to restricted chain mobility below T_g. In this case, viscosity follows a Williams–Landel–Ferry (WLF) behavior near T_g and transitions to Arrhenius behavior only at higher temperatures (**Figure 1-7 (b)**) [27].

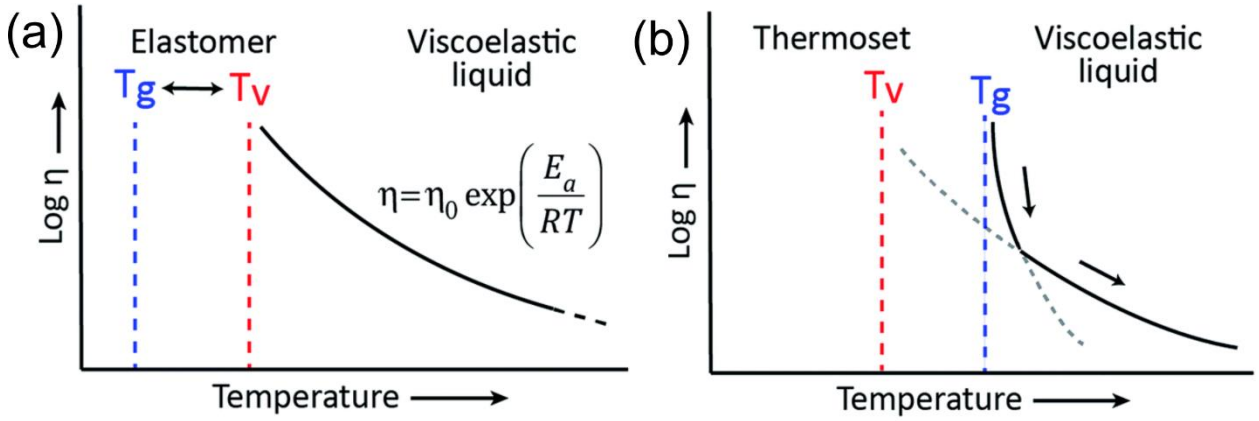

Figure 1-7 Schematic of phase behavior evolution of vitrimers across different temperature regions [27].

1.3.2 Types of dynamic bonds in epoxy vitrimers

Depending on the chemistry used to introduce reconfigurability, epoxy vitrimers can be categorized by their dynamic bond types, including transesterification, disulfide exchange, and imine exchange, each offering unique advantages in network design.

1.3.2.1 Epoxy vitrimers based on transesterification

Epoxy groups readily react with carboxylic acids or anhydrides to form ester linkages, accompanied by the formation of hydroxyl groups [4, 33, 34]. In the presence of catalysts such as Lewis's acids or organic bases, reversible transesterification can occur between these esters and hydroxyls under elevated temperatures [35]. This exchange reaction induces topological rearrangement of the network, making transesterification one of the most extensively studied mechanisms in epoxy vitrimer research (**Figure 1-8**) [29].

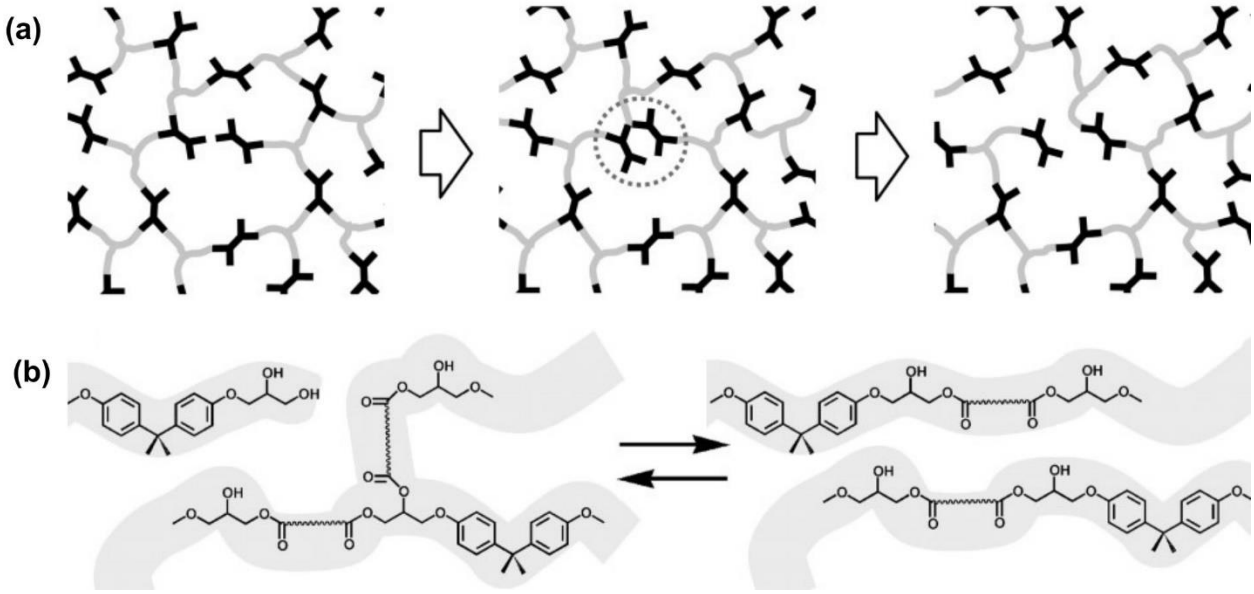

Figure 1-8 (a) Topological rearrangements via exchange reactions preserving the network integrity; (b) Illustration of transesterification in hydroxyl-ester networks [29].

1.3.2.2 Epoxy vitrimers based on disulfide exchange

Disulfide bonds are relatively weak covalent bonds capable of undergoing dynamic exchange without the need for external catalysts—even at room temperature. The dynamic properties of disulfide bonds mainly originate from three pathways: (a) thermally or UV-induced disulfide bond exchange; (b) cleavage of disulfide bonds through radical mechanisms; and (c) nucleophilic substitution within disulfide bonds triggered by the attack of external thiolate anions [36]. A common strategy involves incorporating disulfide-containing curing agents into commercial epoxy resins. As shown in **Table 1-1**, representative examples include 4,4′-diaminodiphenyl disulfide (4-AFD) [37], 3-dithiodipropionic acid (DPTA) [38], and 2,2′-diaminodiphenyl disulfide (2-AFD) [39]. These systems demonstrate excellent self-healing and recyclability, although the high cost of disulfide compounds may limit large-scale applications.

Table 1-1 Overview of bio-based epoxy vitrimer containing disulfide exchange.

Epoxy resin monomer	Curing agent	T_g (°C)	Tensile strength (MPa)	Remolding condition	Reference
Epoxidized soybean oil (ESO)	4-AFD	34.0	3.0	180 °C, 20 MPa, 10 min	[37]
cardanol-based epoxy	DPTA	-2.2	0.4	150 °C, 1 h	[38]
DGEBA	2-AFD	108.5	57.7	220 °C, 10 MPa, 5h	[39]

1.3.2.3 Epoxy vitrimers based on imine bonds

Imine bonds (C=N), formed by the condensation of aldehydes and primary amines, are another class of dynamic covalent structures. They exhibit reversible behavior through mechanisms such as imine condensation, exchange, and imine metathesis (**Figure 1-9**) [40]. These systems offer catalyst-free network rearrangement and multifunctional capabilities such as self-healing, degradability, and recyclability. Recent studies have successfully integrated imine functionalities into epoxy networks to achieve both high performance and dynamic reconfigurability [41-43].

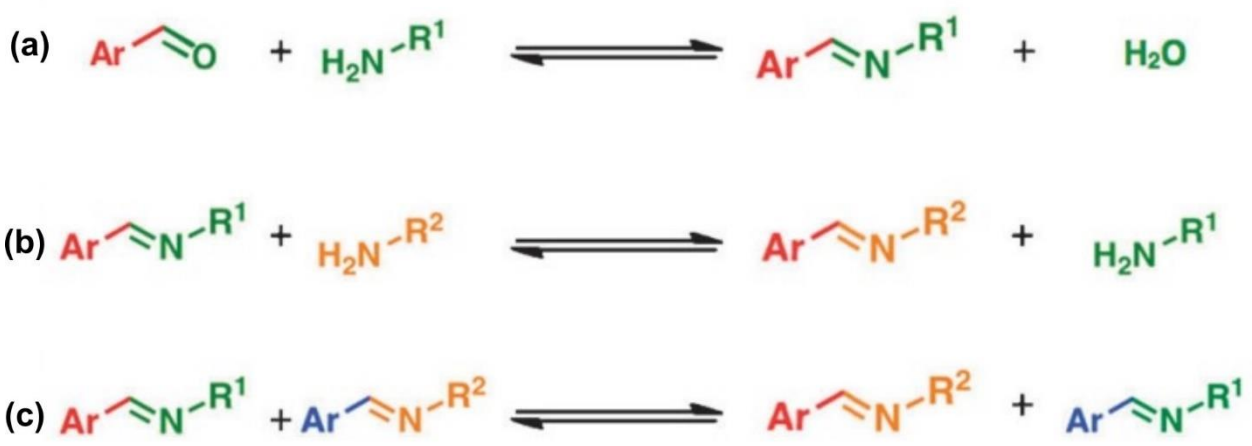

Figure 1-9 The three types of imine reactions: (a) imine condensation, (b) exchange, and (c) metathesis [40].

1.3.3 Bio-based epoxy vitrimers

In response to global initiatives for carbon neutrality and sustainability, bio-based vitrimers have emerged as an eco-friendly alternative to petroleum-derived thermosets. Sustainability in such systems is typically achieved through two main strategies: replacing fossil-based epoxy monomers like DGEBA with monomers derived from renewable sources such as vegetable oils [44], lignin [45, 46], or natural phenolics [47, 48]; and utilizing bio-based curing agents containing functional groups such as carboxylic acids, phenols, or amines to introduce dynamic structures like esters or imines. For example, epoxy soybean oil cured with fatty acids or anhydrides forms ester-based networks that undergo transesterification at elevated temperatures [49]. Aldehydes like vanillin and eugenol, with rigid aromatic backbones, are often employed to design imine-based vitrimers with improved T_g and mechanical strength. On the curing side, bio-derived molecules such as citric acid [50], gallic acid [10], vanillin [51] and lysine [52] are used to introduce multifunctional groups, enabling dynamic covalent crosslinking (**Figure 1-10**). While bio-based vitrimers show great promise in terms of environmental impact and functionality, challenges remain. These include variability in bio-feedstock reactivity, limited control over network architecture, and batch-to-batch performance inconsistency [41].

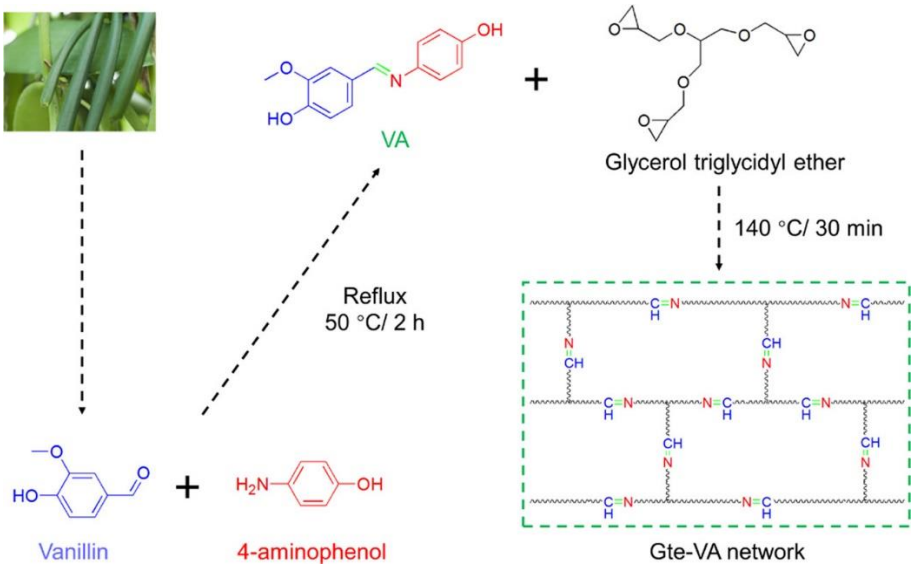

Figure 1-10 Synthetic route of VA and the preparation of epoxy vitrimer [51].

1.3.4 Functional expansion of epoxy vitrimers

As material design has advanced, vitrimers have evolved beyond traditional thermosets into multifunctional of shaping, welding, self-healing, shape memory, and stimuli-responsiveness.

1.3.4.1 Reshaping

Due to the reconfigurable nature of their networks, vitrimers can be reshaped under thermal conditions. This is achieved through dynamic bond exchange, allowing for plastic deformation that becomes fixed upon cooling. This feature is particularly advantageous for complex 3D structures and additive manufacturing. **Figure 1-11** illustrates representative examples of topological rearrangement and reshaping of epoxy vitrimer networks triggered by external stimuli such as heat, light, or water. An epoxy/acid vitrimer film based on transesterification could be reshaped into a new spiral shape by rolling the strip in a metal thin rod, fixing it by tape and keeping it at 160 °C for 2 h (**Figure 1-11 (a)**) [53]. The epoxy acid vitrimer film containing carbon nanotubes was programmed into a stable “V” shape by mechanically deforming it under infrared light with an intensity of 0.84 W/cm^2, followed by maintaining the applied force during continued exposure for 20 s (**Figure 1-11 (b), ii**). This irradiation elevated the temperature to around 180 °C due to the photothermal properties of the nanotubes, which was sufficient to initiate the bond exchange reactions. By repeating the thermal shaping protocol, the material was subsequently

transformed into a “w” shape (**Figure 1-11 (b), iii**) [54]. Once these configurations were fixed, they remained unchanged even when subjected to temperatures exceeding 250 °C, indicating complete stress relaxation and high thermal stability of the reconfigured structure. Abu-Omar et al. demonstrated the water responsive malleability of their vitrimer system, showing that its rigidity and toughness could be adjusted through water absorption. In their study, a vitrimer film was immersed in water for four hours and then stretched over the surface of a round bottom flask. After complete drying, the material retained a stable arc shaped configuration (**Figure 1-11 (c)**) [55]. The reshaped film exhibited excellent mechanical strength and remained undeformed while supporting a load of at least 240 g (**Figure 1-11 (c) iv**).

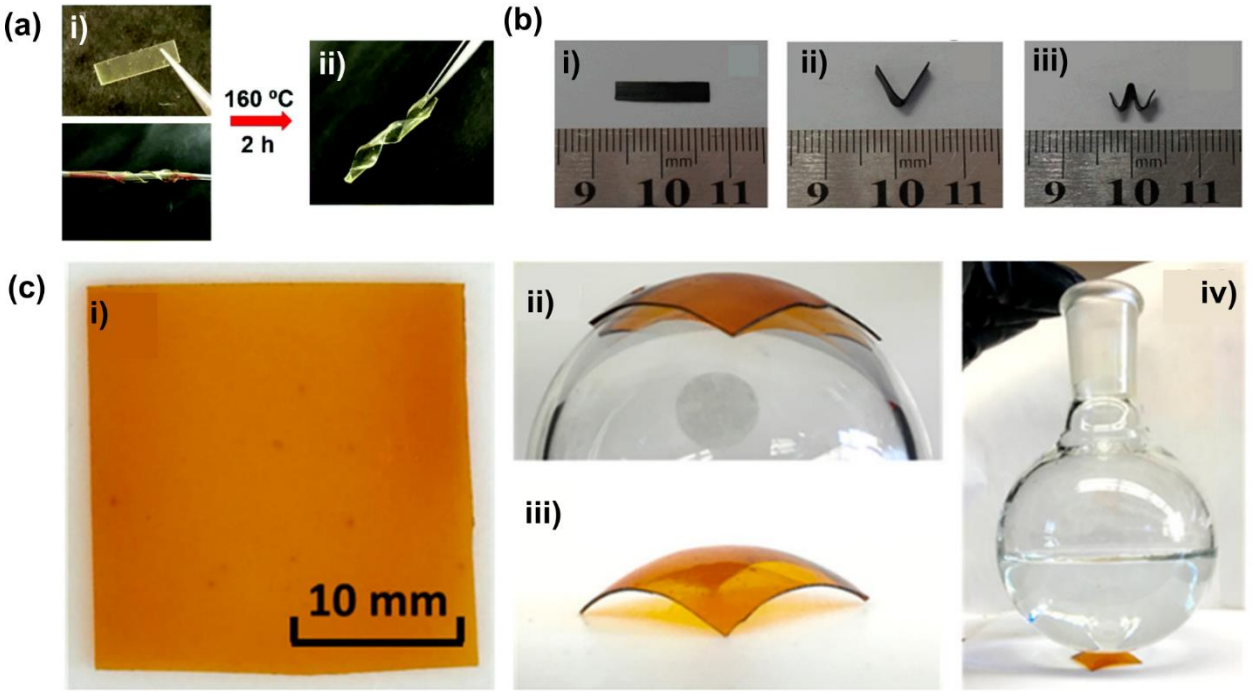

Figure 1-11 (a) Thermal-induced reshaping epoxy vitrimer [53]; (b) Photo-induced reshaping epoxy vitrimer [54]; (c) Water-driven malleability of epoxy vitrimer with imine bonds [55].

1.3.4.2 Welding and self-healing

The welding and self-healing capabilities of epoxy vitrimers are governed by the dynamic covalent bonds embedded in their networks, which enable bond exchange reactions under external stimuli such as heat, light, or moisture [56]. These reactions allow topological rearrangement at material interfaces, facilitating covalent fusion between fractured or separate parts [28, 57]. In literature,

this process is often described as interfacial welding, surface welding, self-welding, or autonomous repair.

The relaxation behavior of vitrimers is controlled by two key temperatures: T_g and T_v. Below T_v, bond exchange reactions are extremely slow, and the network topology remains essentially fixed. When the temperature exceeds T_g or T_v, and the bond exchange becomes sufficiently fast to allow interfacial network rearrangement. Accordingly, welding of vitrimer elastomers is typically performed at $T > T_v$, while welding of vitrimer thermosets requires $T > T_g$ [58].

Figure 1-12 (a) presents representative examples of reshaping and welding in vitrimer materials driven by thermal, photothermal, and hydrothermal stimuli, demonstrating the capability for reversible topological reconstruction [59]. For instance, a liquid crystalline epoxy vitrimer synthesized from diglycidyl ether of 4,4′-dihydroxybiphenyl and sebacic acid were chemically welded at 180 °C for 120 min to form complex soft actuators (**Figure 1-12 (b)**) [60]. In another study, Carbon Nanotube-reinforced vitrimers (CNT-vitrimers) demonstrated light-induced transmission welding and mask-assisted welding, successfully bonding to a wide range of materials with varying chemical compositions and physical properties, including (i) another CNT-vitrimer with identical chemistry, (ii) a control sample without CNTs, (iii) a conventional thermoset epoxy, and even (iv) a thermoplastic polymer substrate (**Figure 1-12 (c)**) [54].

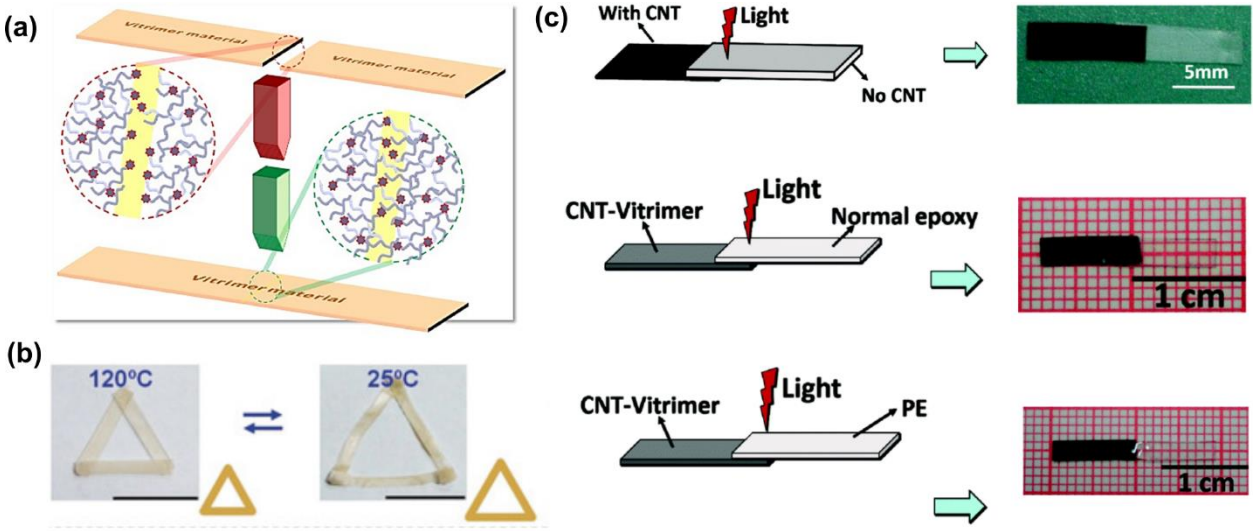

Figure 1-12 (a)Schematic illustration of chemical welding of vitrimer materials [59];(b) Thermally induced welding of epoxy vitrimer [60]; (c) Light-induced welding of epoxy vitrimer [54].

1.3.4.3 Shape memory and stimuli responsiveness

Shape memory polymers (SMPs) are a class of crosslinked polymeric materials capable of programmable deformation and reversible shape transformation under external stimuli such as heat, light, pH, or solvents [61]. They have shown significant potential in biomedical devices, soft robotics, intelligent actuators, and flexible electronics. Conventional thermally responsive SMPs typically exhibit a dual-shape memory effect governed by the T_g [62]. When heated above T_g, polymer chain segments become mobile and can be deformed under mechanical force, accompanied by a decrease in system entropy. Upon cooling below T_g, the temporary shape is fixed. Reheating to temperatures above T_g releases stored elastic energy, allowing the material to recover its original shape. This entropy-driven deformation–fixation–recovery cycle defines the classical elastic shape memory behavior of polymers. However, traditional SMPs are limited to a single deformation-recovery cycle, which restricts their applicability in systems requiring complex geometries or multi-stage shape programming [63].

In contrast, vitrimers combine conventional elastic shape memory behavior with plastic shape reconfiguration due to the presence of dynamic covalent bonds in their networks. When vitrimer materials are deformed under mechanical load at temperatures above the T_v, bond exchange reactions are thermally activated, allowing permanent topological rearrangement of the network. Once cooled, the new shape is fixed and cannot revert to the original geometry upon reheating, as the mechanism is not entropy-based but instead driven by network restructuring through covalent bond exchange. This enables programmable, irreversible shape transformation, allowing vitrimers to undergo multiple cycles of complex and precise 3D shape construction. Furthermore, by tailoring the chemistry of the dynamic bonds, vitrimers can be designed to respond to a range of external stimuli—including temperature, light, moisture, and pH—broadening their potential for integration into advanced aerospace systems, wearable devices, and multifunctional smart materials.

1.4 Flame retardant vitrimer in CFRP

Carbon fiber-reinforced polymer (CFRP) has become indispensable in sectors such as transportation, wind energy, and aerospace, owing to their exceptional properties, including high specific strength, stiffness, multifunctionality, and design flexibility [64, 65]. Over the past decade,

global demand for CFRP has grown steadily, with a compound annual growth rate of approximately 6%, and the market is projected to reach USD 64 billion by 2030 [66]. However, this rapid expansion inevitably results in a substantial increase in CFRP waste, including surplus prepregs, manufacturing scrap, and end-of-life components. In addition, carbon fiber (CF) production remains an expensive and energy-intensive process, further highlighting the urgent need for efficient recycling technologies to manage accumulated CFRP waste and reduce environmental impact [67].

CFRP typically consists of two main components: carbon fibers and a resin matrix. EP is the most widely used matrix, as it forms a highly cross-linked and stable three-dimensional polymer network with excellent mechanical strength and chemical resistance. However, despite its high cross-link density and aromatic structure, EP is intrinsically flammable. Once ignited, it produces large amounts of smoke and releases significant heat, posing serious fire hazards to the cured epoxy matrix and the corresponding CFRP structures. To improve flame retardancy, flame-retardant additives are usually introduced into the epoxy resin through either physical blending (additive type) [68] or chemical bonding (reactive type) [69]. The use of flame-retardant EP can enhance the fire performance of CFRP. Nevertheless, the permanent cross-linked structure of conventional epoxy networks makes recycling of such composites challenging. In addition, the incorporation of flame-retardant components further complicates waste treatment, leading to reduced incineration efficiency, potential environmental risks from landfill leachates or gaseous emissions, and the formation of more complex residues during thermochemical processing.

The development of vitrimers based on dynamic covalent chemistry is considered a promising strategy to address the recycling challenges of flame-retardant carbon fiber-reinforced composites. Vitrimers offer significant potential for extending the service life of both polymer matrices and carbon fiber-reinforced materials, enabling the recovery of carbon fibers under mild conditions and facilitating the reuse of recycled materials. However, although various types of dynamic covalent bonds have been explored in vitrimer systems, only a limited number of studies to date have focused on the design and development of sustainable and flame-retardant CFRP.

1.4.1 Ester exchange approach

Transesterification is one of the most widely used dynamic covalent exchange reactions in CANs [70, 71]. As shown in **Figure 1-13(a)**, Chen et al [72] reported a flame-retardant epoxy vitrimer system prepared using DGEBA as the epoxy resin matrix, a 9,10-dihydro-9-oxa-10-phosphaphenanthrene-10-oxide (DOPO)-based diacid as a co-curing agent, and 1,5,7-triazabicyclo dec-5-ene (TBD) as the catalyst for transesterification. The resulting vitrimer exhibited excellent repairability and reprocessability, with no significant loss in mechanical or flame-retardant properties after reprocessing. However, alkaline catalysts or metal salts commonly used in transesterification reactions are often expensive, toxic, and prone to migration from the resin matrix, potentially affecting the long-term stability and reprocessability of the material.

Zhang et al [73] introduced glycerol into an epoxy–anhydride curing system and found that the hydroxyl groups in glycerol first reacted with anhydride to generate carboxylic acids, which subsequently attacked epoxy groups to form β-hydroxy ester linkages. In this way, the system could be cured via thermal stimulation without catalysts. Currently, there are two main approaches for using free hydroxyl groups as multifunctional transesterification modifiers to prepare flame-retardant thermosetting resins. The first approach involves directly incorporating phosphorus-containing flame-retardant groups into curing agents or resin monomers to construct vitrimer networks. For example, Li et al [74] synthesized a DOPO-based anhydride as a co-curing agent for epoxy resin and used triethanolamine (TEOA) as a transesterification modifier to develop a reprocessable and degradable flame-retardant epoxy resin (**Figure 1-13(b)**). This resin demonstrated stable flame retardancy after reprocessing, and the resulting CFRPs could be repaired by hot pressing and allowed for non-destructive recovery of carbon fibers in ethanolamine solution. The second approach involves the design and synthesis of phosphorus-containing polyols, introducing free hydroxyl groups along with flame-retardant functionalities to achieve both flame retardancy and recyclability. For instance, Li et al [75] synthesized a phosphorus-containing diol with a tertiary amine structure, 2-(bis(2-hydroxyethyl)amino)ethyl diphenylphosphinate (DPEA), and applied it as a transesterification modifier in an epoxy–anhydride system to construct a dynamic ester-linked vitrimer network, which was further used as the matrix for CFRP (**Figure 1-13(c)**). The phosphinate groups in DPEA covalently bonded with the epoxy network, imparting inherent flame retardancy to both the vitrimer and the CFRP. Moreover, the tertiary amine and reactive primary hydroxyl groups in DPEA accelerated the transesterification reactions, enhancing

the reprocessability of the vitrimer and enabling the repair and recycling of CFRP. Nevertheless, challenges remain when using free hydroxyl groups as multifunctional transesterification modifiers. Their relatively low catalytic efficiency can limit the reprocessing performance of vitrimer systems. Additionally, while adjusting the number of free hydroxyl groups can help tailor cross-link density, this often leads to reduced network cross-linking, potentially compromising the overall mechanical properties of the resin [76].

Recently, Zhao et al [77] proposed the use of N-acylated phthalimide (NAPI), which can undergo direct catalyst-free ester exchange reactions at approximately 100 °C without relying on hydroxyl groups. This strategy enables the construction of CANs and overcomes common issues associated with traditional transesterification, such as catalyst toxicity, poor compatibility, and undesirable side reactions involving hydroxyl groups. However, the application of ester exchange reactions in the development of sustainable, flame-retardant thermosetting materials based on this new mechanism remains relatively limited and warrants further investigation.

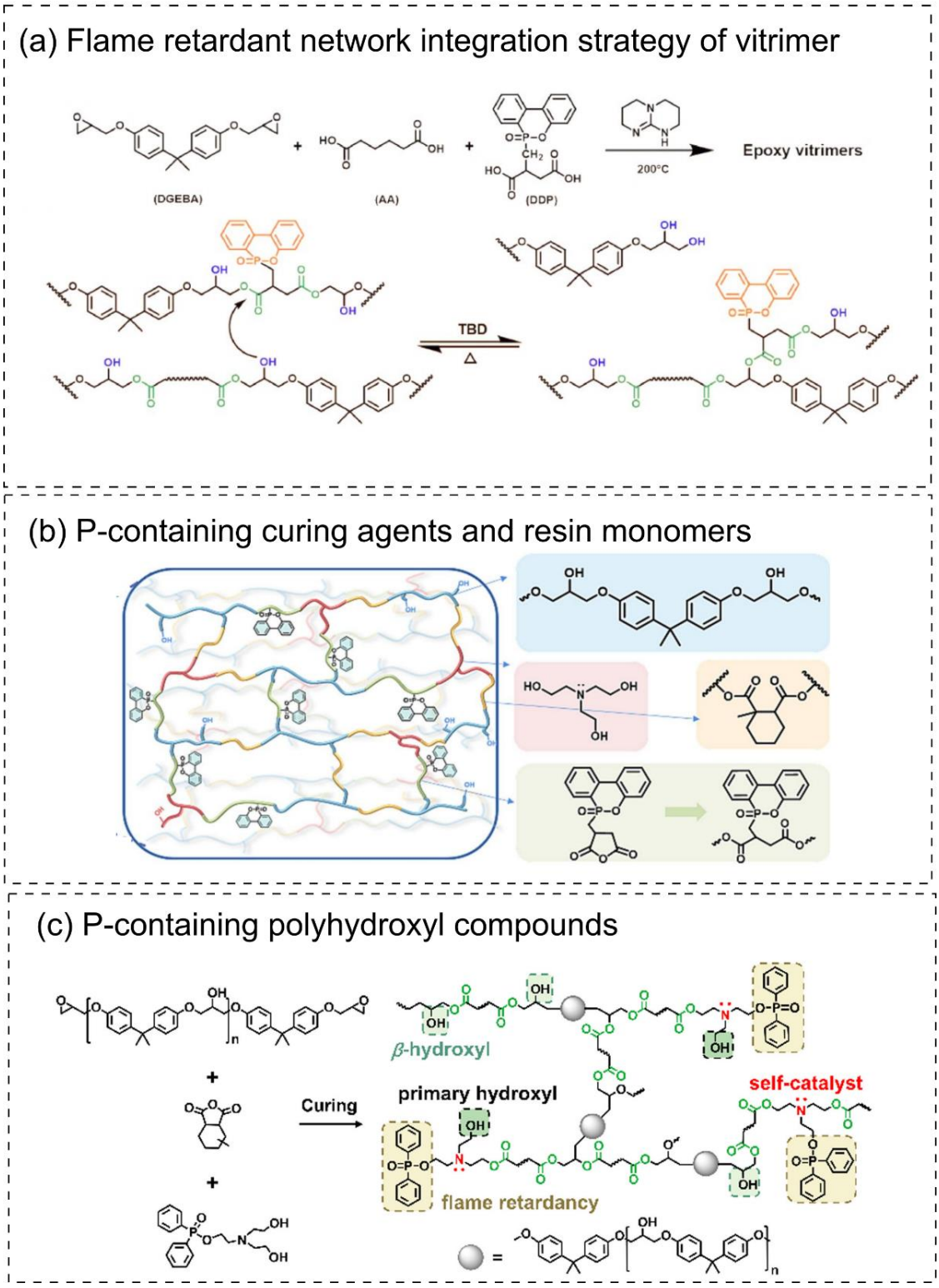

Figure 1-13 Designing strategies for flame retardant ester-based CANs [72]. (a) flame retardant network integration strategy of ester-based CANs;(b) P-containing curing agents and resin monomers [74]; (c) P-containing polyhydroxyl compounds [75].

1.4.2 Disulfide exchange approach

There are two main strategies for preparing flame-retardant disulfide-crosslinked epoxy resins. One approach is to introduce flame-retardant elements directly into the epoxy monomer, followed by curing with a disulfide-containing curing agent. For example, Wang et al [78] grafted DOPO onto the DGEBA molecular chain and subsequently cured it with 2- AFD, producing a flame-retardant disulfide-based epoxy vitrimer (**Figure 1-14 (a)**). This material could be rapidly reprocessed at elevated temperatures by hot pressing. The incorporation of phosphorus moieties and disulfide bonds into the network structure enabled a synergistic combination of flame retardancy, self-healing, and reprocessability.

The second strategy involves designing curing agents that incorporate both flame-retardant elements and disulfide bonds. Dai et al [79] synthesized a curing agent containing both disulfide linkages and phosphonate groups to prepare flame-retardant vitrimers (**Figure 1-14 (b)**). The resulting materials exhibited enhanced flame retardancy while maintaining excellent reprocessability and mechanical performance. In disulfide-containing vitrimer systems, in addition to the flame-retardant effect of phosphorus, the sulfur components can release SO_x gases and sulfur-rich radicals during combustion, which contribute to gas-phase flame inhibition. However, the emission of SO_x gases may introduce smoke toxicity, which limits the widespread application of such systems in CFRP.

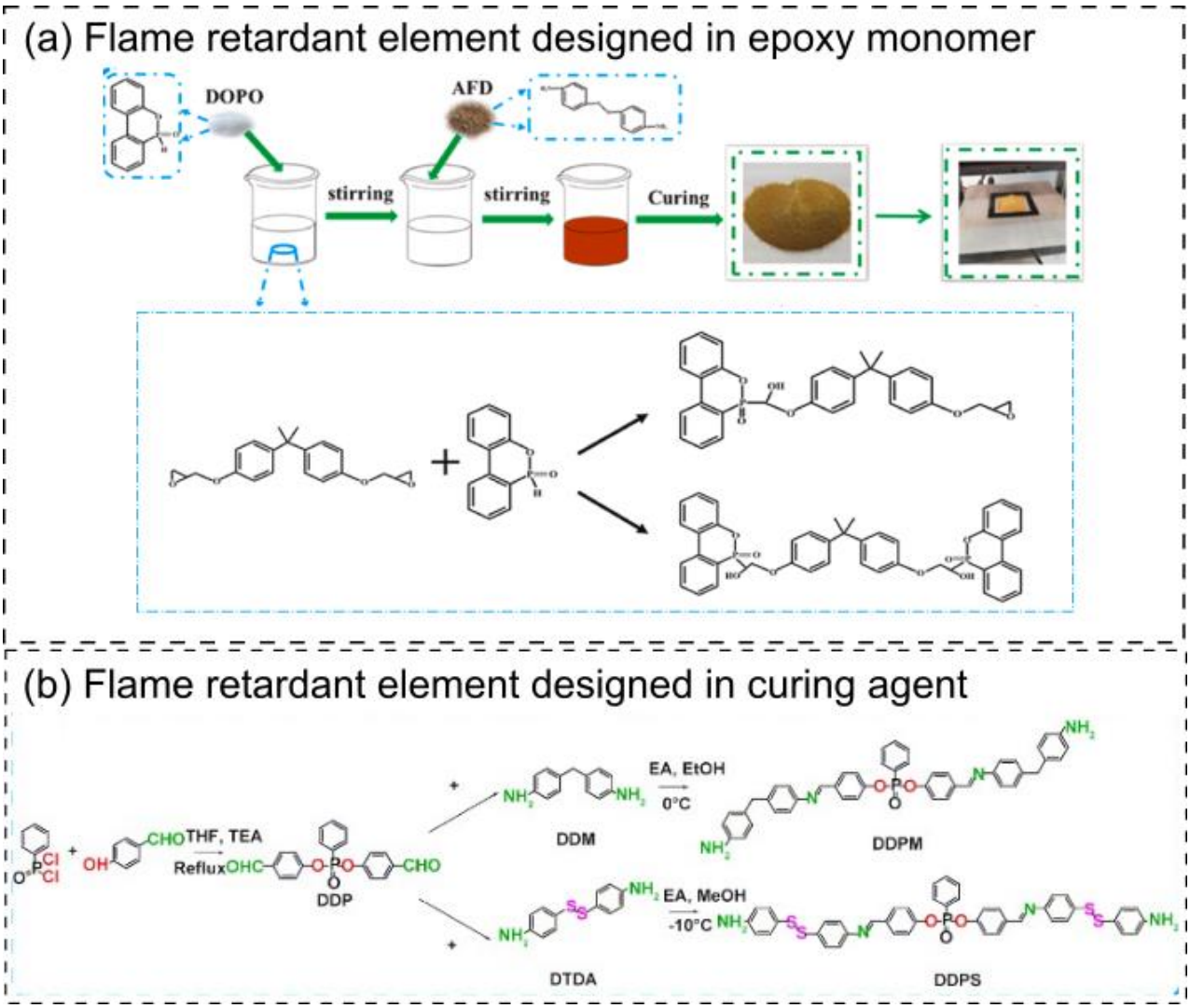

Figure 1-14 Designing strategies for flame retardant disulfide-based CANs. (a) Incorporating flame-retardant elements into epoxy monomers [78]; (b) Incorporating phosphate and disulfide bonds into the curing agent [79].

1.4.3 Imines exchange approach

Imine exchange is an important type of dynamic covalent reaction that has recently been introduced into epoxy vitrimer networks to impart excellent reprocessability, recyclability, and chemical degradability. Compared to transesterification, imine bonds can undergo rapid exchange under relatively mild conditions without the need for catalysts. Furthermore, imine bonds can be easily formed through condensation reactions between aldehydes and amines, offering flexibility in molecular design. Two main approaches have been developed for introducing imine bonds into

epoxy systems: the one-pot method, in which imine bonds are formed in situ during the curing process [80], and the more common approach of pre-synthesizing epoxy monomers or curing agents that already contain imine functionalities and blending them into the epoxy network [81].

Highly aromatic imine structures have been shown to promote char formation through crosslinking and rearrangement reactions at elevated temperatures, effectively blocking heat and mass transfer during combustion and enhancing flame retardancy [41] [82]. For instance, Weng et al [83] prepared an all-aromatic imine crosslinked epoxy vitrimer that exhibited good flame retardancy even at a high reprocessing temperature of 230 °C. However, excessive rigidity in such networks can hinder the dynamic exchange of imine bonds, highlighting the need to carefully balance the content of imine linkages or incorporate flexible epoxy resins or curing agents to optimize the dynamic behavior of imine-based CANs.

Inspired by flame retardancy strategies in ester-based vitrimers, researchers have also explored the incorporation of phosphorus-containing flame-retardant elements into imine-based systems [84]. Adding such structures can improve flame retardancy, but their steric hindrance and specific functional groups may also affect the curing behavior, processing performance, and mechanical properties of the resulting networks. For example, a phosphorus-nitrogen-imine-containing curing agent was synthesized to produce a flame-retardant epoxy vitrimer that could be reprocessed by hot pressing at 100 °C for 3 min [85]. However, excessive imine content led to relatively flexible molecular chains, resulting in inferior mechanical properties and weatherability. Similarly, Duan et al [86] developed an epoxy monomer containing both imine bonds and DOPO groups, which exhibited significant steric hindrance effects. Thus, when incorporating phosphorus structures into imine-based CANs, it is essential to balance the impact of these structures on dynamic exchange behavior, processability, and mechanical performance.

In the context of CFRP, the introduction of imine bonds to enable chemical degradation of the matrix and simultaneous recovery of both thermoset resin and carbon fibers has attracted significant interest. For example, Taynton et al [87] developed degradable polyimine composites based on imine condensation between dialdehydes, diamines, and triamines. Their results showed that an excess of diamine facilitated matrix degradation into soluble oligomers and allowed recovery of carbon fibers. Liu et al [42] synthesized a degradable epoxy resin from vanillin, methylcyclohexanediamine, and epoxy resin, which, when combined with carbon fibers, produced

CFRP that could be degraded in ethylenediamine solution, enabling the recovery of both resin fragments and fibers.

However, the development of flame-retardant imine-based vitrimer CFRP that simultaneously achieve high mechanical performance, flame retardancy, and recyclability remains largely unexplored but highly promising [88, 89]. Most current studies have not yet integrated flame retardancy with the dynamic and degradable nature of imine-based vitrimer CFRP. Additionally, comprehensive studies on system design, processing optimization, and long-term performance under service conditions are still lacking.

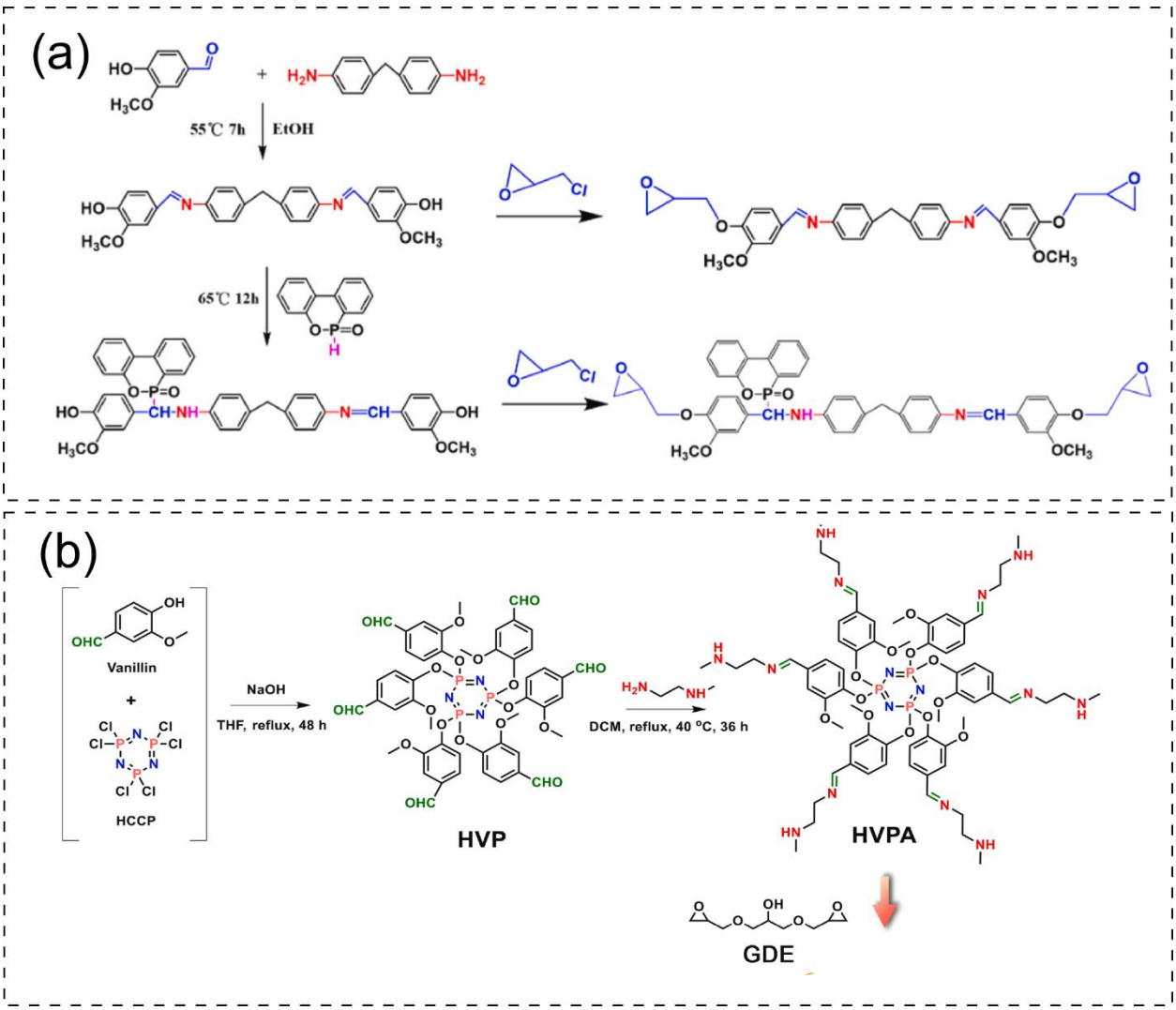

Figure 1-15 Designing strategies for flame retardant imine-based CANs. (a) Incorporating flame-retardant elements into epoxy monomers [82];(b) Incorporating flame-retardant elements and imine bonds into the curing agent [85]

CHAPTER 2
Objectives of This Study

Imine-based vitrimer systems demonstrate notable advantages, including catalyst-free, green processing, tunable network architectures, and the ability of aromatic imine structures to promote char formation for enhanced flame retardancy. However, current research on imine-based flame-retardant vitrimer systems remains scarce, with most studies focusing on the intrinsic resin properties. There is still a lack of systematic research addressing their application in continuous fiber-reinforced composites. This dissertation follows the research theme of "structure design–property optimization–practical application", aiming to develop recyclable, flame-retardant, bio-based epoxy vitrimer systems and to promote their sustainable manufacturing and engineering applications in continuous fiber-reinforced composites. The specific objectives are as follows:

(i) Based on the design of dynamic covalent networks, to develop bio-based epoxy vitrimer resin systems incorporating imine bonds and phosphorus-containing structures, thereby achieving integrated flame retardancy, thermal reprocessability, and recyclability.

(ii) Based on network structure optimization, to explore optimal stoichiometric ratios between epoxy monomers and curing agents, and to implement co-polymerization strategies of flexible and rigid epoxy monomers for solvent-free melt processing, overcoming the limitations of solvent-based fabrication.

(iii) Based on engineering-scale process development, to design and construct a semi-automated hot-melt prepregging system, optimize vitrimer resin rheology and gel time, and fabricate continuous fiber-reinforced vitrimer composites with superior flame retardancy and mechanical performance.

(iv) Based on structure–property–process relationships, to systematically investigate the influence of vitrimer network structure on composite properties, and to promote sustainable recycling and green applications of next-generation high-performance thermosetting composites.

CHAPTER 3

Materials and Experimental Techniques

3.1 Materials

Epoxy resin (Glycerol triglycidyl ether, Gte, epoxy equivalent weight: 149 g/mol) was provided by Carbosynth Ltd. Tris(4-hydroxyphenyl) methane triglycidyl ether (Tmte) was supplied by biosynth international, Inc. Vanillin, 4-Aminophenol, 1,2-Dimethylimidazole (DMeIm), ethanol, Ethylene Diamine (EDA), Tetrahydrofuran (THF), HCl (1 M), NaOH (1 M), acetone (Ace), dichloromethane (DCM), and N, N-Dimethylformamide (DMF, ACS reagent, ⩾99.8 %), triethylamine, ethyl acetate, phosphorus oxychloride were all provided by Sigma-Aldrich Chemical Co. 9,10-Dihydro-9-oxa-10-phosphaphenanthrene 10-oxide (DOPO, 97%) was provided by TCI EUROPE N.V. Carbon fabrics were provided by R&G Faserverbundwerkstoffe GmbH Composite Technology. The plain weaving carbon fabric (0/90°) had an area weight of 200±5 g/m^2. Deionized water was obtained from the laboratory's filtration system.

3.2 Characterization techniques

3.2.1 Fourier transformation infrared spectroscopy (FTIR)

The FTIR spectrums of Gte, self-made curing agent and epoxy vitrimer were conducted on the FTIR (Nicolet 5700) with the wave number ranging from 4000 to 400 cm^{-1} after 32 scans with a resolution of 4 cm^{-1}.

3.2.2 Nuclear magnetic resonance (NMR)

The ^{1}H NMR, ^{13}C NMR, ^{31}P NMR spectrums of various samples were recorded on the NMR spectrometer (Bruker Avance III HD-WB-400 MHz) at room temperature, using dimethyl sulfoxide (DMSO) as the solvent and tetramethylsilane (TMS) as the internal standard.

3.2.3 Thermogravimetric analyser (TGA)

The thermal decomposition behaviour of epoxy vitrimers were studied by TGA (TA Q50) in nitrogen atmosphere with a heating rate at 10 °C/min. The sample gas purge flow rate was set as 90 mL/min. The weight of the samples around 6 ± 0.5 mg was used for the test at the temperature range between room temperature up to 700 °C.

3.2.4 Differential scanning calorimetry (DSC)

The curing behaviour of epoxy vitrimer were conducted by DSC analyzer (TA Q200). Samples weighing around 5± 0.5 mg were heated from 30 to 200 °C at a rate of 10 °C/min under a nitrogen flow, following ISO 11357.

3.2.5 Dynamic mechanical analysis (DMA)

Dynamic mechanical analysis (DMA) experiments were performed using a TA Instruments DMA Q800. Tensile deformation was applied to sample plaques with dimensions of 8.0 mm × 35.0 mm × 1.0 mm. Measurements were taken from -50 °C to 150 °C at a heating rate of 3 °C/min and an oscillation frequency of 1 Hz. The cross-linking density of the epoxy vitrimers was calculated using the following eq 1:

$$V_e = \frac{Er'}{3\mathrm{RT}} \tag{1}$$

Where V_e is the cross-linking density (mol/cm^3), R is 8.314 (cm^3·MPa/mol·K), T is T_g + 50 in the rubbery state (°C), and Er' is the storage modulus in the rubbery state (MPa).

Stress relaxation tests were conducted on a Q800 DMA device using samples with dimensions of 18.0 mm × 6.0 mm × 1.0 mm. Each sample was subjected to a constant strain of 1%, and the modulus of the samples was monitored over time until it reached a steady value.

The activation energy (E_a) for stress relaxation of sample was determined using the Arrhenius equation:

$$\tau^*(\mathrm{T}) = \tau_0 \exp\left(\frac{E_a}{\mathrm{RT}}\right) \tag{2}$$

where T represents the test temperature, τ_0 denotes the characteristic relaxation time at infinite temperature, and R is the universal gas constant.

3.2.6 Tensile test

The mechanical properties of the epoxy vitrimer were conducted using an Instron 5966 universal testing machine, following the ASTM D638-14 standard. Dog-bone-shaped specimens (30.0 mm × 3.0 mm × 4.0 mm) were prepared using previously described molding methods. The tensile tests were performed at a crosshead speed of 10 mm/min, with at least five specimens tested to determine the average mechanical properties.

The tensile test of CF monofilaments was performed using a Textechno textile testing machine. Carbon fiber monofilaments were randomly selected, and the test speed was set to 1 mm/min.

The mechanical properties of GTV-4-CF were evaluated using a CMT4204 universal testing machine (MTS Systems) following the ASTM D882 standard. The sample dimensions were 100.0 mm × 10.0 mm × 2.0 mm.

The flexural properties of the fiber-reinforced composites were evaluated by three-point bending tests. The specimen dimensions were 70 mm × 12 mm, with a span length of 64 mm, maintaining a span-to-thickness ratio of 32:1 in accordance with ASTM D7264. A universal testing machine with a maximum load capacity of 100 kN was used to record the load–displacement curves. For each test series, at least three specimens were tested at a crosshead speed of 1.0 mm/min to ensure the reproducibility and consistency of the results.

Calculation of the flexural strength (σf) for rectangular cross section is as eq 3:

$$\sigma f = \frac{1.5FL}{bd^2} \tag{3}$$

Where σf is the flexural strength (MPa), F is the load at a given point on the load–deflection curve (N), L is the support span (mm), b is the width of the test beam (mm), and d is the depth of the tested beam (mm).

3.2.7 Scanning electron microscopy (SEM)

The SEM images were obtained using an EVO MA15 analyzer at an accelerating voltage of 10 kV to examine the morphology of the tensile section of the vitrimer, as well as the original and recycled carbon fibers (CFs), all of which were coated with a thin gold layer to enhance imaging quality.

3.2.8 Raman

Raman spectra of original and recycled CFs were measured using a DXR2xi Raman imaging microscope (Thermo Fisher Scientific) with a 532 nm laser, an exposure time of 60 s, and a laser power of 12 mW.

3.2.9 Shape fixity (SF)

The shape fixity (SF) ratio was studied using image analysis with ImageJ software (v1.53). A 50 × 12 mm² specimen was first heated to 130 °C for 10 min to ensure it reached a rubbery state. The specimen was then bent and placed into a mold. After cooling to room temperature, the temporary

shape was obtained by removing the specimen from the mold. The permanent shape was recovered by heating the specimen above its T_g. The shape recovery stage was carried out at 130 °C for 10 min to compare the shape recovery performance of GTV-4.

The SF was calculated using the following eq 4:

$$SF\ (\%) = \left(1 - \frac{\theta_S - \theta_F}{\theta_S}\right) \times 100 \quad (4)$$

Where θ_s represents the angle of the mold, and θ_F is the angle of the fixed shape after removal from the mold.

3.2.10 Self-healing

The self-healing capabilities of epoxy vitrimer were evaluated by heating the samples at 140 °C. Cracks were introduced using a blade with a 45° cutting edge at the center of the sample. The topology of the induced cracks was then characterized using optical profilometry with a ZETA Z-20 optical profilometer (Zeta Inc.). After initial characterization, the samples were thermally activated via convective heating in a conventional oven to trigger the healing mechanism. The repaired cracks were subsequently analyzed by optical profilometry. Surface topology, both before and after healing, was examined using profilometer images processed with MountainsMap analysis software.

3.2.11 Limiting oxygen index (LOI)

LOI values were measured by using FTT (Fire Testing Technology). LOI instrument with sheet dimensions of 130.0 mm × 6.5 mm × 3.2 mm according to ASTM D2863.

3.2.12 Vertical burning test (UL-94)

The UL-94 was measured by an FTT UL-94 flame chamber according to ASTM D3801. The dimensions of the specimen were 125.0 mm × 12.7 mm × 3.2 mm. Every sample was tested five times until the results were stable.

3.2.13 Cone calorimeter test (CCT)

The CCT was performed according to ISO 5660-1 by the FTT cone calorimeter. Specimens with the size of 100.0 mm × 100.0 mm × 4.0 mm were tested in the heat flux of 50 kW/m^2 with 25.0 mm in horizontal mode.

3.2.14 Thermogravimetric infrared spectroscopy (TG-IR)

The TG-IR spectrums were carried out on a Nicolet 5700 spectrometer. The samples were tested under an air atmosphere at a heating rate of 10 °C/min from 50 °C to 700 °C.

3.2.15 Gel fraction and swelling experiments

The gel fraction was measured by using the immersion method. The samples (W_0) were sequentially immersed in DMF at room temperature for 24 h. Subsequently, the samples were dried in vaccum at 80 °C for 24 h and then weighed again (W_1). The gel fraction was determined by eq 5:

$$GF = \frac{W_1}{W_0} \times 100\% \quad (5)$$

The swelling ratios were measured by immersing the samples (W_0) sequentially into H_2O,1wt% HCl, 1 wt% NaOH, acetone, and DMF at room temperature for 24 h. Afterward, the samples were taken out from the solutions. Excess solvent on the surface was removed using filter paper, and the swollen samples were weighed (W_2). The swelling ratio was determined by eq 6.

$$SR = \frac{W_2 - W_0}{W_0} \times 100\% \quad (6)$$

3.2.16 Gel time

The gel time was determined using the wire-drawing method.

CHAPTER 4

Bio-based Flame-retardant Epoxy Vitrimer: Flame Retardancy and Recyclability

4.1 Introduction

CFRP has been widely used in high-performance structural applications such as aerospace, high-speed rail, and automotive industries due to their excellent specific strength, specific modulus, dimensional stability, and corrosion resistance [65]. However, the thermosetting matrix commonly used in CFRP is inherently non-recyclable, and its flammability significantly limits its application in safety-critical environments. Consequently, achieving a balance between flame retardancy and recyclability has become a key challenge in the development of next-generation composite materials [90, 91].

Vitrimers have attracted considerable attention for their ability to combine the structural integrity of thermosets with the reprocessability of thermoplastics, providing an effective pathway to overcome the recyclability limitations of traditional thermosetting polymers [92]. As discussed in Chapter 1, various DCNs, such as transesterification, disulfide exchange, and imine exchange, have been successfully introduced into epoxy systems, enabling properties such as reshaping, welding, and closed-loop recycling. However, compared to extensive research on mechanical and dynamic properties, the flame-retardant performance of vitrimer materials remains relatively underexplored, particularly for imine-based vitrimers, whose intrinsic char-forming ability alone is often insufficient to meet stringent flame-retardant standards. Therefore, the development of imine-based vitrimers that exhibit both high flame retardancy and dynamic network behavior is of great significance for expanding their use in high-performance thermosetting systems.

In recent years, DOPO and its derivatives as organophosphorus flame retardants, have attracted widespread attention from academia to industry because of its good chemical reactivity and excellent effectiveness as flame retardant [86]. Incorporating DOPO or its derivatives into EP, whether through chemical reactions or physical blending, endows the resulting materials with long-lasting flame retardancy and environment toletance [93]. Tang et al [94] synthesized an aromatic imine-containing DOPO-based reactive flame retardant (DOPO-AI) for the preparation of an EP, featuring enhanced flame-retardant and mechanical properties. When the mass of DOPO-

AI was 20% of Diglycidyl ether bisphenol F epoxy resin (DGEBF), the flame-retardant epoxy vitrimer EP/20DOPO-AI passed the V-0 rating in the UL-94 test with the limiting oxygen index (LOI) of 35.4%. In the cone calorimetry test, the peak heat release rate (pHRR) and total heat release (THR) of EP/20DOPO-AI decreased by 26% and 27%, compared to pristine EP. The mechanism analysis showed that during the combustion, the free radicals generated by the decomposition of the DOPO structure in DOPO-AI trapped H· and OH· radicals to interrupt the free radical chain reaction in the gas phase. In the condensed phase, the phosphorus and aromatic imine in DOPO-AI promoted the matrix to form a dense char laver that prevented the exchange of oxygen and heat as compared to pristine EP, EP/20DOPO-AI exhibited enhanced tensile strength and storage modulus, which were attributed to the high rigidity of DOPO and aromatic imine. In another example, Yang et al [82] designed two vanillin-based epoxy monomers with excellent flame retardancy and good reprocessability. The first epoxy monomer VAD-EP contained two Schiff base bonds obtained by vanillin and 4,4′-Diaminodiphenylmethane (DDM), while the other epoxy monomer VDP-EP featured a Schiff base bond formed through an addition reaction between the P-H bond of DOPO and the Schiff-based bond. The epoxy materials were then cured by a D230 diamine hardener by adjusting the proportion of VAD-EP and VDP-EP monomers. When the mass ratio was 8:2, A8P2-D230 achieved the fire retarding UL-94 V0 rating and a LOI value of 27.0% with only 0.66% phosphorus content. This behavior was ascribed to free radical scavenging and condensed phase mechanisms. Additionally, the material showed a high-stress relaxation rate, excellent self-healing capability, reprocessability, and degradation behaviors, due to the presence of dynamic imine bonds in the topological crosslinking network. This approach simultaneously addressed the recycling concerns and achieved satisfactory flame retardancy for EPs.

Most reported networks still rely on fossil-derived epoxy monomers, such as DGEBA. Due to the endocrine-disrupting and reproductive toxicity concerns associated with BPA, its use is increasingly restricted, particularly in the European Union. This has driven growing interest in the development of green, safe, and sustainable bio-based epoxy systems [95, 96]. Among these, Gte has emerged as a promising candidate due to its commercial availability, BPA-free nature, structural stability, high reactivity, and excellent processability—making it an ideal substitute for traditional petroleum-based epoxies. Nevertheless, research on flame-retardant vitrimer systems derived from Gte remains scarce, and the development of high-performance, fully bio-based vitrimer materials still faces challenges related to efficiency, cost, and industrial feasibility.

In this chapter, we reported a facile strategy to prepare high-performance bio-epoxy vitrimers (Gte-VA-DOPO, GVD), which exhibited high flame retardancy, reprocessability, recyclability, and excellent mechanical properties. A commercial biomass-derived epoxy monomer, Gte, was subsequently cured with a vanillin-based hardener (VA) and DOPO to prepare epoxy vitrimers with high performance and versatility. First, their chemical structure was determined. Then, we systematically investigated the thermal and mechanical behavior, the intrinsic flame retardancy, the reprocessability, and the recyclability of the bio-epoxy vitrimers.

4.2 Synthesis of vanillin-based hardner and epoxy vitrimer

4.2.1 Synthesis of vanillin-based hardner

The vanillin-based hardener (VA) was prepared according to the procedure reported elsewhere [51]. Vanillin (240 mmol, 18.24 g) and 4-aminophenol (570 mmol, 13.08 g) were dissolved in 510 mL water and 210 mL ethanol, respectively, and then mixed in a 1000 mL flask. The reaction was then performed by stirring a magnetic stirring bar at 50 °C for 2 h. VA, yellow powder with a yield of 80%, was obtained by vacuum filtration, washed three times with water, and dried at 80 °C.

4.2.2 Preparation of epoxy vitrimers

DOPO was first mixed with Gte while heating at 100 °C with mechanical stirring for 5 min to get a transparent liquid. The temperature increased to 140 °C, and the vanillin-based VA and catalyst DMeIm were added to the former mixture under mechanical agitation for 4 min to obtain a homogenous liquid mixture. Finally, the mixture was transferred rapidly to a mold, and cured at 140 °C for 30 min. The cured epoxy vitrimers containing 1, 3, 5, 7 wt% DOPO are denoted as GVD1, GVD3, GVD5, and GVD7, respectively. A pristine epoxy vitrimer (GV) without DOPO was prepared using the same procedure. **Table 4-1** summarizes the specific formulation details, while the synthesis route is depicted in **Scheme 4-1**.

Table 4-1 Composition of epoxy vitrimer

Sample	Gte (g)	DOPO (g)	VA (g)	Catalyst (g)
Neat GV	54.6	0	44.4	1
GVD1	54.1	1	43.9	1
GVD3	53.0	3	43.0	1
GVD5	51.9	5	42.1	1
GVD7	50.8	7	41.2	1

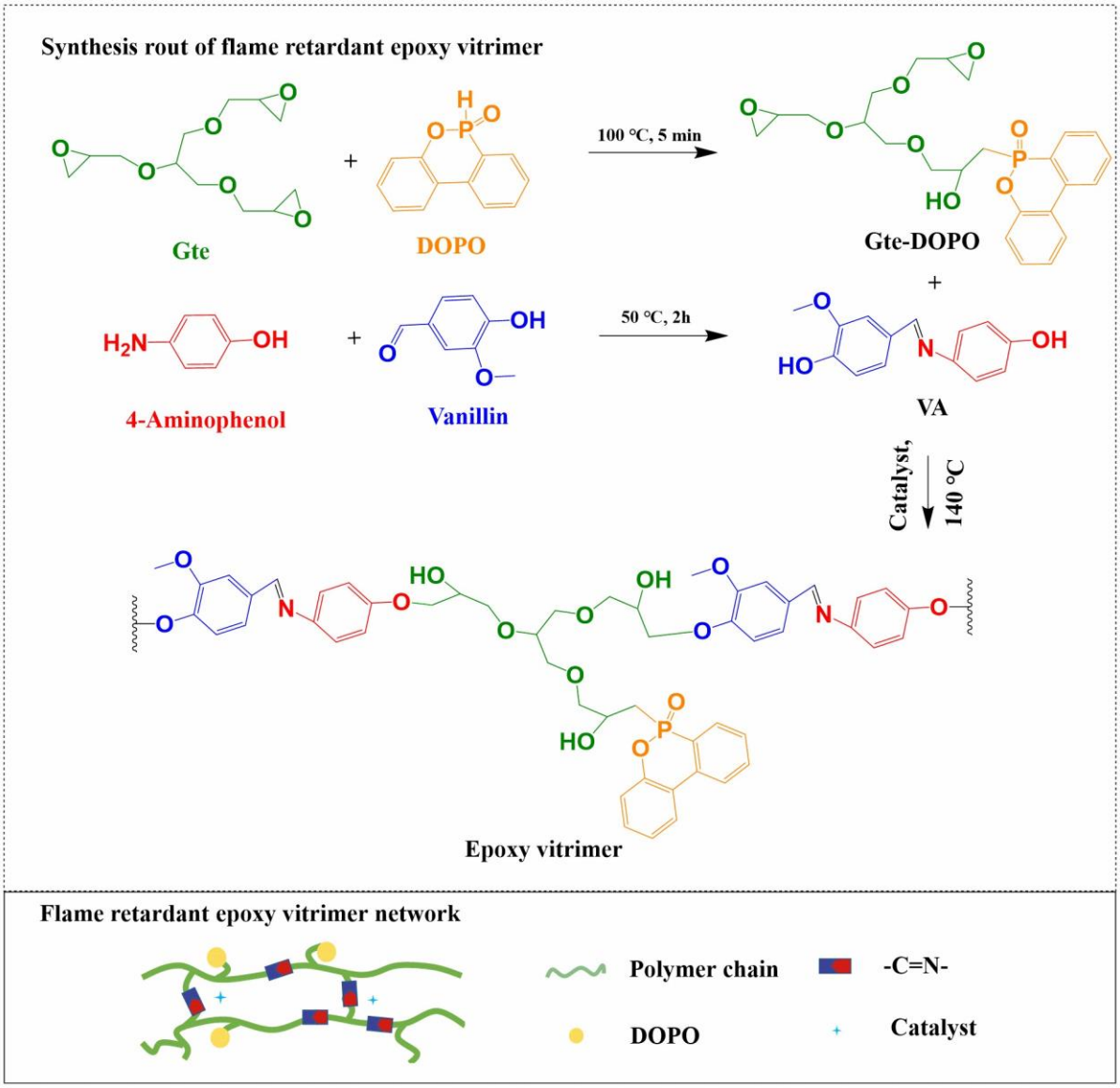

Scheme 4-1 Synthetic pathway and molecular structure of the flame-retardant epoxy vitrimer network.

4.3 Characteristics of VA and properties of epoxy vitrimers

4.3.1 Characteristics of VA

Figure 4-1 (a) shows the ^{1}H NMR spectrum of the VA with chemical shifts at δ=8.34 (s, 1H, a (-CH=N-)), 7.49 (d, 1H, b (Ar-H)), 7.27 (dd, 1H, c (Ar-H)), 7.13-7.12 (m, 2H, d (Ar-H)), 6.88 (d, 1H, e (Ar-H)), 6.79-6.77 (m, 2H, f (Ar-H)), 3.84 (s, 3H, g (-OCH_3)) ppm, indicating seven distinct hydrogen environments. The characteristic absorption band of amino group (3340 cm^{-1}) of 4-aminophenol and aldehyde group (1697 cm^{-1}) of vanillin were not observed in the FT-IR spectrum of VA (**Figure 4-1 (b)**) while a new absorption belonging to imine was observed at 1620 cm^{-1}. The ^{1}H NMR and FTIR results confirmed the successful synthesis of VA.

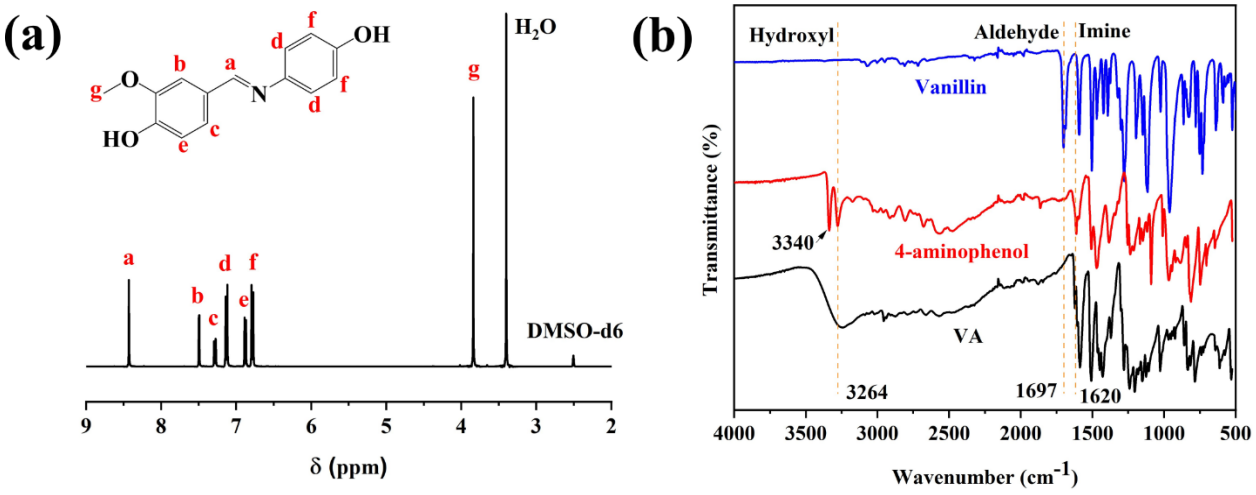

Figure 4-1 (a) ^{1}H NMR spectrum of VA; (b) FTIR spectra of vanillin, 4-aminophenol, and VA.

4.3.2 FTIR and DSC of GVD epoxy vitrimers

Figure 4-2(a) presents the FTIR spectra of GV and GVD5. In both epoxy networks, no characteristic absorptions were observed at 910 cm^{-1} (epoxide C–O stretching vibration) or 847 cm^{-1} (epoxide C–O–C deformation vibration), indicating that the epoxy groups were almost completely consumed during the curing process. Additionally, a broad absorption band appeared at 3450 cm^{-1}, corresponding to hydroxyl groups generated by the ring-opening of the epoxy groups in Gte. A distinct absorption at 1620 cm^{-1}, attributed to imine (C=N) groups, was observed in both GV and GVD5 spectra, confirming the existence of imine bonds. The FTIR spectrum of DOPO exhibited characteristic peaks at 2430 cm^{-1} (P–H stretching vibration), 1592 cm^{-1} (P–C), 1236

cm^{-1} (P=O), and 925 cm^{-1} (P–O). However, these characteristic absorptions were not detected in the GVD5 spectrum, likely due to the low DOPO content. To further verify the reaction between DOPO and epoxy groups, 30 g of DOPO was reacted with 38.6 g of Gte at 100 °C for 5 min, yielding a transparent liquid denoted as Gte-30DOPO. In the FTIR spectrum of Gte-30DOPO, the absorption corresponding to the P–H bond at 2430 cm^{-1} disappeared, while the peaks at 1592 cm^{-1}, 1236 cm^{-1}, and 925 cm^{-1} were enhanced, confirming a pre-reaction between the epoxy groups and P–H bonds of DOPO.

Furthermore, the reaction behavior between Gte and DOPO was investigated by DSC. As shown in **Figure 4-2(b)**, the DSC curve of GV exhibited a broad exothermic peak over a wide temperature range, corresponding to the curing process of the epoxy network. DOPO displayed a sharp endothermic peak at approximately 118 °C, associated with its melting transition. In contrast, the GVD5 sample showed two characteristic thermal events around 115 °C: an exothermic curing peak and a mild endothermic peak. These results further confirmed that a reaction occurred between the epoxy groups and P–H bonds, indicating successful grafting of DOPO onto the epoxy molecular chains.

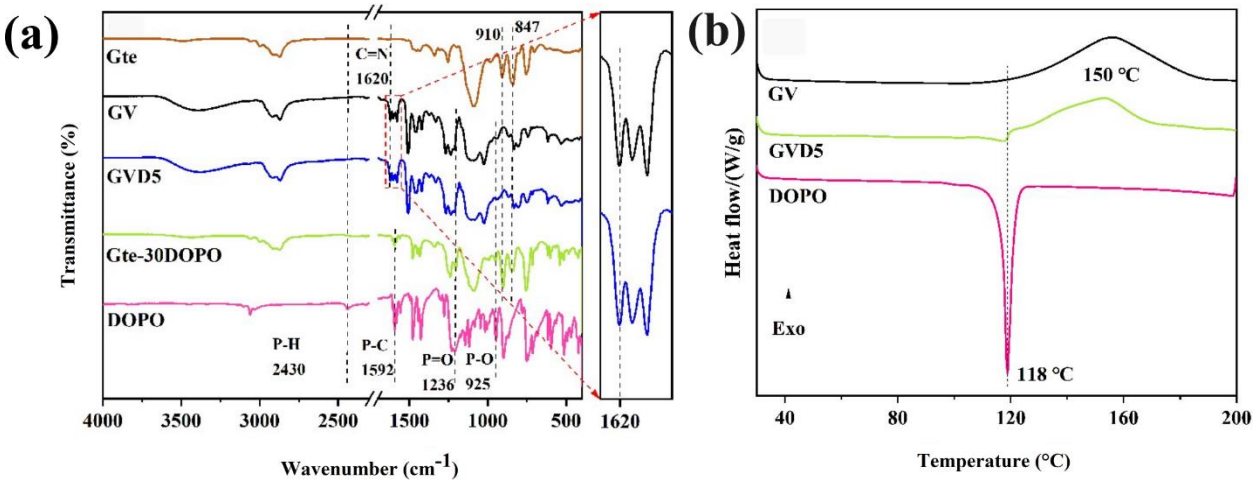

Figure 4-2 (a) FTIR spectra of Gte, GV, GVD5, Gte-30DOPO, and DOPO; (b) DSC curves of GV, GVD5, and DOPO.

4.3.3 Thermal degradation behavior of GVD epoxy vitrimers

The thermal degradation behaviors of epoxy vitrimers were investigated using TGA in the N_2 atmosphere. The TGA and DTG curves were displayed in **Figure 4-3(a) and (b)**, respectively, and

the key parameters including 5 wt% degradation temperature ($T_{5\%}$), maximum degradation temperature (T_{max}), and residual weight at 690 °C ($R_{690°C}$) were listed in **Table 4-2**. Under N_2 conditions, all epoxy vitrimers exhibited a two-step degradation. The first DTG peaks at about 200-305 °C suggested that part of the C=N double bonds were broken into more stable C-N single bonds, which could be further recombined into amine nitrogen rings [85]. The degradation of other stable bonds resulted in the second DTG peak. The $T_{5\%}$ values for GV, GVD1, GVD3, GVD5, and GVD7 indicate that the thermal stability of GVD vitrimers was approximately equivalent to that of GV vitrimer. The $R_{690°C}$ of GVD epoxy vitrimers was higher than GV. The improved charring capability of GVD epoxy vitrimers could be attributed to two key aspects. Firstly, the epoxy vitrimers containing imine bonds in their main chain were converted to nitrogen-containing six-membered heterocyclic compounds at high temperatures, thereby enabling heat-induced self-crosslinking of the polymer chains and improved carbonization [97]. Secondly, the presence of phosphaphenanthrene moieties led to the aggregation and amplification of the carbonization effect [98]. Furthermore, it is worth noting that GVD7 exhibited the highest residual char content (36.1 %) at 690 °C, as it had the highest phosphorus content.

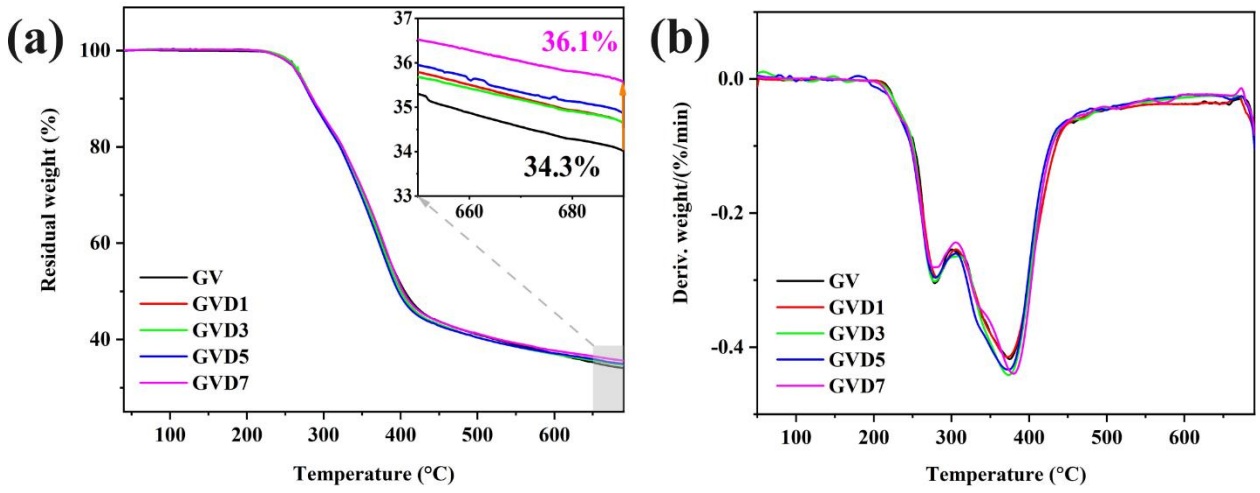

Figure 4-3 (a) TGA and (b) DTG curves of GV, GVD1, GVD3, GVD5 and GVD7 in N_2 atmosphere.

Table 4-2 Key parameters of GV and GVD epoxy vitrimers in TGA and DTG analysis.

Sample	$T_{5\%}$[a] (°C)	T_{max1}[b] (°C)	T_{max2}[c] (°C)	$R_{690°C}$[d] (%)
GV	269	278	375	34.3
GVD1	269	281	372	35.2
GVD3	268	278	373	35.2
GVD5	266	279	373	35.4
GVD7	268	279	380	36.1

a: Temperature at 5% weight loss; b: Temperature at first maximum weight loss rate; c: Temperature at second maximum weight loss rate; d: Residue at 690 °C.

4.3.4 UL-94 and LOI of GVD epoxy vitrimers

The flame-retardant properties of epoxy vitrimers were evaluated via LOI and UL-94 vertical burning tests. The results are presented in **Table 4-3**. The GV sample rapidly ignited and was unable to self-extinguish under the UL-94 test. Consequently, it did not achieve any rating according to the UL-94 standard, and the LOI value was only 28.7%. However, the incorporation of flame retardant DOPO into the system substantially improved the LOI values and UL-94 level of GVD epoxy vitrimers. When the DOPO content was more than 5 wt.%, the epoxy vitrimer was able to self-extinguish within 4 s following a 10 s ignition period. The GVD5 displayed a UL-94 V-0 rating without any dripping and exhibited a LOI of 31%. Therefore, it can be dictated that the addition of DOPO exhibited a clear positive impact on improving the flame retardancy of the epoxy vitrimer.

Table 4-3 LOI and UL94 results obtained for the epoxy vitrimers.

Sample	LOI (%)	Vertical burning test after ignitions		Dripping	UL94 Rating
		av-t_1 (s)	av-t_2 (s)		
GV	28.7	60.0	/	Yes	NR
GVD1	28.9	60.0	/	No	NR
GVD3	29.1	8.4	1.3	No	V-1
GVD5	31.0	2.2	0.9	No	V-0
GVD7	31.5	2.3	0.0	No	V-0

4.3.5 Combustion behavior of GVD epoxy vitrimers

The CCT was used for further analyzing the flame-retardant performance. The curves and data obtained from the CCT for the epoxy vitrimers are illustrated in **Figure 4-4** and **Table 4-4**, respectively. The addition of DOPO exhibited almost no effect in the time to ignition (TTI) for epoxy vitrimers. However, the increasing content of DOPO yielded a gradual decrease in the heat release rate (HRR) and total heat release (THR).

The pHRR and THR of GV were 888 kW/m^2 and 74.1 MJ/m^2, respectively, whereas GDV5 demonstrated a sharp reduction to 549 kW/m^2 and 53.6 MJ/m^2, registering a decrease of 38.2% and 26.3% in comparison to GV. This decrease in pHRR and THR corroborated the superior flame retardancy, found in the results of LOI and UL-94. The presence of DOPO was key to such improvement, as the decomposition of phosphorous substances in the early combustion stage promoted the formation of a dense carbon layer, insulating the internal epoxy matrix from external oxygen and heat. Furthermore, the PO·, PO_2·, and phenoxy radicals generated during combustion effectively quenched combustion reactions involving H· and OH· [78]. Along with pHRR and THR, the other two important parameters for assessing fire safety performance are the fire performance index (FPI) and fire growth rate (FGR). In general, a high-performance flame-retardant material features a high FPI value and a low FGR value [99]. As shown in **Table 4-4**. The GVD7 displayed the highest FPI of 0.053 m^{2}s/kW and the lowest FGR of 4.1 kW/m^2/s, further demonstrating the best flame retardancy among the samples investigated here. Average effective heat combustion (EHC) values of GVD epoxy vitrimers also decreased with increasing DOPO content, implying the gas-phase quenching capability of DOPO [100].

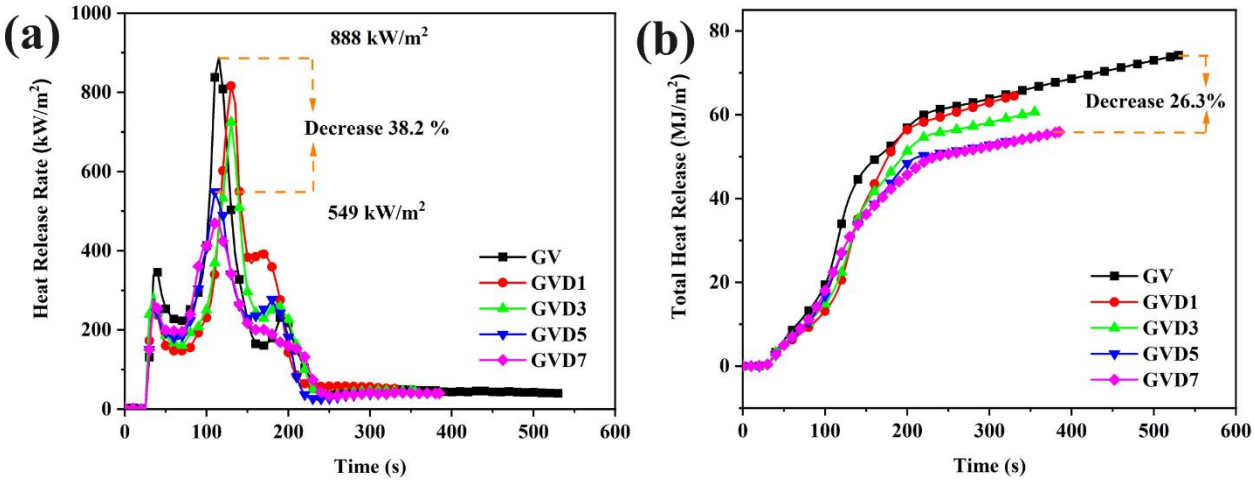

Figure 4-4 (a) HRR and (b) THR curves of GV, GVD1, GVD3, GVD5 and GVD7.

Table 4-4 Data of epoxy vitrimers in CCT.

Sample	TTI (s)	pHRR (kW/m²)	THR (MJ/m²)	T_{pHRR} (s)	FPI[a] (m²s/kW)	FGR[b] (kW/m²/s)	EHC/ (MJ/kg)	Residue at 300 s (%)
GV	26	888	74.1	115	0.028	7.7	17.10	28.6
GVD1	27	816	64.5	130	0.030	6.3	15.63	29.7
GVD3	27	725	60.6	130	0.034	5.6	11.13	30.7
GVD5	26	549	53.6	110	0.045	5.0	13.87	31.4
GVD7	26	473	55.9	115	0.053	4.1	13.26	32.1

a: fire performance index, FPI=TTI/pHRR (TTI: time to ignition); b: fire growth rate, FGR=pHRR/T_{pHRR} (T_{pHRR}: time to pHRR).

The residue at the testing time of 300 s of epoxy vitrimers increased from 28.6 wt% for GV to 31.4 wt% for GVD5, suggesting partial flame-retardant activity in the condensed phase. Furthermore, inspection through digital photography and SEM images revealed that the burning residue of GVD epoxy vitrimers was much denser than that of GV (**Figure 4-5**). The chemical

component of the char residues was further studied by EDS, as shown in **Figure 4-5(f)** and **Table 4-5**. As for GV, the contents of C, O, and N elements were 87.4, 10.3, and 2.3 wt%, respectively. In contrast, besides C, O, and N elements, the char residues of GVD1, GVD3, GVD5, and GVD7 contained P elements which were 0.7, 1.1, 1.7, and 1.9 wt%, respectively. For GVD1, GVD3, GVD5, and GVD7, the presence of P element in the char residues indicated that phosphoric compounds were produced to encourage the establishment of the thermally stable char layer and subsequently increase the char yield, further demonstrating improved flame retardancy of GVD epoxy vitrimers in the condensed phase [101].

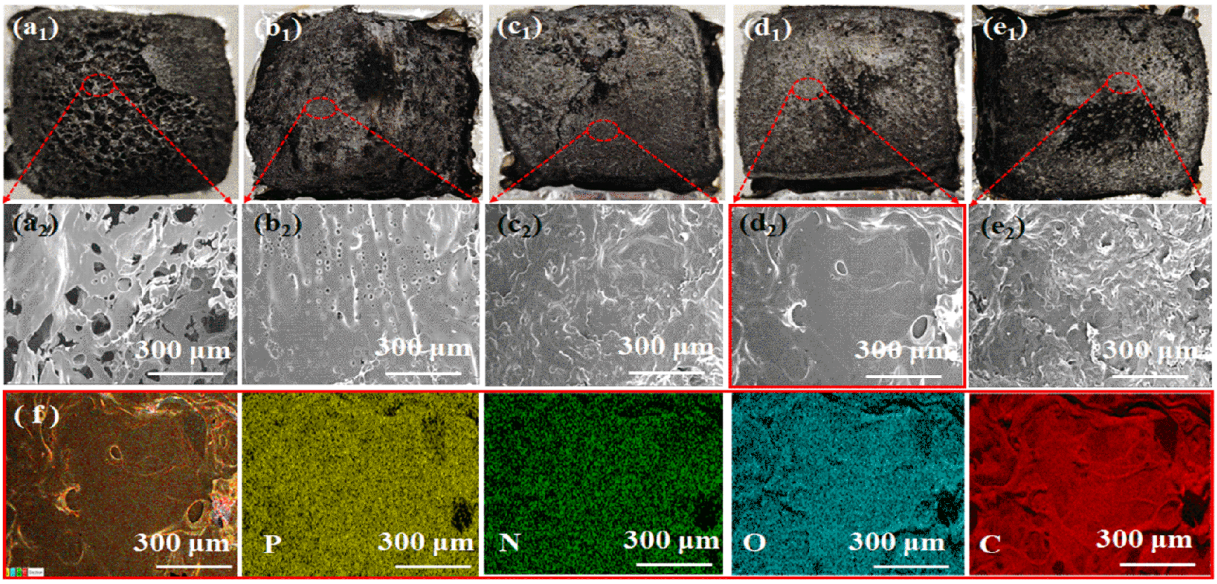

Figure 4-5 Digital photographs of (a1) GV, (b1) GVD1, (c1) GVD3, (d1) GVD5, (e1) GVD7 after combustion; SEM micrographs of (a2) GV, (b2) GVD1, (c2) GVD3, (d2) GVD5, (e2) GVD7 after combustion (f) EDS elemental mapping images of GVD5.

Table 4-5 Elemental composition and content of the residual char.

Sample	C(Wt%)	O(Wt%)	N(Wt%)	P(Wt%)
GV	87.4	10.3	2.3	0
GVD1	81.3	13.5	4.5	0.7
GVD3	80.2	14.1	4.6	1.1
GVD5	82.8	13.1	2.4	1.7
GVD7	83.3	13.2	1.6	1.9

4.3.6 TG-IR of gaseous products of GVD epoxy vitrimers

Real-time tracking of volatiles from two epoxy vitrimers was performed by TG-IR. The spectra of the pyrolysis products extracted from GV and GVD5 at different times are shown in **Figure 4-6(a) and (b)**. The main gaseous products of GV were non-flammable gases (NO_3, 3778 cm^{-1}), water (3650 cm^{-1}), carbon dioxide (CO_2, 2360 cm^{-1}), and aromatic compounds (1510 cm^{-1}) [102]. The pyrolysis products of GVD5 vitrimers were like those of GV, albeit with a few notable differences. Specifically, the emergence of P=O, P-O, and P-O-Ph (phosphorus-containing compounds) at 1234, 1170, and 930 cm^{-1} indicated the presence of DOPO and its derivatives in the gas phase [103]. These phosphorus-containing compounds were anticipated to contribute to the flame retardancy performance in the gas phase by effectively quenching OH· or H· free radicals.

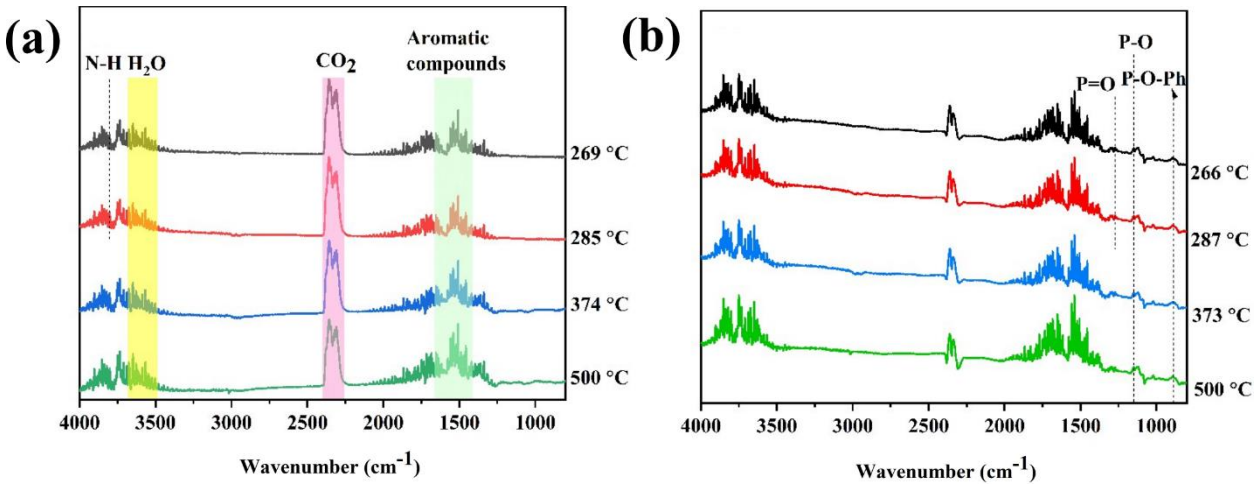

Figure 4-6 TG-IR spectra of gaseous products for (a) GV and (b) GVD5.

Considering the results from different analyses described above, the flame-retardant action mechanism of GVD epoxy vitrimers is summarized in **Scheme 4-2**. In GVD epoxy vitrimers, DOPO displayed a positive role in both the gas phase and condensed phases. In the condensed phase, the presence of phosphorus in GVD epoxy vitrimers can facilitate dehydration and char formation, enhancing the material's ability to inhibit the release of heat and oxygen [102]. Furthermore, GVD epoxy vitrimers generate phosphorus-containing free radicals such as PO· and HPO·, which can effectively quench active radicals, including H· and OH· originated during combustion [103], further terminating the combustion chain reaction in the gas phase. The combined effects in the condensed phase and the gas phase led to superior flame retardancy.

Additionally, the -C=N- group present in the vitrimers, has also been reported to improve flame retardancy to some extent. It is important to note that flame-retardant mechanisms are complex, which warrants more meticulous investigations in future research works.

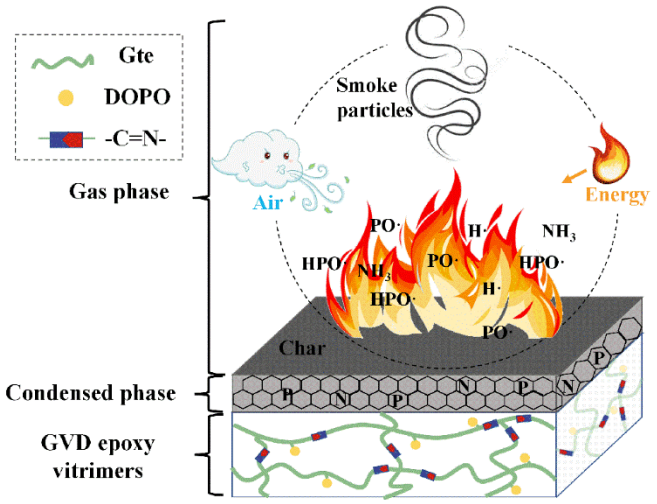

Scheme 4-2 Schematic illustration of combustion mechanism.

4.3.7 Mechanical properties of GVD epoxy vitrimers

Achieving a balance between enhancing flame retardancy and maintaining or improving mechanical properties is of paramount importance in the application of epoxy vitrimers. We investigated the mechanical performance of the epoxy vitrimers by performing DMA and tensile tests. The curves of loss factors (tan δ) and storage modulus (E') obtained by DMA are displayed in **Figure 4-7(a)**, and the corresponding data were presented in **Table 4-6**. The tan δ of the GV shifted to a higher temperature range with increasing the DOPO content, due to the presence of rigid DOPO which restricted the chain mobility [104]. For instance, GVD7 possessed a T_g (~80 °C) much higher than that of the GV (~75.4 °C). The E' at 40 °C of GVD decreased with the content of DOPO increasing, but only the E' of GVD3 was larger than that of GVD1. These results were explained by the crosslinking density of epoxy thermosets, which was calculated by eq (1) and presented in **Table 4-6**. Compared to the GV samples, the crosslinking density of the GVD vitrimers decreased as the DOPO content increased, because the epoxy value of the epoxy resin decreased after the epoxy group of Gte reacting with the P-H of DOPO, resulting in the decrease of the amount of epoxy group for forming crosslinking sites in the epoxy thermosets [105, 106].

This was the reason why the E' of GVD1, GVD3, GVD5, and GVD7 were lower than that of GV. Compared with GVD1, the E' of GVD3 increased by 2.6%, but the crosslinking density of GVD3 was lower. This result demonstrated that the enhancement of mechanical properties caused by rigid DOPO exceeded the decrease of mechanical properties caused by lower crosslinking density [107].

The results of the tensile tests are presented in **Figure 4-7 (b)** and **Table 4-6**. All the samples exhibited typical tensile behavior of hard plastic. While comparing with GV, GVD epoxy vitrimers with DOPO concentration up to 5 wt% showed very similar tensile strength. However, for a DOPO content of 7 wt%, the tensile strength decreased from 51±3 MPa for GV to 40±2 MPa for GVD7. Furthermore, the increasing DOPO content yielded a decrease in the elongation at the break of epoxy vitrimers. The decreased mechanical property was owing to the steric hindrance of DOPO in the network [108]. Interestingly, the tensile modulus of GV was 2681±140 MPa, whereas GVD7 exhibited a tensile modulus of 2958±190 MPa, representing the maximum increment of 10.3 %. The increased tensile modulus was reasonably attributed to the enhanced rigid structure of the network such as aromatic rings and impurity atoms with increasing DOPO content [109].

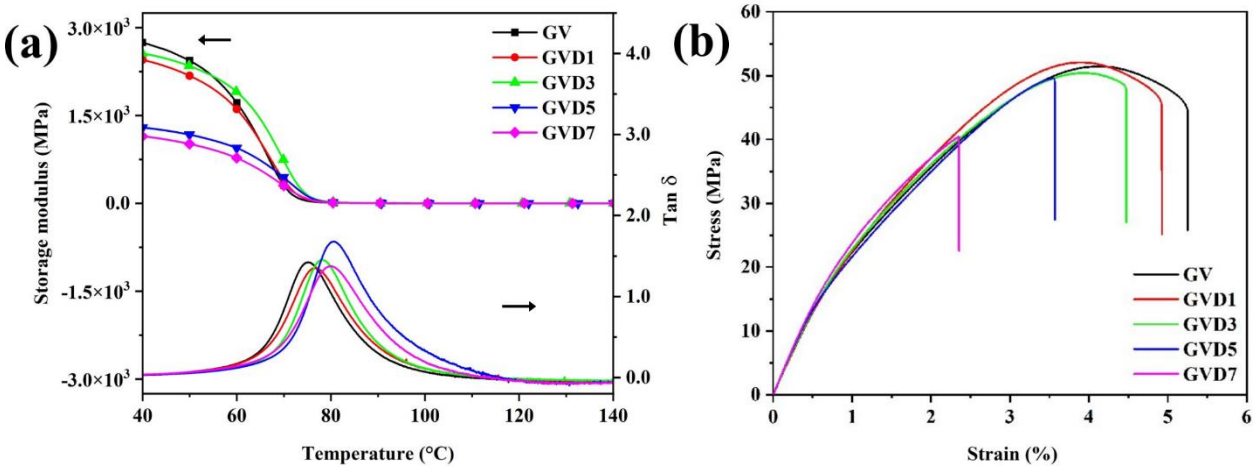

Figure 4-7 (a) DMA curves of E' and tan δ against temperature, (b) stress-strain curves obtained during tensile tests for GV and GVD epoxy vitrimers.

Table 4-6 Mechanical properties of GV and GVD epoxy vitrimers obtained from DMA and tensile tests

Sample	DMA test results					Tensile test results		
	Storage modulus (MPa)	T_g (°C)	T_g+50 °C	E_r'[a] (MPa)	V_e[b] (10^{-3} mol/cm^3)	Tensile modulus (MPa)	Tensile strength (MPa)	Elongation at break (%)
GV	2907	75.4	125.4	3	0.9	2681±140	51±3	5.3±0.2
GVD1	2535	76.9	126.9	2	0.6	2701±80	51±2	4.9±0.5
GVD3	2601	78.2	128.2	2	0.6	2709±100	50±2	4.5±0.4
GVD5	1325	80.6	130.6	1	0.3	2796±170	49±3	3.6±0.5
GVD7	1185	80	130	1	0.3	2958±190	40±2	2.4±0.3

a: storage modulus; b: crosslink densities.

4.3.8 Reprocessing and recycling of GVD epoxy vitrimers

We chose the GVD5 sample to characterize the reprocessability and recyclability of GVD epoxy vitrimers due to their superior flame retardancy among the GVD systems. The reprocessing behavior was investigated via a hot press in a compression molding machine. As shown in **Figure 4-8 (a)**, the GVD5 powder could be successfully remolded into a completely integrated sample at 140 °C, because of topology rearrangement induced by imine metathesis and chain mobility at high temperatures [110].

A transamination process occurs between the network with imine bonds and the network containing amino groups [56]. Therefore, to decompose GVD5 completely, ethylenediamine (EDA) was chosen. 0.1 mol/L EDA solution (solvent: DMF) completely dissolved GVD5 at 50 °C within 2 h, as shown in **Figure 4-8 (b)**. Since the amine-imine exchange reaction was reversible, the complete network could be recycled after the evaporation of the EDA solution. Chemically recycled GVD5 was obtained by hot pressing at 140 °C for 10 min after drying.

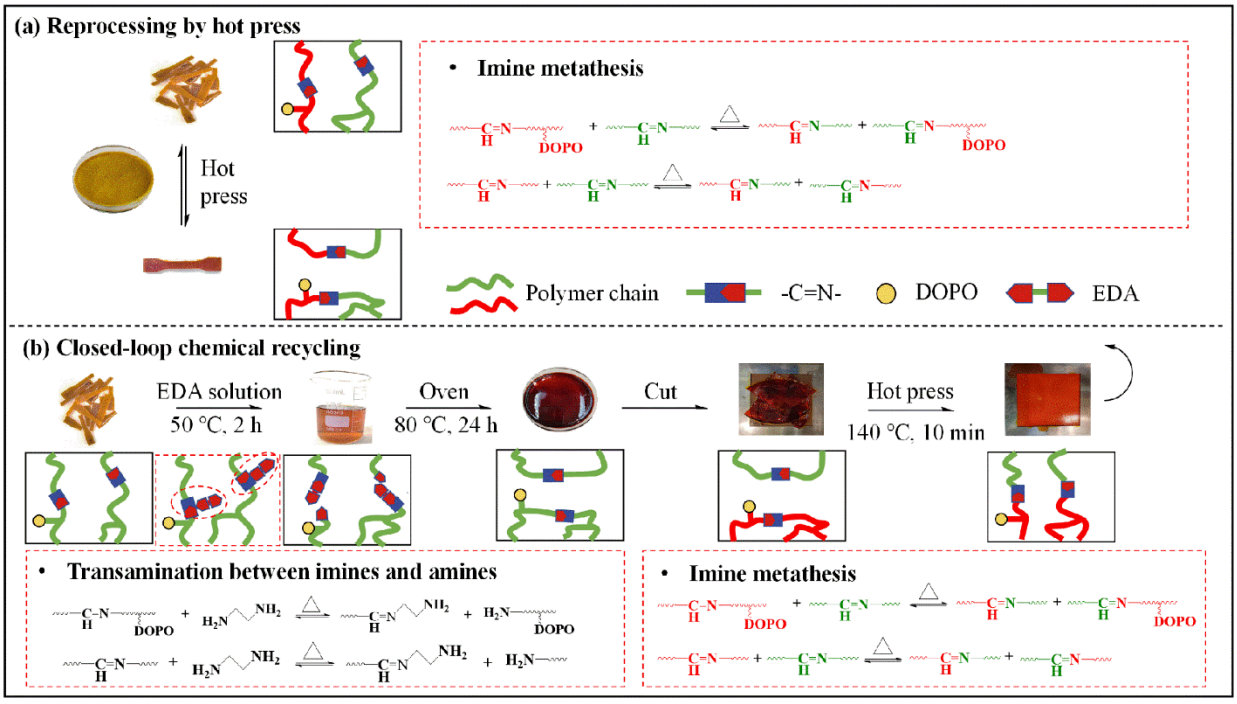

Figure 4-8 (a) hot press reprocessing of GVD5, (b) closed-loop chemical recycling of GVD5.

The mechanical properties and structures of reprocessed GVD5 were measured to evaluate their reprocessability and recyclability. **Figure 4-9 (a) and (b)** show the stress-strain curves and FTIR spectra of GVD5 and reprocessed GVD5 samples, and characteristic indicators are summarized in Figure 3-9 (c). The tensile strength remained at 100% and 87.8% of the original value, even after undergoing two rounds of reprocessing two times. The consistent FTIR spectra of the reprocessed GVD5 further confirmed that the chemical structure of GVD5 remained unchanged during reprocessing.

The recycling efficiency, defined as the ratio of tensile strengths before and after recycling, was calculated to be 93.9 %, as shown in **Figure 4-9 (a) and (c)**. We speculate two main reasons accounting for this result: (1) once broken, covalent bonds such as C-C, P-O, and P=O cannot be repaired during decomposition, and (2) the solvent in GVD5 was not completely removed. As displayed in **Figure 4-9 (c)**, the FTIR spectra of the chemically recycled GVD5 remained unaltered, with the C=N- peak at 1620cm-1, which was consistent with the original GVD5. These findings asserted the good recyclability of GVD5 featuring imine bonds.

To assess the performance status of our work, the comparison to the recent publications associated with the epoxy vitirmer containing imine bonds was carried out [85, 91, 99, 111, 112], as shown in **Figure 4-9 (d)**. In terms of LOI value, our work presented the best performance in fire safety. In terms of mechanical properties, the tensile strength is at a moderate level, however, the recycling efficiency of stress reaches 100%. These features provide great potential for the biobased thermoset for versatile applications.

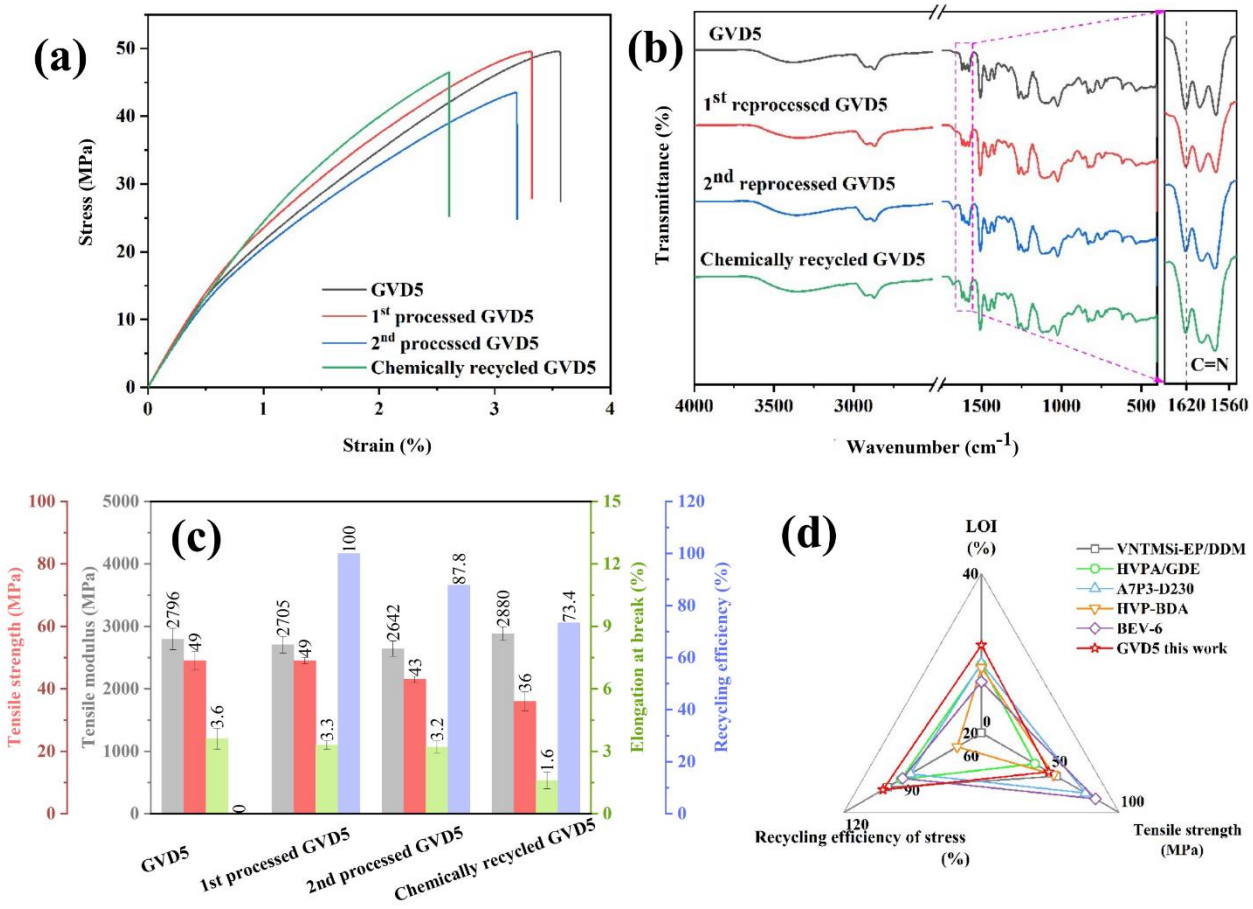

Figure 4-9 (a) Stress-strain curves, (b) FTIR spectra, (c) tensile strength, tensile modulus, elongation at break, and recycling efficiency of the GVD5 and reprocessed GVD5 samples, and (d) Radar map probing optimal LOI, tensile strength, and recycling efficiency of the stress of imine bond epoxy vitrimers [85, 91, 99, 111, 112].

4.4 Summary

In summary, this work presented a facile approach for producing high-performance bio-epoxy vitrimers exhibiting high flame retardancy and mechanical performances. The addition of flame-retardant material DOPO within the epoxy matrix significantly enhanced the flame retardancy, even at a low loading of DOPO. GVD5, featuring a DOPO content of 5 wt% within the epoxy, achieved a V-0 rating in the UL-94 test, with a relatively high LOI value of 31%. Furthermore, the pHRR and THR of GVD5 decreased by 38.2 % and 26.3 %, respectively, compared to the pristine epoxy GV, owing to the high efficiency of DOPO. Notably, GVD epoxy vitrimers demonstrated good reprocessability and recyclability due to the presence of imine bond crosslinks. Additionally, GVD5 exhibited similar mechanical properties like those of GV. The findings of this work demonstrate the multifunctionality of commercial bio-epoxy resins, expanding their utility in high-performance applications.

CHAPTER 5

Biobased Epoxy Vitrimer: Mechanical Enhancement and Smart Functionalities

5.1 Introduction

Prepregs are key intermediate materials in the fabrication of CFRP, typically consisting of continuous CF impregnated with thermosetting resins [113, 114]. They offer excellent molding uniformity and storage stability and serve as the fundamental platform for achieving structural integration and automated manufacturing of high-performance composites. Among various resin systems, epoxy-based prepregs have long been the preferred matrix material for advanced composites due to their outstanding interfacial adhesion, low curing shrinkage, chemical resistance, and excellent mechanical performance [115, 116]. However, conventional epoxy resins are predominantly derived from non-renewable petroleum resources and form irreversible three-dimensional crosslinked networks upon curing, resulting in limited degradability and recyclability. These drawbacks pose significant challenges for their broader application in the context of green manufacturing and circular economy.

Currently, the fabrication of prepregs is mainly carried out through two techniques: solvent impregnation and hot-melt impregnation. The solvent impregnation method reduces resin viscosity by adding organic solvents, thereby facilitating fiber impregnation; it is simple to operate and requires relatively low equipment costs [117]. However, solvent residues may adversely affect composite performance and introduce environmental and health risks. In contrast, the hot melt impregnation method reduces viscosity by heating the resin, eliminating the need for solvents. This approach offers a cleaner, more efficient process flow, with lower emissions, and is increasingly favored in industrial-scale production due to its alignment with the principles of green manufacturing.

In the chapter 3, a flame-retardant bio-based imine vitrimer system was developed, achieving a balance between flame retardancy and recyclability. However, this system exhibited high reactivity and a narrow processing window, which are unfavorable for prepregs fabricating use hot-melt impregnation method. Common strategies to address these limitations include reducing resin viscosity [118-120], modifying molecular structures or adjusting reaction formulations [121, 122].

However, these methods often improve processability at the expense of mechanical strength. Therefore, how to extend the processing window while maintaining excellent mechanical performance remains a critical scientific challenge in promoting the practical application of vitrimer materials.

In recent years, various material design strategies have been proposed to optimize the structure and performance of vitrimer systems. For example, incorporating nanofillers such as functionalized SiO_2 [123], graphene [124], Fe_3O_4 [125], and carbon nanotubes [126] can enhance mechanical properties and impart smart functionalities. However, the adsorption of polymer chains onto the surface of nanoparticles may suppress topological rearrangement, thereby reducing the vitrimer's self-healing capability and recyclability. Compared with nanofiller strategies, resin blending offers greater flexibility and design freedom in balancing material performance and dynamic network behavior. By blending flexible and rigid resin components, the network architecture, crosslinking density, and relaxation behavior can be effectively tuned. For instance, blending polyurethane segments has been shown to enhance toughness and processing properties in thermoplastic vitrimer systems, while the introduction of rigid epoxy monomers improves strength in epoxy-based systems [127]. Nevertheless, poor compatibility between mixed networks may still impair recyclability and reprocessing efficiency.

Based on these considerations, this chapter proposes a simple and generalizable network tuning strategy to achieve melt-processable, high-performance imine-based vitrimers. Initially, the stoichiometric ratio between the aliphatic epoxy monomer Gte and the bio-based imine curing agent VA was optimized to reduce system reactivity and enable hot-melt processing. However, the resulting materials exhibited incomplete curing and unsatisfactory mechanical properties. To overcome this, a novel vitrimer formulation (GTV-4) was developed by blending Gte with a rigid aromatic epoxy monomer, tris(4-hydroxyphenyl) methane triglycidyl ether (Tmte), followed by curing with VA to construct a densely crosslinked network. The resulting GTV-4 system exhibited a wide processing window of up to 45 min, along with excellent processability, self-healing ability, shape memory performance, and recyclability. The prepared carbon fiber-reinforced composites not only retain shape memory functionality but also allowed for efficient and non-destructive fiber recovery using amine solvents. This study provides new insights and design references for developing imine-based epoxy vitrimers with extended processing windows, superior mechanical

properties, thermal self-healing, and degradability, as well as their application in hot-melt prepreg processing and multifunctional carbon fiber-reinforced composites.

5.2 Synthesis of vanilllin based hardner and epoxy vitrimer

5.2.1 Synthesis of vanillin-based hardner

The preparation method is the same as that in Section 4.2.1 and will not be repeated here.

5.2.2 Preparation of epoxy vitrimers

The GV epoxy vitrimers were synthesized via condensation reaction of Gte, VA, and catalyst. By varying the stoichiometric ratio of epoxy groups in Gte to hydroxyl groups in VA (1:1, 2:1, and 3:1), the resulting products were designated as GV-1 (1), GV-1 (2), and GV-1, respectively. For the preparation of GV-1 (1) and GV-1 (2), Gte, VA, and 1,2-dimethylimidazole (DMeIm) were mixed in a beaker, stirred for 4 min, then poured into molds and cured at 140 °C for 1 h.

To further optimize the network structure and enhance material performance based on GV-1, a series of GTV epoxy resin vitrimers was synthesized using Gte, Tmte, VA, and catalyst through condensation reaction. Depending on the molar ratio of Gte to Tmte (9:1, 7:3, and 5:5), the resulting products were labeled as GTV-2, GTV-3, and GTV-4, respectively. Both GV-1 and the GTV series samples were prepared using the same process: Gte and Tmte were first mixed at 80 °C for 5 min to obtain a homogeneous resin mixture (14.00 g), followed by the addition of VA (4.00 g) and DMeIm (0.18 g), with continued stirring for 15 min. After degassing for 10 min, the mixture was poured into aluminum molds of predetermined dimensions and cured at 140 °C for 1 h. The detailed formulation is provided in **Table 5-1**.

Table 5-1 Formulations of the vitrimer GV and GTV

Sample	Gte (g)	Tmte (g)	VA (g)	Catalyst (g)	Epoxy/-OH	Gel time (min)
GV-1 (1)	14.00	-	12.00	0.18	1/1	4
GV-1 (2)	14.00	-	8.00	0.18	2/1	5
GV-1	14.00	-	4.00	0.18	3/1	60
GTV-2	12.60	1.40	4.00	0.18	-	51
GTV-3	9.80	4.20	4.00	0.18	-	48
GTV-4	7.00	7.00	4.00	0.18	-	45

5.2.3 Fabrication of GTV-4-CF

GTV-4 was selected as the matrix resin for the fabrication of carbon fiber-reinforced composite (GTV-4-CF). The designed composition of the composite consisted of 65 wt% carbon fiber and 35 wt% resin. Gte (7 g) and Tmte (7 g) were mixed in a beaker and stirred at 80 °C for 5 min. Subsequently, VA (4 g) and catalyst (0.18 g) were added, and the mixture was further stirred thoroughly at 80 °C. The prepared resin was then used to impregnate carbon fiber fabric by manual lay-up to produce prepregs. Three layers of prepregs were cut, stacked, and enclosed in a polytetrafluoroethylene (PTFE) bag, followed by hot-press curing at 140 °C under a pressure of 10 MPa for 1 h.

5.3 Characteristics of epoxy vitirmer

5.3.1 Synthesis, thermal and mechanical properties of epoxy vitrimer

As shown in **Table 5-1**, the gel times of GV-1(1) and GV-1(2) were 4 min and 5 min, respectively, while GV-1 exhibited a significantly prolonged gel time of 60 min. This was mainly attributed to the epoxy-to-hydroxyl molar ratio of 3:1 in GV-1, where the reduced hydroxyl content led to decreased system reactivity, resulting in extended gelation. The longer gel time made this system suitable for melting processing of fiber-reinforced epoxy composites. However, the presence of many unreacted epoxy groups in the network resulted in insufficient crosslink density and a significant reduction in mechanical properties. To improve the overall performance of the system without substantially affecting the gelation time, Tmte was introduced to further optimize the formulation in this study.

The synthetic route for GTV is shown in **Scheme 5-1**. The bio-based epoxy vitrimer (GTV), incorporating dynamic imine bonds, was synthesized by curing a mixture of Gte and Tmte with the bio-based curing agent VA. The dynamic nature of the imine bonds enables network rearrangement via imine metathesis, as shown in **Scheme 5-2**, which imparts the resulting GTV vitrimer with excellent self-healing, shape memory, degradability, and recycling properties.

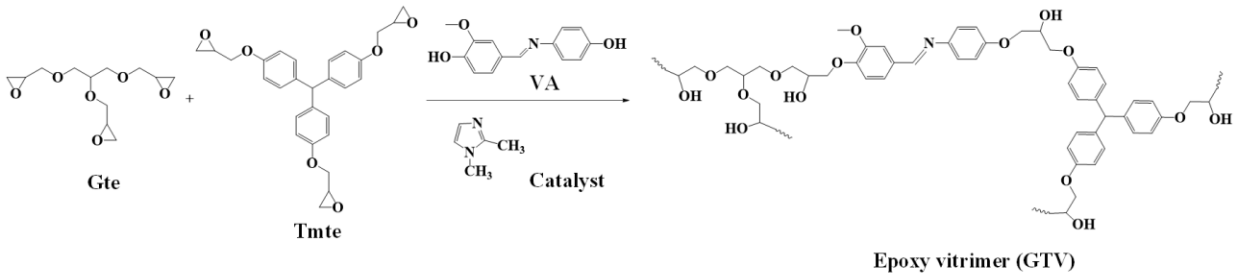

Scheme 5-1 Possible mechanism of curing reactions for epoxy vitrimer.

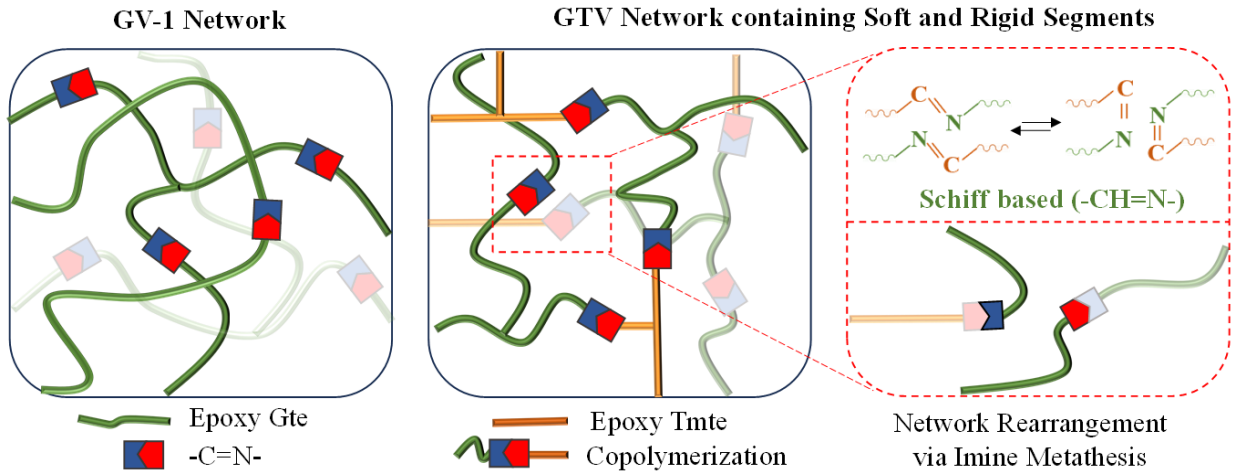

Scheme 5-2 Network rearrangement of epoxy vitrimer via imine metathesis.

The functional groups of epoxy vitrimers were analyzed by FTIR spectra (**Figure 5-1(a)**). The VA sample exhibits a characteristic peak at 1620 cm^{-1}, which corresponds to the C=N vibration (imine bond) [81, 128], indicating the presence of imine groups within its molecular structure. As the reaction progresses, the GV-1, GTV-2, GTV-3, and GTV-4 samples retain this peak at 1620 cm^{-1}, confirming the successful incorporation of imine bonds.

The curing behavior of GV-1 and GTV was investigated via DSC analysis. This study allowed us to optimize the curing treatment to achieve a high level of conversion in the new glass-ceramic systems. Both systems exhibit broad exothermic peaks, suggesting effective reactions between hydroxyl and epoxy groups (**Figure 5-1(b)**). The exothermic peak for GV-1 occurs at 140 °C, while GTV-4 peaks at 170 °C with a broader profile. The latter is attributed to the high-temperature

ring-opening of Tmte, because it is an aromatic amine, regarded as the aliphatic amine of Gte, which partially overlaps with the main exothermic process.

DMA was used to analyze the thermomechanical properties of all materials. **Figure 5-1(c)** illustrates the variation in tan δ curves and storage modulus with temperature, while key data derived from these measurements are summarized in **Table 5-2**. The T_g was identified from the peak of the tan δ curve, was found to be 18.5 °C for GV-1, 30.1 °C for GTV-2, 55.1 °C for GTV-3, and 91.1 °C for GTV-4. As the proportion of aromatic epoxy resin in the formulation increases, the T_g of the samples also rises, owing to the enhanced rigidity of the final material.

Using Flory's ideal rubber elasticity theory, the crosslink density was determined from the storage modulus in the rubbery state (T_g + 50 °C). The calculated values are presented in **Table 5-2**, the crosslink densities for GV-1, GTV-2, GTV-3, and GTV-4 were 177 mol/m³, 160 mol/m³, 185 mol/m³, and 788 mol/m³, respectively. When the storage modulus at 0 °C gradually increased for GTV-2 and GTV-3, indicating that the intrinsic rigidity of the Tmte structure contributes to enhancing the storage modulus at an appropriate crosslink density. However, despite its significantly higher crosslink density, GTV-4 exhibited a lower storage modulus at 0 °C (1446 MPa) compared to GTV-3 (1858 MPa). A possible explanation is that the high Tmte content may have induced microphase separation, thereby negatively impacting the storage modulus.

Thermal stability of the cured materials was assessed through thermogravimetric analysis (TGA). **Figure 5-1(d)** and **Table 5-2** show that all materials remain thermally stable up to nearly 200 °C, allowing for safe relaxation tests to be conducted below this temperature. DTG curves for all samples reveal two degradation peaks: the first, near 300 °C, is associated with imine bond degradation, while the second, around 400 °C, corresponds to the epoxy resin network degradation.

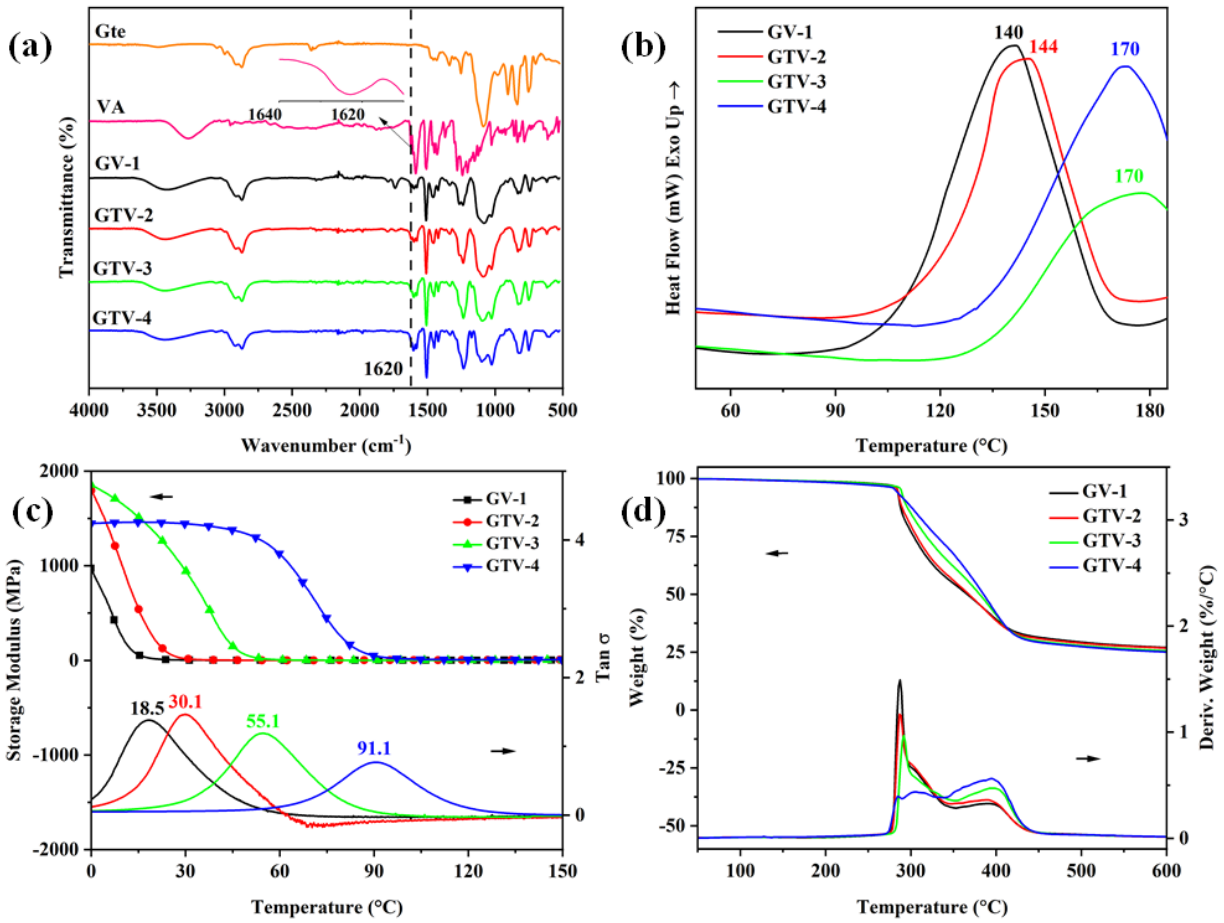

Figure 5-1 (a) FT-IR spectra, (b) DSC curves, (c) Storage modulus curves and Tan Delta curves, (d) Thermogravimetric curves and DTG curves of GV-1, GTV-2, GTV-3, and GTV-4.

Table 5-2 DMA and TGA parameters of the GV-1 and GTV vitrimers

Sample	T_g - DMA (°C)	E′[a] at 0 °C (MPa)	v_e[b] (mol/m^3)	T_{max1} (°C)	T_{max2} (°C)
GV-1	18.5	973	177	287.8	397.6
GTV-2	30.1	1810	160	287.8	400.6
GTV-3	55.1	1858	185	290.9	401.6
GTV-4	91.1	1446	788	305.2	399.6

a: storage modulus; b: crosslink densities.

The mechanical properties of GV-1, GV-1 (1), and GTV were evaluated through uniaxial tensile tests (**Figure 5-2(a), Table 5-3**). The tensile strength and Young's modulus of GV-1 were merely 0.8 MPa and 1 MPa, respectively, due to incomplete curing. In contrast, the tensile strength and Young's modulus of GTV increased with the stoichiometric ratio of Tmte, reaching maximum values of 73.4 MPa and 1069 MPa for GTV-4, which are 92 and 1069 times higher than those of GV-1, respectively. However, the fracture strain of GTV-4 (7 %) was significantly lower than that of GV-1 (60 %), as the introduction of benzene ring structures enhanced rigidity and crosslinking density, thereby restricting polymer chain extensibility.

GV-1 (1) is an epoxy vitrimer with an adjusted stoichiometric ratio of epoxy to hydroxyl groups adjusted to 1:1. It exhibited a tensile strength of 51.2 MPa, a fracture strain of 2 %, and a Young's modulus of 2713 MPa. Compared to GV-1 (1), GTV-4 demonstrated a 43.3% increase in tensile strength and a 250 % improvement in fracture strain. **Figure 5-2(b)** compares the tensile strength and Young's modulus of various epoxy vitrimer materials, highlighting the superior mechanical performance of GTV-4.

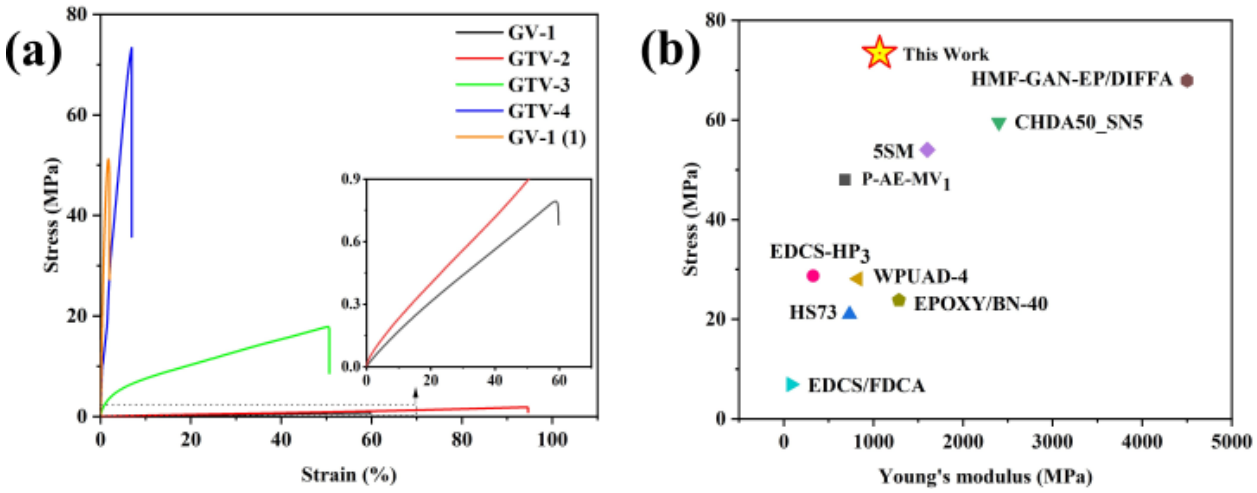

Figure 5-2 (a) Stress-strain curves of GV-1, GV-1(1), GTV-2, GTV-3, and GTV-4, (b) Comparison of tensile stress and Young's modulus with GTV-4 [38, 129-136].

Table 5-3 Young's modulus, tensile stress, and fracture strain of the GV-1 and GTV vitrimers in tensile test

Sample	Young's Modulus (MPa)	Tensile Stress (MPa)	Fracture Strain (%)
GV-1	1±0.2	0.8±0.1	60±38
GTV-2	2±0.5	1.7±0.5	95±43
GTV-3	36±4	17.7±1.8	51±28
GTV-4	1069±110	73.4±3.2	7±1
GV-1 (1)	2713±94	51.2±4	2±0.2

Figure 5-3 presents the fracture surface morphology of different vitrimer samples after tensile testing, analyzed using SEM. The fracture surface of GV-1 (**Figure 5-3(a)**) appears relatively smooth with minimal plastic deformation, indicative of a brittle failure mechanism [137]. This observation aligns with its low Young's modulus and rupture stress. The presence of unreacted epoxy groups likely contributes to the weak crosslinking density, resulting in inadequate stress transfer and premature failure. As the Tmte content increases in GTV-2 (**Figure 5-3(b)**) and GTV-3 (**Figure 5-3(c)**), the fracture surfaces become progressively rougher, exhibiting fibrillated and layered morphologies. These features suggest enhanced plastic deformation and energy dissipation, facilitated by increased crosslinking density and dynamic imine bond exchange. GTV-4 (**Figure 5-3(d)**), with the highest Tmte content, displays a highly fractured morphology with extensive microcracking, characteristic of brittle failure [138]. The transition from a smooth to a progressively more fractured surface correlates with the increasing rigidity and crosslinking density, highlighting the critical role of the Gte-to-Tmte ratio in tuning the mechanical properties and fracture behavior of the epoxy vitrimer system.

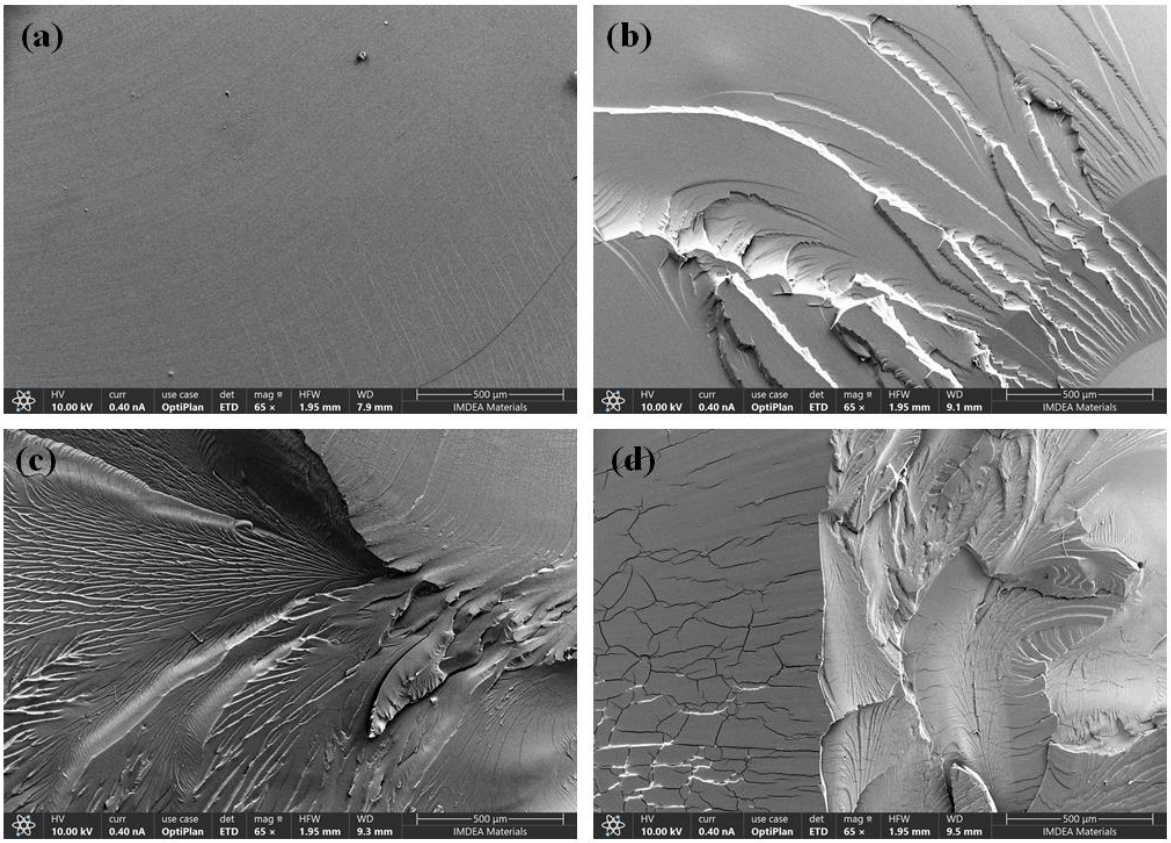

Figure 5-3 SEM images of the epoxy vitrimers: (a) GV-1, (b) GTV-2, (c) GTV-3, (d) GTV-4.

Stress relaxation is a fundamental property of vitrimers, allowing for repair, recycling, and advanced functionalities such as self-healing and programmability [139]. In vitrimers with imine bonds, stress is alleviated through topological rearrangement, driven by imine exchange reactions at elevated temperatures [140, 141]. The influence of temperature on the stress relaxation behavior of GTV-4 was analyzed through stress relaxation tests conducted at temperatures above the glass transition in the rubbery state (T_g + 50 ºC), since the rearrangement of the network requires a high mobility state of the polymeric chains. As the temperature increased, stress relaxation accelerated, as evidenced by the shift of the relaxation curves to shorter timescales illustrated in **Figure 5-4(a)**. The relaxation time ($\tau*$), defined as the time at which the normalized modulus reached 37 % of the initial modulus (G/G_0 = 1/e), was 353.6 s at 110 °C, which progressively decreased to 285.4, 273.7, 189.5, and 197.6 s at 120, 130, 140, and 150 °C, respectively. This trend is attributed to the enhanced activation of imine exchange reactions at elevated temperatures, promoting network rearrangement and accelerating stress relaxation [140].

The activation energy (E_a) for stress relaxation of GTV-4 was determined using the Arrhenius equation, calculated by eq 2. A linear correlation was observed for GTV-4 when plotting ln(τ) against 1/T, as shown in **Figure 5-4(b)**, confirming that its relaxation follows Arrhenius behavior. The E_a, calculated from the slope of this linear relationship, was 21.26 kJ/mol, falling within the reported range of 20.35–129 kJ/mol for vitrimers with dynamic imine bonds [142].

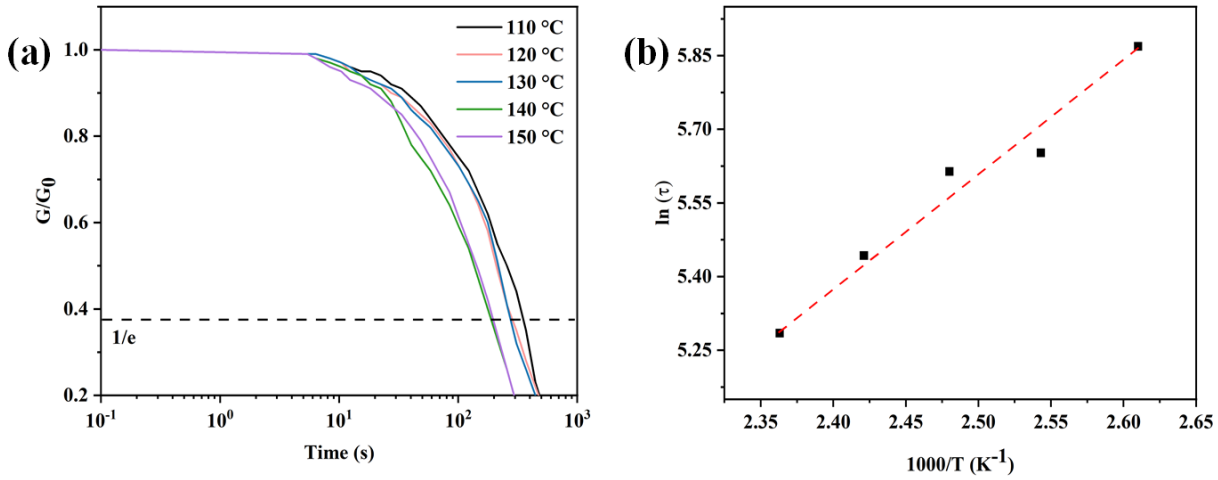

Figure 5-4 (a) Variation of relaxation modules over time at different temperatures for GTV-4, (b) Dependence of relaxation time on temperature for GTV-4.

5.3.2 New functionalities of GTV-4: self-healing, shape memory and recycling

The GTV-4 epoxy vitrimer demonstrated better stretchability than GV-1, prompting further investigation into its self-healing, shape memory, degradation, and recycling capabilities. The self-healing efficiency is shown in **Figure 5-5**, where cracks in GTV-4 were visibly recovered after a convective healing process. Similarly, profile contours before and after healing confirmed a nearly flat surface post-recovery.

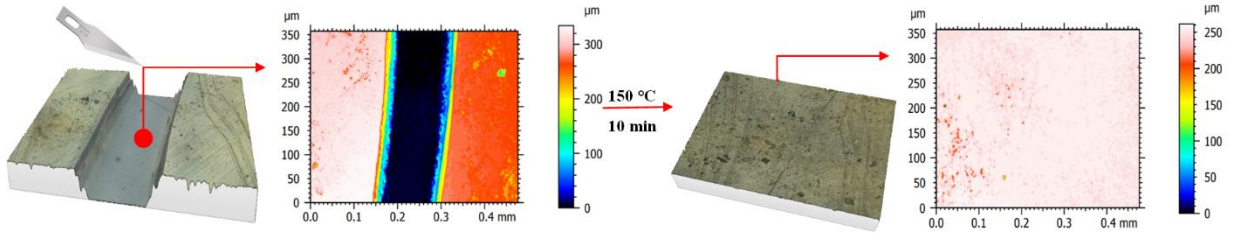

Figure 5-5 Self-healing photographs and map contours before and after at 150 °C

GTV-4 demonstrated outstanding shape memory performance, as illustrated in **Figure 5-6**. A rectangular specimen was deformed into a 'U' shape at 110 °C (above its T_g) under an external force and subsequently cooled to room temperature. Upon releasing the force, the temporary 'U' shape remained intact. When reheated to 110 °C, the sample returned to its original rectangular form, confirming T_g-based shape memory behavior.

Additionally, GTV-4 exhibited triple-shape memory characteristics at elevated temperatures. At 150 °C, the rectangular sample was reshaped into a 'spiral' configuration and held for 30 minutes before cooling to room temperature, fixing the new form. Upon reheating to 110 °C, the spiral transitioned into an 'I' shape, which was then cooled to preserve this intermediate state. When the temperature increased back to 110 °C, the "I" shape transformed into the spiral. Finally, upon heating to 150 °C, the original rectangular shape was fully restored via dynamic bond exchange.

The shape memory effect in GTV-4 is primarily entropy-driven. In its permanent state, molecular chains adopt a conformation with maximum entropy, corresponding to thermodynamic stability. When heated above the transition temperature (T_{trans}, either T_g or the topological transition temperature T_v), molecular mobility increases, allowing external deformation to shift the chain conformation to a lower entropy state. Cooling below Ttrans locks the molecular structure in this temporary shape. Upon reheating in a stress-free environment, the molecular chains regain mobility, restoring their highest entropy conformation and returning the material to its initial form. This mechanism governs the triple-shape memory behavior of GTV-4, dictated by T_g and T_v [130].

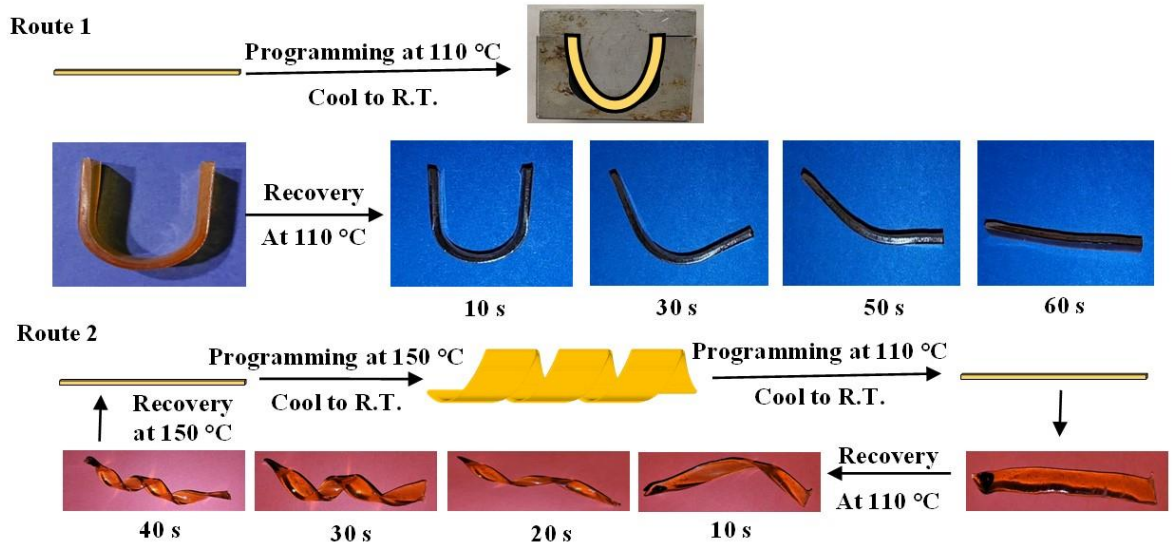

Figure 5-6 Shape memory photographs of GTV-4.

The chemical degradation of GTV-4 was evaluated using EDA solution (solvent: DMF). After soaking and stirring at 50 °C for 2 h, GTV-4 completely dissolved due to reversible amine-imine exchange reactions between the network's imine bonds and the amino groups in the solvent [2, 143] (**Figure 5-7(a)**).

Recycling tests demonstrated that GTV-4 retained its tensile properties (**Figure 5-7(b) and Table 5-4**) after chemical degradation. Following the first recycling, the tensile strength was 71 MPa, with a fracture strain of 4 %. The tensile strength retention efficiency was 96.7 %, while fracture strain efficiency was 57.1 %. After the second recycling, the tensile strength was 67.6 MPa, with the same fracture strain, showing efficiencies of 92.1 % and 57.1 %, respectively. These results highlight that the dynamic imine bonds enable GTV-4 epoxy vitrimer to achieve excellent self-healing, shape memory, chemical degradation, and recycling performance.

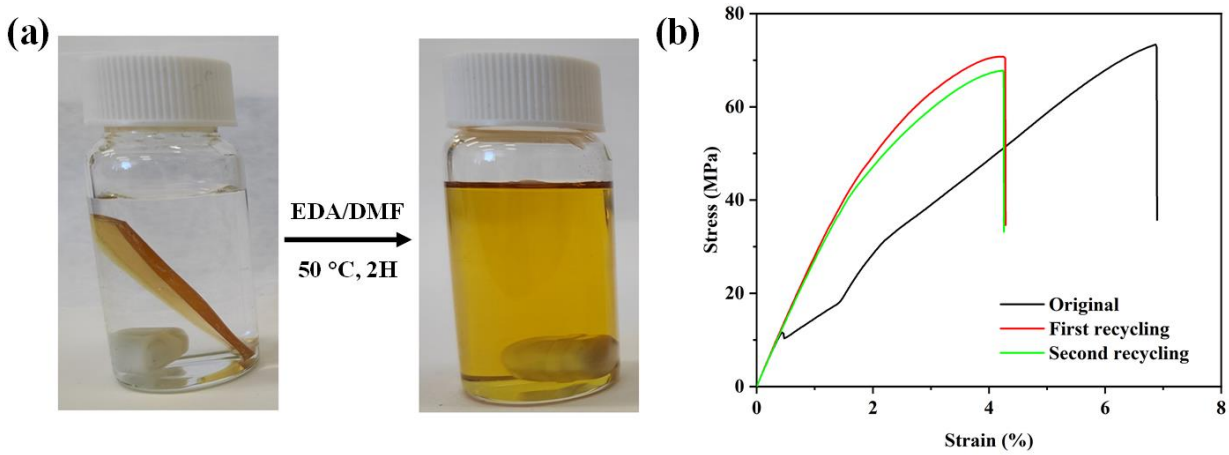

Figure 5-7 (a) Photographs of GTV-4 degradation in EDA solutions, (b) Original, first recycling and second recycling tensile curves of GTV-4.

Table 5-4 Tensile stress and fracture strain of recycling GTV-4 in tensile test.

Sample	Tensile Stress (MPa)	Fracture Strain (%)
Original	73.4±3.2	7
First recycling GTV-4	71±0.6	4
Second recycling GTV-4	67.6±0.5	4

5.3.3 Preparation and properties of GTV-4-CF

CFRP are typically composed of CF embedded within a polymer matrix. Given the excellent mechanical properties of the GTV-4 system, GTV-4 was selected as the matrix resin for CFRP fabrication. The GTV-4 resin was preheated at 80 °C, followed by manual lay-up to prepare GTV-4 prepregs. Three layers of prepregs were stacked to fabricate the GTV-4-CF composite, with a CF weight fraction maintained at 65%.

The GTV-4-CF exhibits T_g-based shape memory behavior. As shown in **Figure 5-8(a)**, a rectangular sample was bent to various angles at 130 °C and held for 30 min before being cooled to room temperature, effectively locking the deformed shape. Upon reheating to 130 °C, the sample recovered its original rectangular shape. The shape fixity ratios (S_F, the formula for eq 4) of the GTV-4-CF in different angle molds exceeded 85%, demonstrating excellent shape memory performance.

To assess whether the GTV-4-CF develops surface defects during shape memory bending recovery, we compared its tensile strength after shape recovery with that of the original GTV-4-CF. As shown in **Figure 5-8(b)** and **Table 5-5**, the tensile strength of the GTV-4-CF after one recovery remained 98.4% of the original, while after two and three recoveries, the tensile strengths were 94.3% and 68.4%, respectively. These conclusions indicate that during the shape memory deformation process within two times, the GTV-4-CF exhibits minimal surface defects in the bending region, which have negligible impact on its mechanical properties.

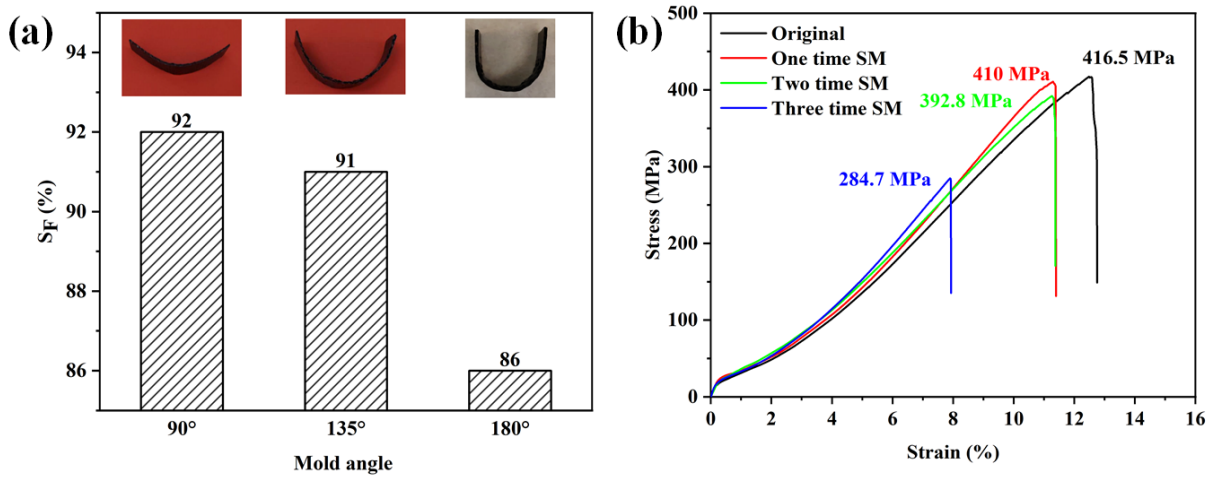

Figure 5-8 (a) Shape fixity ratios of GTV-4-CF, (b) Tensile curves of GTV-4-CF in its original state, after one, two, and three shape memory cycles.

Table 5-5 Tensile stress and fracture strain of GTV-4-CF and CTV-4-CF after one, two, and three shape memory cycles.

Sample	Tensile Stress (MPa)	Fracture Strain (%)
GTV-4-CF	416±20	13±1
One time SM	410±5	11±1
Two-time SM	393±10	11±1
Three-time SM	285±5	8±1

Finally, we investigated the degradation of the GTV-4-CF. As noted earlier, Schiff bases readily react with amine. Thus, we immersed a rectangular sample of the GTV-4-CF in an EDA solvent (solvent: DMF) and degraded the matrix at 50 °C for 2 h, followed by recycling the dispersed CFs. Initially, the GTV-4-CF was fully submerged in the EDA solvent, which caused the matrix to swell. The Schiff base underwent aminolysis with EDA, leading to a gradual degradation of the polymer network. After 2 h, the Schiff bases in the matrix were completely degraded by EDA. **Figure 5-9** illustrates the entire degradation process. The solution turned from colorless and transparent to yellowish, leaving behind clean CFs and achieving mild recycling of the CFs.

Figure 5-9 Photographs of the GTV-4-CF polymer before and after degradation in EDA solusion.

The surface morphology of CFs before and after recycling was examined using SEM, as depicted in **Figure 5-10**. Compared to the virgin CFs (**Figure 5-10(a)**), the recycled CFs (**Figure**

5-10(c)) exhibited a smooth surface, free of residual matrix resin at the interface. Additionally, enlarged SEM images of a single CF monofilament, both before (**Figure 5-10(b)**) and after recycling (**Figure 5-10(d)**, revealed no discernible differences. This confirms that the GTV-4 matrix resin underwent complete degradation during the recycling process.

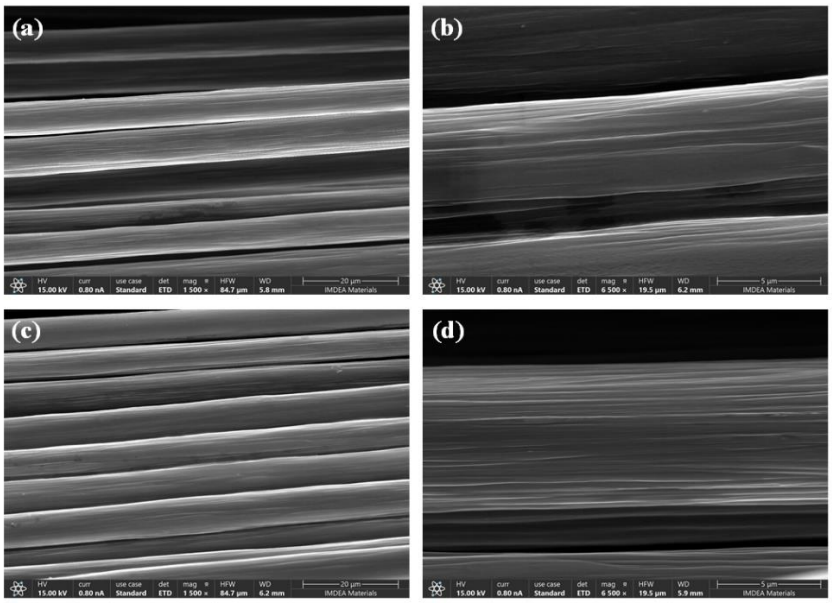

Figure 5-10 SEM of (a) virgin CFs, (b) virgin CF monofilament, (c) recycled CFs, and (d) recycled CF monofilament.

The Raman spectrum of recovered fibers exhibited a carbon peak like that of the original fibers, suggesting that the surface of the CFs was minimally affected during recycling (**Figure 5-11(a)**). To further assess any changes in the mechanical properties of the carbon fiber (CF) monofilaments post-recycling, a detailed analysis was performed. As shown in **Figure 5-11(b)**, the rupture stress and rupture strain of the recycled CF monofilaments were nearly identical to those of the virgin fibers, with the tensile strength retaining 97% of its original value. These results indicate that the recycled CFs maintain similar surface morphology, chemical structure, and mechanical properties to the virgin fibers, making them suitable for reuse in CFRPs fabrication. This study demonstrates an effective non-destructive recycling process and establishes a closed-loop system for CFs in CFRP applications.

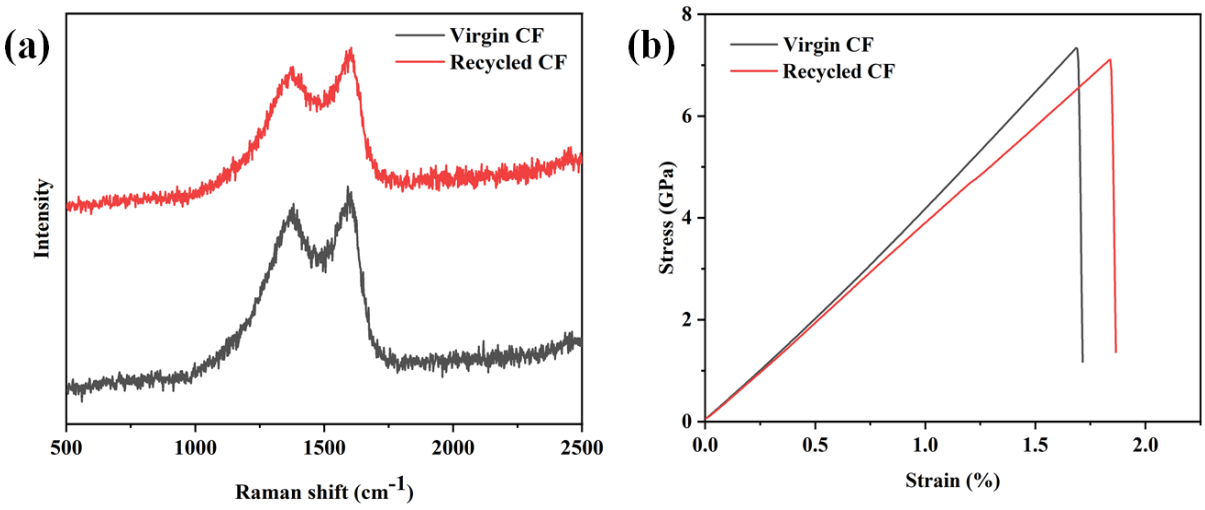

Figure 5-11 (a) Raman spectra of virgin and recycled CF, (b) The stress-strain of virgin and recycled CF monofilaments.

5.4 Summary

This study developed a high-performance bio-based epoxy vitrimer system, GTV-4, through systematic screening of gel time and processing performance, effectively addressing the challenges of narrow processing windows and mechanical limitations in epoxy vitrimer systems for hot-melt prepreg applications. By optimizing the network structure with glycerol triglycidyl ether (Gte), tris(4-hydroxyphenyl) methane triglycidyl ether (Tmte), and a bio-based imine-containing curing agent, the GTV-4 resin achieved a gel time of approximately 45 min at 80 °C, providing a stable processing window for melt-based prepreg fabrication. The resulting GTV-4 resin exhibited excellent overall performance, with a T_g of 91.1 °C, tensile strength of 73.4 MPa, Young's modulus of 1069 MPa, and elongation at break of 7 percent, along with remarkable self-healing ability, shape memory behavior, and recyclability. Based on this vitrimer matrix, carbon fiber-reinforced composites containing 65 weight percent fiber were fabricated through melt prepreg processing. The composites demonstrated outstanding mechanical performance with a tensile strength of 414.6 MPa, maintained excellent shape memory functionality, and enabled efficient, non-destructive fiber recovery using amine solvents. This work provides an effective design strategy to expand the application potential of imine-based epoxy vitrimers in the development of sustainable, high-performance composite materials.

CHAPTER 6

Biobased Flame-Retardant Epoxy Vitrimer: Processability, Flame Retardancy and Mechanical Strength

6.1 Introduction

CFRPs are widely used in aerospace, defense, and advanced transportation sectors due to their excellent specific strength, dimensional stability, and fatigue resistance [144-146]. In these high-performance applications, increasing demands are placed on the safety, sustainability, and recyclability of composite materials [147, 148]. In this context, the development of novel vitrimer-based prepreg systems that simultaneously exhibit flame retardancy, bio-based origin, and recyclability has emerged as a promising strategy to meet the requirements of green manufacturing and circular economy.

Commercial thermoset prepregs are typically supplied in roll form and can be directly laid over complex molds without the need for handling liquid resins, significantly improving manufacturing efficiency and ensuring product consistency [149, 150]. The matrix resin in prepregs usually undergoes three stages: the A-stage (unreacted), B-stage (partially crosslinked), and C-stage (fully cured) [151]. The B-stage is particularly critical for processing and storage, as the extent of reaction directly determines the viscosity, drapability, and final molding behavior [152]. Excessive reactivity during this stage can cause premature gelation and poor fiber impregnation, while insufficient curing may lead to resin flow, deformation, or poor shape retention [153, 154]. Therefore, precise control over the curing kinetics in the B-stage is one of the main technical challenges in prepreg resin design.

Although numerous prepreg products are available on the market, their matrix resins are predominantly based on conventional thermosets with limited degradability and poor reprocessability [155, 156]. Furthermore, their development has remained largely disconnected from recent advances in materials science, especially in smart polymer networks. Vitrimers, characterized by dynamic covalent bonds, offer a promising platform for next generation prepregs by enabling thermal reprocessability, recyclability, and self-healing [157]. However, most reported vitrimer systems have been optimized for batch processing or small-scale molding and remain unsuitable for continuous prepreg production [158-161]. Specifically, issues such as viscosity

control, processing window, thermal stability, and flame retardancy must be simultaneously addressed. As such, there is a clear need to construct a vitrimer resin system with balanced reactivity, excellent flame resistance, and favorable rheological behavior for scalable prepreg applications.

To address these challenges, this chapter presents the design and synthesis of a novel phosphorus-containing imine-based bio-derived curing agent (FROH), which is combined with glycerol triglycidyl ether (Gte) to formulate a vitrimer resin network that can be cured under catalyst-free conditions. This system offers excellent melt-processing adaptability. A semi-automated hot-melt impregnation process is employed to prepare continuous carbon fiber prepregs, which are subsequently consolidated into multi-layer flame-retardant CFRP (Gte-FROH-CF) composites through hot-pressing. The resulting materials are systematically evaluated in terms of mechanical performance, flame retardancy, and recyclability, providing insights into their potential for application in the sustainable manufacturing of high-performance composites.

6.2 Construction of the semi-automated hot-melt impregnation equipment

To evaluate the suitability of the developed bio-based epoxy vitrimer resin system for hot-melt prepreg processing, a continuous prepreg fabrication device was designed and constructed in this study. This setup aims to achieve efficient and uniform impregnation of reinforcing fibers with molten resin under controlled temperature and tension conditions, thereby producing prepreg tapes with stable quality and controllable properties.

The entire prepregging system consists of four functional zones, like **Figure 6-1** and **Figure 6-2**: (a) fiber unwinding unit, (b) resin heating and impregnation unit, (c) roller compaction unit, and (d) winding unit. Initially, continuous reinforcing fibers (e.g., carbon or glass fibers) are guided into the system through a tension-controlled unwinding device. Guide rollers are used to maintain fiber alignment and apply appropriate tension, ensuring uniform and consistent impregnation in the subsequent processing stage. The fibers then enter the resin impregnation zone, which is equipped with a temperature-controlled heating chamber. Here, the vitrimer resin is heated to a preset temperature range where its viscosity is sufficiently reduced to allow thorough infiltration without excessive flow. The temperature is optimized based on the rheological characteristics of the resin system to achieve effective fiber wetting while preventing premature curing.

After resin impregnation, the fiber bundle passes through the roller compaction unit, where it is lightly compressed by a pair of heated rollers. This step ensures uniform distribution of resin among the fibers and precisely controls the resin content to avoid issues such as excessive resin accumulation, which could hinder subsequent processing or degrade the mechanical performance of the final composites. If necessary, the impregnated fibers are subjected to preliminary cooling and are then collected into rolls at the winding unit under constant tension, ensuring the dimensional stability and structural integrity of the prepreg tapes.

Throughout the prepreg fabrication process, key operational parameters—including resin bath temperature, impregnation speed, roller gap, and winding tension—can be monitored and adjusted in real time to meet the process requirements of different resin formulations. This prepregging setup not only serves as a practical platform for evaluating the processing performance of the bio-based vitrimer resin system developed in this work but also provides a reliable foundation for future studies on continuous prepreg applications involving other thermally processable resin systems.

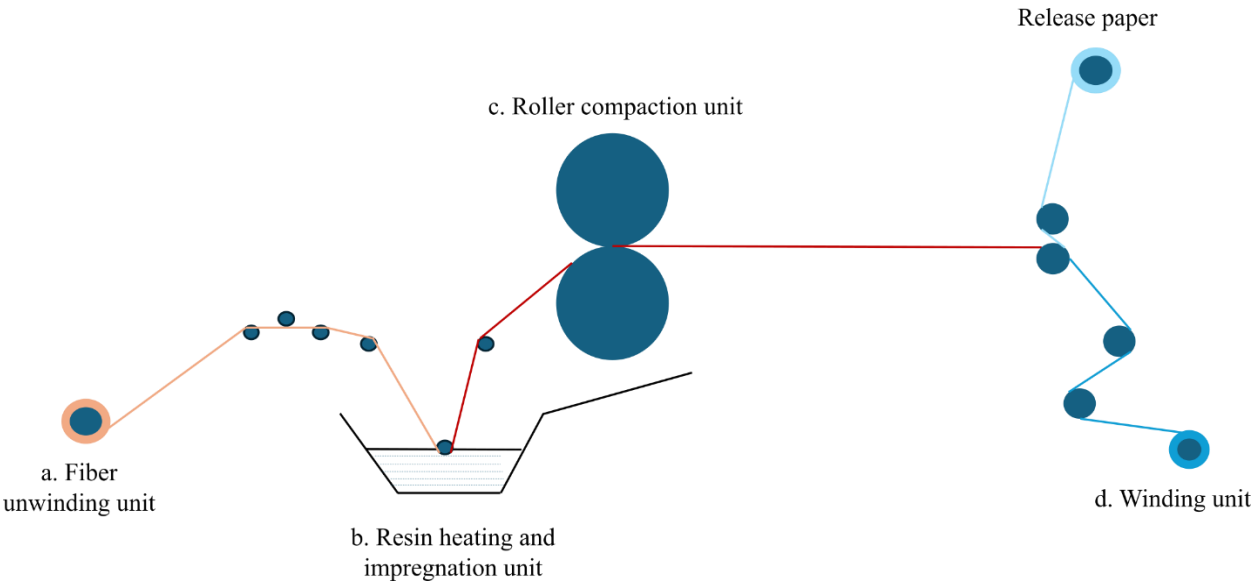

Figure 6-1 Simplified schematic of the prepreg fabrication device.

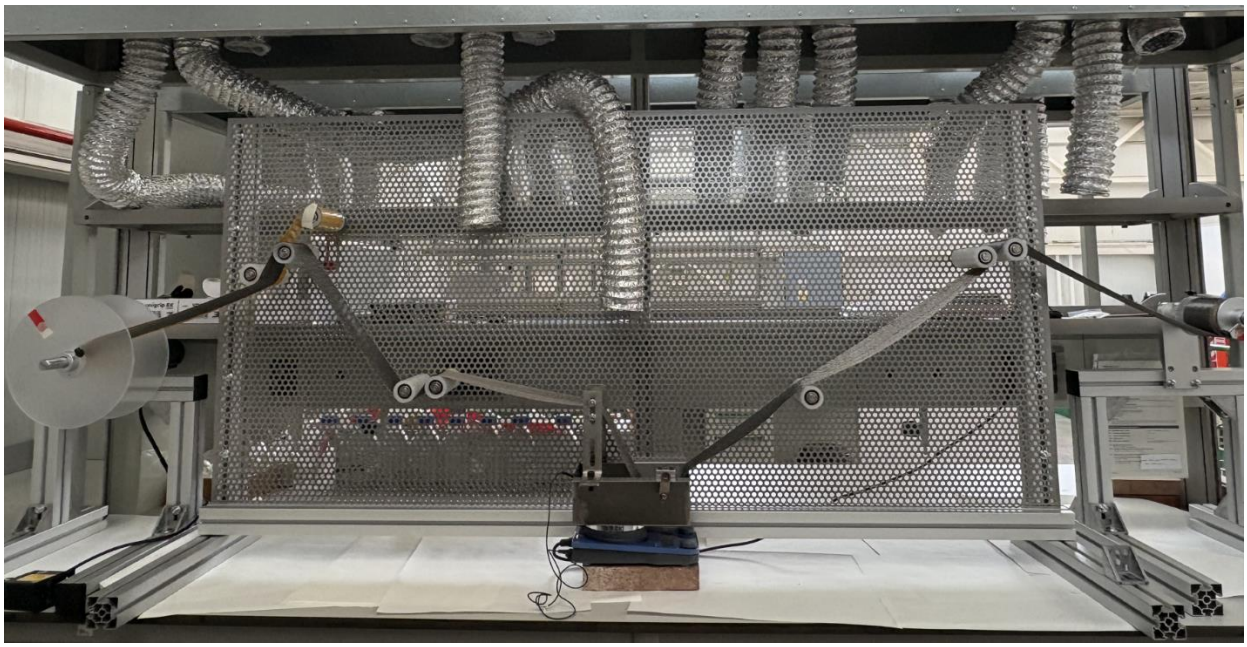

Figure 6-2 Photograph of the self-assembled prepreg device.

6.3 Preparation of curing agent and epoxy prepreg

6.3.1 Preparation of FRA

FRA was synthesized by a quintessential condensation reaction between vanillin and phosphorus oxychloride [162]. First, Vanillin (45.6 g, 0.3 mol) and triethylamine (30.3 g, 0.3 mol) were mixed and dissolved in 200 mL ethyl acetate in a 500 mL three neck flask equipped with a mechanical stirrer. Then, 15.3 g (0.1 mol) of phosphorus oxychloride was added dropwise into the flask at 0 °C. After maintaining the reaction at 0 °C for 30 min, we stirred it at 25 °C for 24 h. when the reaction was complete, the mixture was poured into about 1000 mL of deionized water. Then. The mixture continued to stir for 30 min to cool down to room temperature. After removing the solution through suction filtration, a white solid was collected. Then the collected white solid was recrystallized with ethanal and then dried at 70 °C for 24 h in a vacuum oven.

6.3.2 Preparation of FROH

5 g of FRA was fully dissolved in 22 mL of N,N-dimethylformamide (DMF), and 1.09 g of p-aminophenol was dissolved in 20 mL of ethanol. The two solutions were then mixed under magnetic stirring at 50 °C for 2 h. After mixing, 100 mL of deionized water was added, resulting

in a milky white emulsion. The mixture was centrifuged at 10,000 rpm for 10 min, and the resulting precipitate was dried in an oven at 80 °C to remove residual moisture.

6.3.3 Preparation of epoxy prepreg

In this study, the Gte-VA system described in Chapter 3 was selected as a reference sample. Two types of bio-based epoxy vitrimer prepregs were prepared: Gte-VA prepreg (non-flame-retardant) and Gte-FROH prepreg (flame-retardant). Unidirectional carbon tape with a surface density of 200 g/m² was used as the reinforcement in both cases.

Due to the short gel time of the Gte-VA system (approximately 5 min), it was not suitable for the melt impregnation method. Therefore, a solvent-based method was employed. Specifically, Gte and VA were mixed at a mass ratio of 1:0.8 (corresponding to an epoxy-to-hydroxyl molar ratio of 1:1) and reacted at 140 °C for 4 min. The mixture was then rapidly cooled to room temperature and dissolved in tetrahydrofuran (THF) at a ratio of 1.3 g resin to 7 mL solvent. A 10 cm × 12 cm carbon fiber fabric was immersed in the resin solution, and dried in an oven to evaporate the solvent, yielding the Gte-VA prepreg.

In comparison, the Gte-FROH system exhibited a longer gel time, making it suitable for melt processing. A semi-automated prepreg fabrication system was employed. Gte and FROH were first mixed at a mass ratio of 1:1 (corresponding to an epoxy-to-hydroxyl molar ratio of 1:1) at 100 °C to obtain a homogeneous and transparent resin. Continuous carbon fibers were then passed through the molten resin bath, and excess resin was removed using rollers positioned at the outlet of the resin tank, followed by winding to produce Gte-FROH prepregs, as shown in **Figure 6-3**.

Figure 6-3 A fabricated roll of continuous fiber-reinforced prepreg with a width of 10 cm.

6.3.4 Preparation of carbon fiber reinforced composites

Sixteen layers of Gte-VA and Gte-FROH prepregs were stacked and hot-pressed to fabricate carbon fiber-reinforced composites with an approximate thickness of 2 mm. The Gte-VA laminates were cured at 140 °C for 2 h, while the Gte-FROH laminates were cured at 200 °C for 2 h. The resulting composites exhibited uniform thickness and good interfacial adhesion, and were subsequently used for evaluations of mechanical properties, flame retardancy, and recyclability.

6.4 Characterization of FROH and properties of Gte-FROH

6.4.1 Characterization FRA and FROH

A phosphorus-containing bio-based intermediate monomer, FRA, was synthesized through a straightforward condensation reaction between $POCl_3$ and vanillin. Based on this intermediate, FROH were further prepared by introducing 4-aminophenol (**Scheme 6-1**).

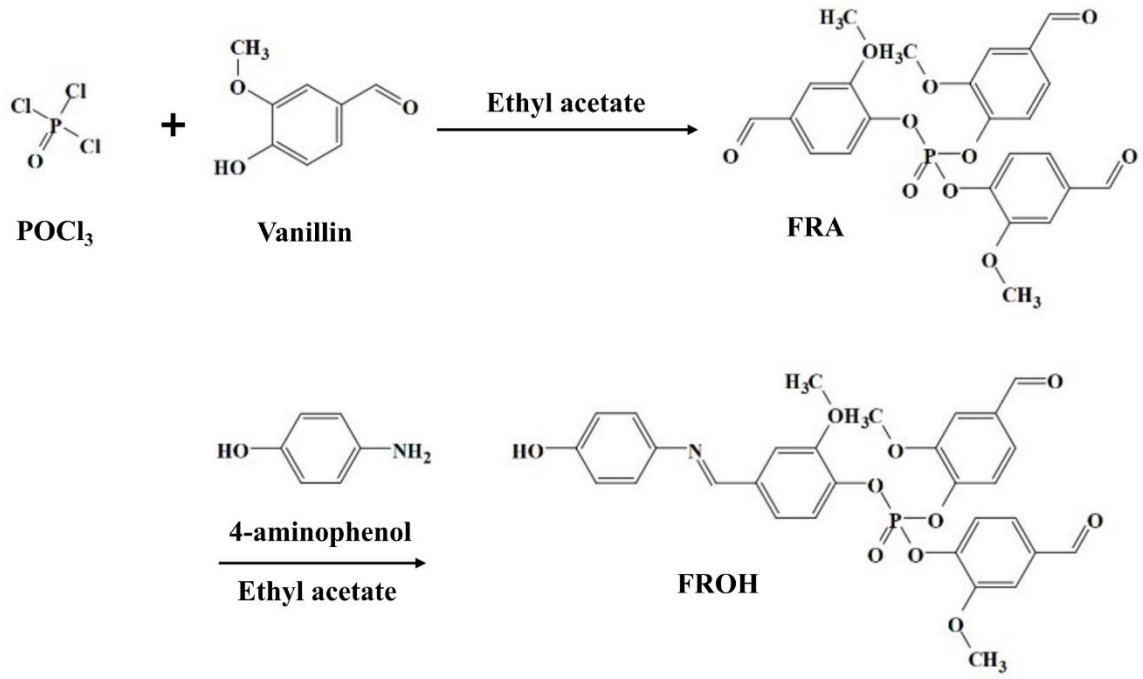

Scheme 6-1 Possible mechanism for FRA and FROH.

To confirm the chemical structure of FRA, ^{1}H NMR, ^{13}C NMR and ^{31}P NMR were employed. As shown in **Figure 6-4 (a)**, the signal at 9.9 ppm corresponds to the proton of the –CHO group. The multiplet signals in the range of 7.4–7.6 ppm is attributed to aromatic protons (H2, H3, H4),

while the peak at 3.8 ppm corresponds to the methyl protons (–CH_3). In the ^{13}C NMR spectrum of FRA (**Figure 6-4 (b)**), eight distinct carbon signals are observed, which are in complete agreement with the proposed chemical structure. The strong signal at 190.5 ppm corresponds to the aldehyde carbon (C1), and the peaks at 151.4, 144.4, 134.7, 124.6, 121.7, and 111.2 ppm are attributed to the aromatic carbon (C6, C5, C2, C3, C4, and C7, respectively). The signal at 56.1 ppm is assigned to the methoxy carbon (C8). In the ^{31}P NMR spectrum of FRA (**Figure 5-4 (c)**), a single peak appears at 18.7 ppm, indicating that the condensation reaction between vanillin and $POCl_3$ has been completed successfully [163, 164].

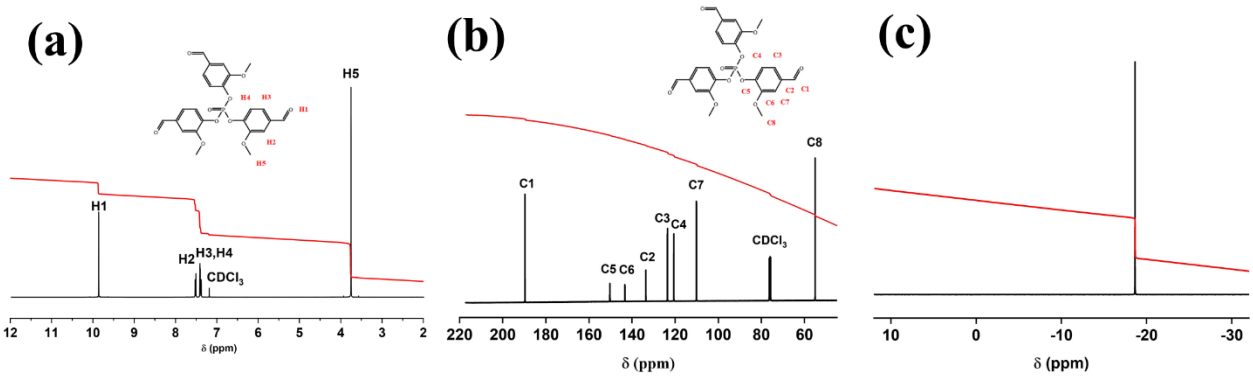

Figure 6-4 (a) ^{1}H NMR, (b) ^{13}C NMR and (c) ^{31}P NMR spectra of FRA.

As shown in **Figure 6-5**, In the FTIR spectrum of FRA, the characteristic absorption peak at 1704 cm^{-1} is attributed to the stretching vibration of the carbonyl group (C=O), indicating that the aldehyde structure of vanillin is preserved after reaction. The strong absorption band observed at approximately 1284 cm^{-1} corresponds to the P=O stretching vibration, while the signal at 1026 cm^{-1} is associated with P–O bond vibrations. These characteristic peaks confirm the successful condensation reaction between vanillin and $POCl_3$, resulting in the formation of the intermediate FRA. For FROH, a new absorption peak appears at 1620 cm^{-1}, corresponding to the stretching vibration of the imine bond (C=N). This observation indicates that the aldehyde group in FRA has reacted with the amino group of 4-aminophenol to form a Schiff base. In the FTIR spectrum of the cured epoxy vitrimer Gte-FROH, the disappearance of the characteristic epoxy peaks at 847 cm^{-1} and 910 cm^{-1} demonstrates the complete consumption of epoxy groups during the curing process. A broad band at 3375 cm^{-1} is observed, attributed to O–H stretching vibrations, confirming the ring-opening reaction of epoxy groups and the generation of hydroxyl functionalities. Additionally, the retention of the imine (C=N) peak at 1620 cm^{-1} confirms the

incorporation of dynamic covalent bonds into the polymer network. The presence of P=O (1284 cm^{-1}) and P–O (1026 cm^{-1}) vibrations further validate the successful synthesis of the phosphorus-containing, flame-retardant epoxy vitrimer system.

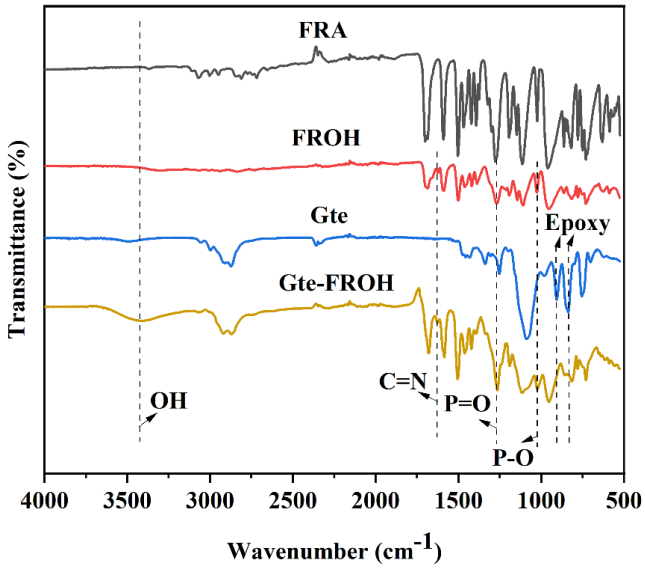

Figure 6-5 The FTIR spectra of FRA, FROH and Gte-FROH.

The curing behavior of the Gte-FROH system was investigated by DSC, as shown in **Figure 6-6 (a)**. The curing reaction proceeds over a broad temperature range, with a main exothermic peak centered around 205 °C, indicating that the primary crosslinking process occurs near this temperature. The onset of the exothermic signal appears at approximately 160 °C, corresponding to the initial stage of the curing reaction. The relatively low hydroxyl content and steric hindrance of the FROH structure reduce its reactivity with the epoxy groups of Gte, resulting in a slower reaction rate and higher activation energy. Consequently, the curing window shifts toward higher temperatures. Based on these results, 180 °C was initially selected as the curing temperature.

To determine the optimal curing time, **Figure 6-6 (b)** shows the gel fraction of Gte-FROH cured at 180 °C for 30, 60, 90, 120, 150, and 180 min, calculated by eq 5. The gel fraction reached approximately 90 wt% at 150 min and further increased to 97 wt% at 180 min, indicating nearly complete curing. **Figure 6-6 (c) and (d)** present optical images of samples cured at 180 °C for different durations (30–180 min), before and after 24 h immersion in DMF. Samples cured for less than 150 min exhibited swelling and cracking in DMF due to residual unreacted epoxy groups

within the network (calculated by eq 6). In contrast, the sample cured for 180 min demonstrated excellent resistance to DMF, confirming the formation of a stable crosslinked network. Therefore, curing at 180 °C for 180 min was established as the optimal condition for subsequent preparation and characterization of the Gte-FROH vitrimer system.

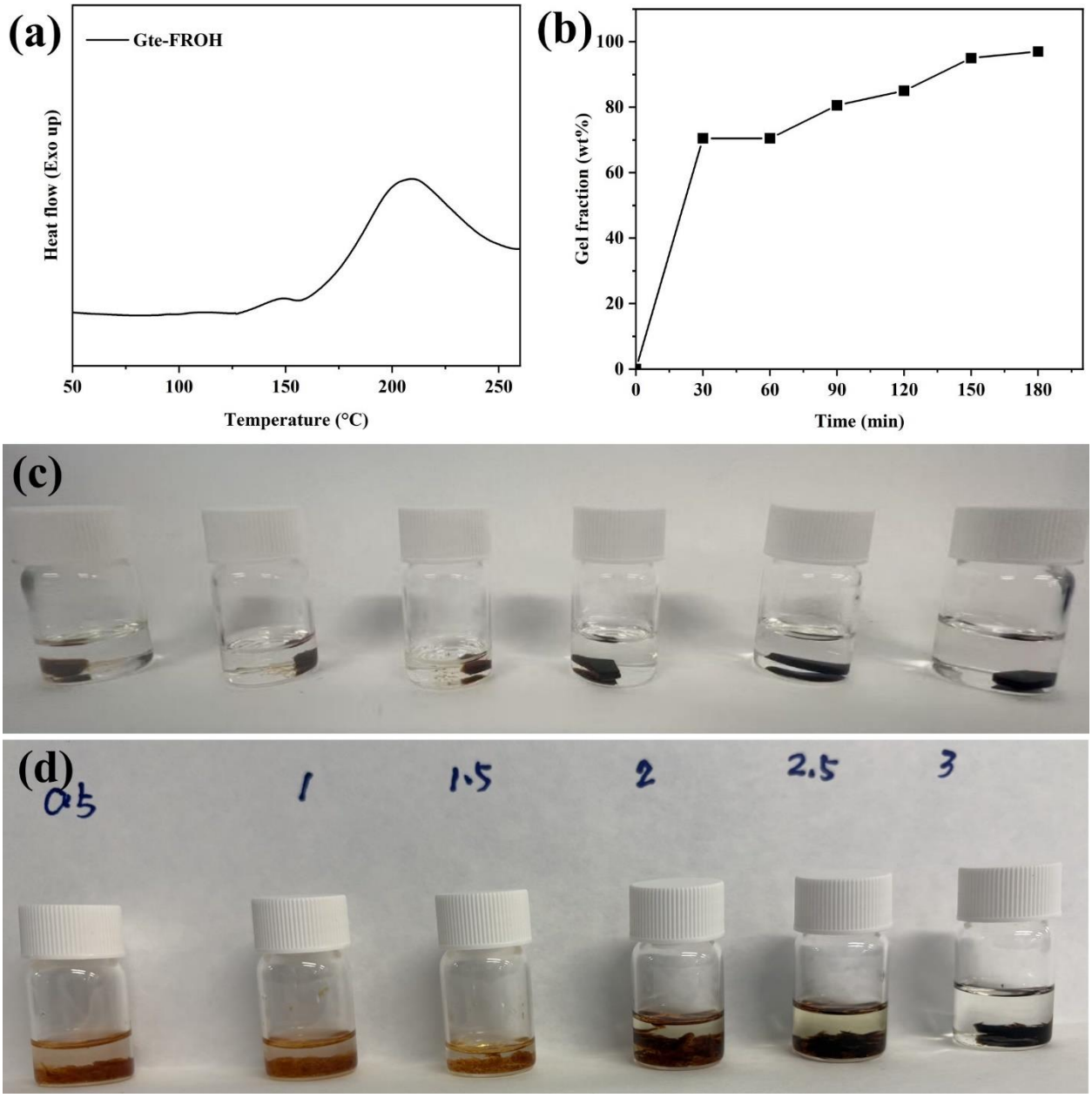

Figure 6-6 (a) DSC curve of Gte-FROH under non-isothermal conditions; (b) gel fraction of Gte-FROH cured at 180 °C for different times (30–180 min); (c) Images of cured samples before 0 h DMF immersion; (d) Images of cured samples after 24 h DMF immersion.

Figure 6-7 presents the viscosity–temperature profile of the Gte-FROH system during heating. The resin exhibits a typical reaction-induced viscosity behavior characteristic of thermosetting systems. As the temperature increases from 30 °C to 90 °C, the viscosity decreases significantly. Within the processing window of 90–160 °C, the viscosity remains stable in the range of approximately 100–300 mPa·s, demonstrating excellent flowability. When the temperature exceeds 160 °C, a sharp rise in viscosity is observed, indicating the onset and acceleration of the crosslinking reaction. According to literature reports, resin systems suitable for melt impregnation processing typically require a viscosity range of 100–1000 mPa·s during the impregnation stage to ensure adequate fiber wetting while minimizing resin migration or loss [165]. The Gte-FROH system maintains an ideal viscosity window between 90 °C and 160 °C, exhibiting excellent processability for melt-based prepreg fabrication.

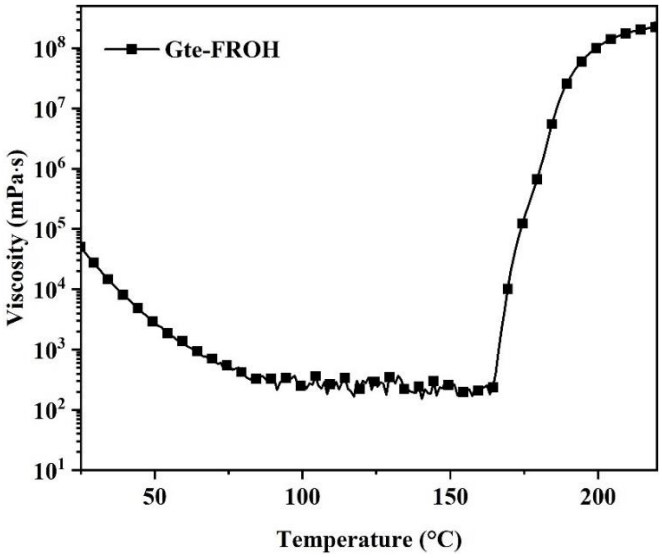

Figure 6-7 Viscosity–temperature curve of Gte–FROH resin during heating.

In addition, the gel time of the system at 100 °C was evaluated, The Gte-FROH system exhibited a gel time of 590 min at 100 °C, indicating a relatively slow curing rate and an extended processing window at this temperature. This characteristic is advantageous for continuous melt impregnation processes used in prepreg manufacturing. In summary, the Gte-FROH resin not only meets the rheological requirements for melt-based prepreg processing but also offers a wide processing window, making it a promising matrix resin for continuous fiber prepreg applications.

6.4.2 Thermal and mechanical properties of Gte-FROH

The thermomechanical properties of the Gte-VA and Gte-FROH systems were evaluated by DMA, as shown in **Figure 6-8**. The tan δ curves clearly show that Gte-FROH exhibits a lower T_g of 60.3 °C, compared to 75.4 °C for Gte-VA. Additionally, the damping peak of Gte-FROH is significantly lower than that of Gte-VA, indicating greater segmental flexibility. This enhanced flexibility is primarily attributed to the molecular architecture of FROH, which not only features π–π conjugation between aromatic rings and imine bonds but also incorporates P–O linkages that introduce internal rotational freedom, increasing chain mobility [166-168]. In contrast, the Gte-VA system relies solely on π–π interactions between aromatic rings and imine bonds, resulting in a more rigid network.

Moreover, the storage modulus curves reveal that Gte-FROH maintains a higher modulus than Gte-VA in the rubbery region (above T_g), indicating superior mechanical support at elevated temperatures. Despite its lower T_g, the Gte-FROH system demonstrates enhanced thermal stability of the cured network. According to the classical rubber elasticity theory, the crosslink densities of Gte-FROH and Gte-VA at $T_g + 50$ °C were calculated to be 919.0 mol/m³ and 302.2 mol/m³, respectively (**Table 5-1**). This higher crosslink density confirms the superior storage modulus performance of Gte-FROH in the rubbery state and reflects the formation of a denser, more stable crosslinked network.

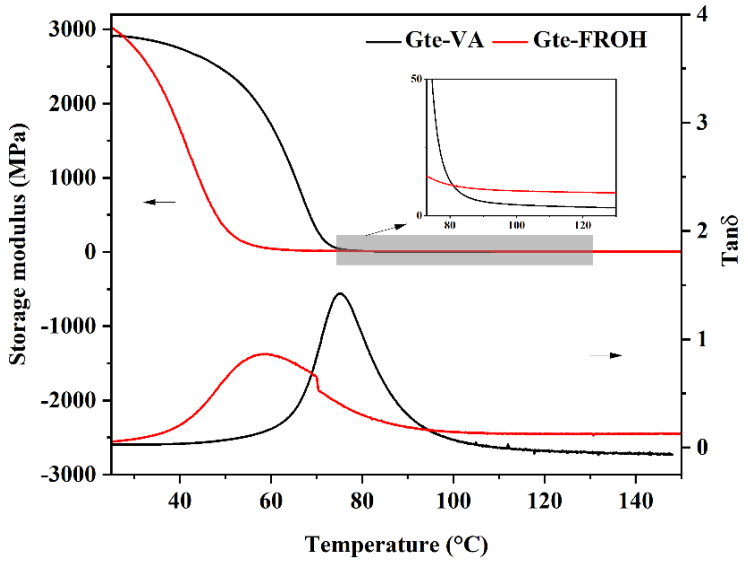

Figure 6-8 DMA curves of Gte-VA and Gte-FROH.

Table 6-1 DMA and tensile parameters of Gte-VA and Gte-FROH.

Sample	Gte-VA	Gte-FROH	2mm Gte-FROH-CF
T_g[a] (°C)	75.4	60.3	/
V_e[b] (mol/m^3)	302.2	919.0	/
Tensile strength (MPa)	49.7±1.0	31.2±2.0	/
Elongation at break (%)	4.1±0.1	17.6±0.5	/
Maximun Load (N)	/	/	546.0±20.0
σf[c] (MPa)	/	/	1024.5±50.0

a: glass transition temperature; b: crosslink density; c: flexural strength.

The thermal stability of Gte-FROH and Gte-VA was evaluated by thermogravimetric analysis (TGA) under a nitrogen atmosphere, as shown in **Figure 6-9** and **Table 6-2**. The initial decomposition temperature ($T_{5\%}$) of Gte-VA was 269 °C, which is close to that of Gte-FROH at 271 °C, indicating that the two materials exhibit similar thermal stability in the early decomposition stage.

However, the two systems show distinct thermal behaviors during the main degradation stage (approximately 250–450 °C). Gte-FROH exhibits a higher mass loss rate and a sharper DTG peak, suggesting a more concentrated degradation process with a faster reaction rate. In contrast, Gte-VA displays two separate degradation peaks, corresponding to the decomposition of imine bonds and the subsequent breakdown of the polymer backbone.

Notably, the char residue of Gte-FROH at high temperatures is significantly higher than that of Gte-VA. At 690 °C, the char yield of Gte-FROH reached approximately 49.7%, compared to 34.3% for Gte-VA. This difference is likely due to the introduction of phosphate-containing groups in FROH, which promote char formation during thermal decomposition and contribute to the development of a more stable carbonaceous structure, thereby enhancing thermal stability and potential flame retardancy [97, 111, 169].

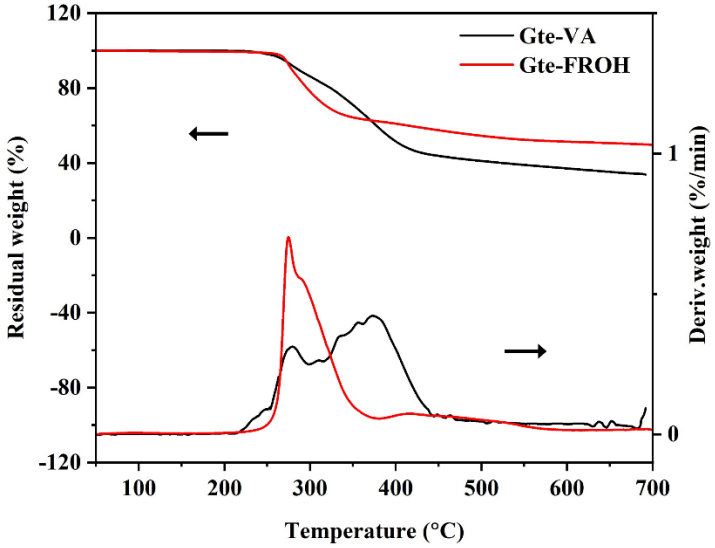

Figure 6-9 TGA curve of Gte-VA and Gte-FROH.

Table 6-2 TG and DTG data of Gte-VA and Gte-FROH at N_2 atmosphere.

Sample	$T_{5\%}$[a] (°C)	T_{max1}[b] (°C)	T_{max2}[c] (°C)	$R_{690°C}$[d] (%)
Gte-VA	269	278	375	34.3
Gte-FROH	271	275	/	49.7

a: Temperature at 5% weight loss; b: Temperature at first maximum weight loss rate; c: Temperature at second maximum weight loss rate; d: Residue at 690 °C.

The mechanical properties of Gte-VA and Gte-FROH were evaluated through tensile testing. As shown in **Figure 6-10** and **Table 6-1**, the stress–strain curves reveal that Gte-VA exhibits a typical brittle fracture behavior, with a tensile strength of 49.7 MPa and an elongation at break of only 4.1 %. This indicates that Gte-VA possesses high stiffness and strength, but limited ductility and toughness, which is characteristic of rigid thermoset materials. In contrast, Gte-FROH demonstrates significantly enhanced ductility, with a maximum tensile strength of 31.2 MPa and a remarkable elongation at break of 17.6 %, reflecting excellent toughness and plastic deformation capacity. This improvement is primarily attributed to the introduction of flexible phosphate (P–O)

linkages in the FROH molecular structure, which increase the chain mobility and thus enhance the material's ability to absorb strain and deform under tensile load [170, 171]. In summary, although the ultimate tensile strength of Gte-FROH is lower than that of Gte-VA, its greatly improved elongation at break highlights its superior overall mechanical performance, making it particularly suitable for applications that demand higher toughness and deformability.

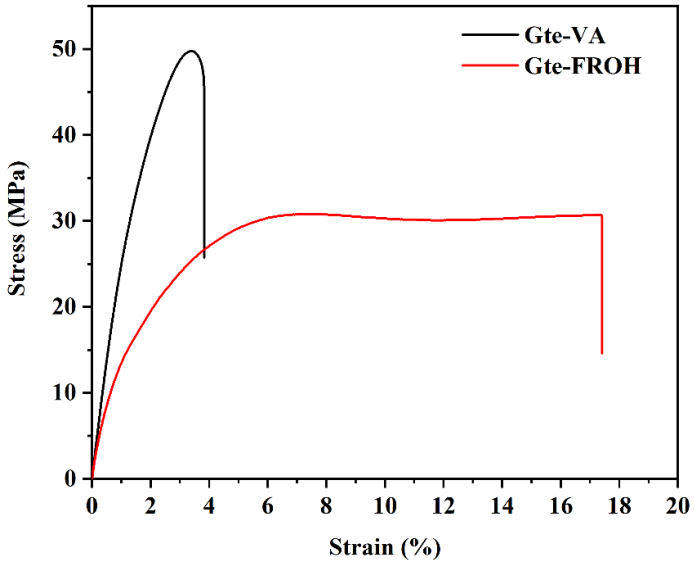

Figure 6-10 Stress-strain curves of Gte-VA and Gte-FROH.

6.4.3 Chemical resistance, reprocessing and degradation

Figure 6-11 illustrates the chemical resistance of the Gte-FROH sample. **Figures 6-11 (a) and (b)** show the morphological changes of the sample before and after immersion for 24 hours at room temperature in various solvents (H_2O, 1% HCl solution, 1% NaOH solution, acetone, and DMF). **Figure 6-11 (c)** presents the corresponding swelling ratios. The results indicate that the Gte-FROH sample maintained its structural integrity in all solvents without cracking or significant damage, demonstrating good dimensional stability and chemical resistance. According to the swelling data, the highest swelling ratio was observed in DMF (7.0%), followed by HCl (5.4%), H_2O (3.3%), and acetone (3.2%), while the lowest swelling ratio was recorded in NaOH (2.1%). The pronounced swelling in DMF is attributed to its strong polarity and high solvent penetration ability. In acidic environments (HCl), chain relaxation or ion exchange within the network may contribute to the increased swelling, whereas the more stable crosslinked structure in alkaline conditions (NaOH) results in superior resistance to swelling. Overall, the Gte-FROH sample exhibits good

chemical resistance across a range of polar solvents, indicating its potential for application in demanding service environments [55, 172].

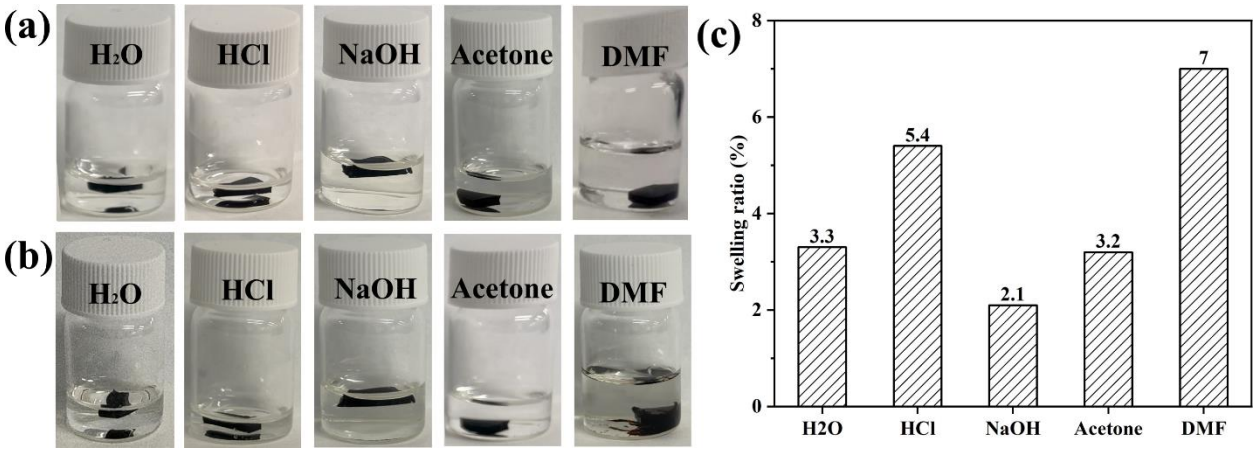

Figure 6-11 Digital photographs of the Gte-FROH in different solvents at room temperature for 0 h (a) and 24 h (b); Swelling ratios of the Gte-FROH network in different solvents for 24 h at room temperature.

Figure 6-12 illustrates the reprocessability and degradability of the Gte-FROH vitrimer system. In **Figure 6-12 (a)**, the cured Gte-FROH sample was ground into powder. **Figure 6-12 (b)** shows the reprocessed film obtained by hot pressing the powder at 180 °C for 30 min, demonstrating excellent reprocessability. This property arises from the dynamic imine bonds embedded in the Gte-FROH network, which undergo reversible exchange reactions upon heating. This dynamic topology enables the reshaping of the vitrimer material, overcoming the irreversible processing limitations of traditional thermosets [173].

There is a reversible amine-imne exchange reaction between the network with imine bonds and the network containing amine groups, **Figure 6-12 (c)** and **(d)** present the degradation behavior of Gte-FROH in a 0.5 mol/L EDA solution (solvent: DMF). Upon immersion at 80 °C for 4 h, the cured material visibly swelled and gradually disintegrated. This degradability offers great promise for the disassembly and recycling of fiber-reinforced composite materials [174, 175].

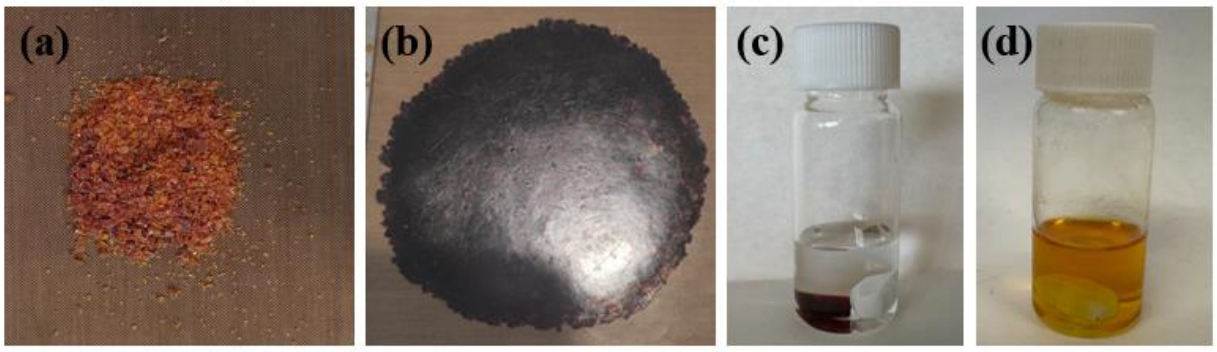

Figure 6-12 (a) Digital photos of Gte-FROH powder, (b) Digital photo of Gte-FROH compression molding; (c) and (d) exchange reaction between the amino group and imine bonds.

6.5 Flame retardancy, mechanical properties and recyclability of carbob fiber reinforced composites

The flame retardancy of Gte-VA-CF and Gte-FROH-CF composites was first evaluated using the UL-94 vertical burning test, and the corresponding results are summarized in **Table 6-3**. The Gte-VA-CF composite did not receive a rating (NR) at a thickness of 2 mm, whereas the Gte-FROH-CF composite achieved a V-0 rating at the same thickness.

Table 6-3 Formulation of the UL-94 results of the testing composites

Sample	t_1 (s)	t_2 (s)	Rating
Gte-VA-CF	>60	-	NR
Gte-FROH-CF	5	8	V-0

In cone calorimeter tests, the peak heat release rate (pHRR) and total heat release (THR) are key indicators used to evaluate the fire hazard of materials, representing the combustion intensity and total heat output, respectively. As shown in **Figure 6-13 (a)** and **(b)** and **Table 6-4**, the combustion performance of Gte-VA-CF and Gte-FROH-CF composites under a heat flux of 50 kW/m² is significantly different. The pHRR and THR of Gte-VA-CF reached 216 kW/m² and 16.8 MJ/m², respectively, while those of Gte-FROH-CF decreased by 40.2% and 64.9%, indicating a milder combustion process and lower fire risk.

The CO_2 release behavior exhibited a similar trend to heat release. As shown in **Figure 6-13 (c)** and **(d)**, the CO_2 production rate and total CO_2 released by Gte-FROH-CF decreased by 42.2% and

65.3%, respectively. This may be attributed to the phosphorus–oxygen (P–O) structures introduced by FROH, which promote the formation of a compact char layer and suppress the release of flammable volatiles into the gas phase [85, 176].

Time to ignition (TTI), which reflects the time required for a material to ignite under radiant heat, is positively correlated with flame retardancy. The TTI of Gte-FROH-CF increased from 37 s (Gte-VA-CF) to 40 s, indicating improved fire resistance.

The effective heat of combustion (EHC), which reflects the activity of flammable volatiles in the gas phase, is calculated as the ratio of total heat release to total mass loss (EHC = THR / mass loss). The EHC of Gte-VA-CF was 58.7 MJ/kg, while Gte-FROH-CF decreased by 22.1%, indicating a reduced contribution of gas-phase combustion and a more pronounced gas-phase flame-retardant effect [177].

During combustion, the generation of smoke and toxic gases such as carbon monoxide poses serious hazards to evacuation and firefighting efforts. Therefore, these parameters are also crucial in evaluating the fire safety of materials [178]. As shown in **Figures 6-13 (e–h)**, the peak smoke production rate (SPR), total smoke production (TSP), peak CO production rate (PCO), and total CO production (TCO) of Gte-FROH-CF were reduced by 52.4%, 73.0%, 40.0%, and 43.0%, respectively, compared to Gte-VA-CF. This demonstrates the superior smoke suppression and toxic gas reduction performance of the FROH-modified system [179].

Furthermore, as shown in **Figure 6-13 (i)**, the residual char yield of Gte-FROH-CF reached 87.1%, significantly higher than the 71.4% of Gte-VA-CF. This further confirms its enhanced condensed-phase flame-retardant behavior through the formation of a more stable char layer.

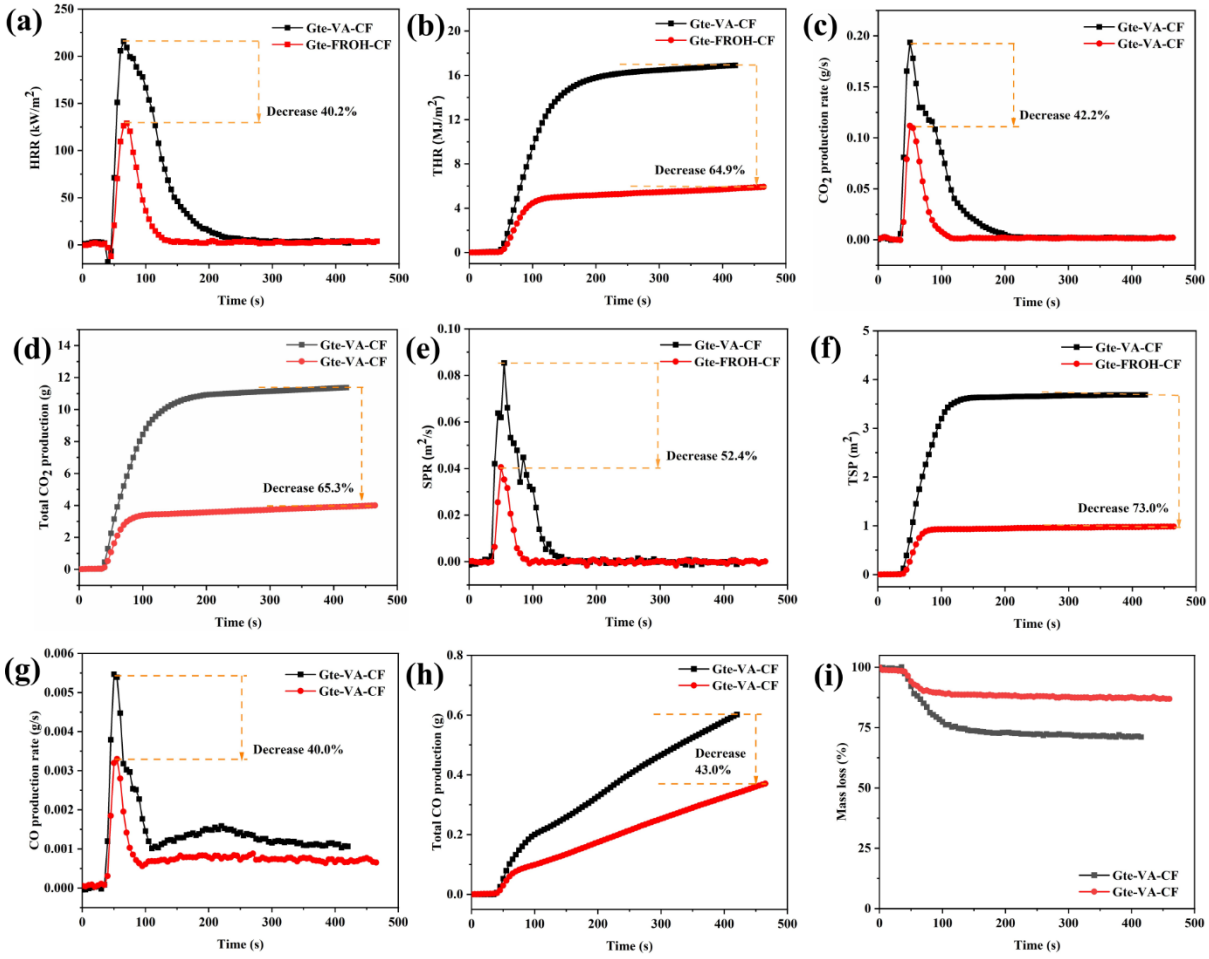

Figure 6-13 Cone calorimeter test results of Gte-VA-CF and Gte-FROH-CF composites under an external heat flux of 50 kW/m^2. (a) Heat release rate (HRR); (b) total heat release (THR); (c) CO_2 production rate; (d) total CO_2 production; (e) smoke production rate (SPR); (f) total smoke production (TSP); (g) CO production rate; (h) total CO production; (i) mass loss.

Table 6-4 Cone calorimeter test results of Gte-VA-CF and Gte-FROH-CF composites

Sample	TTI (s)	pHRR (kW /m^2)	THR (MJ/m^2)	TSR (m^2/m^2)	TSP (m^2)	Mass loss (%)	EHC (kJ/g)	PSP (m^2/s)	PCO (g/s)	TCO (g)
Gte-VA-CF	37	216	16.8	415.4	3.7	71.4	58.7	0.086	0.005	0.604
Gte-FROH-CF	40	129	5.9	109.4	1	87.1	45.7	0.041	0.003	0.344

To further investigate the condensed-phase flame-retardant mechanism of Gte-FROH-CF, **Figure 6-14 (a) and (b)** show the digital images of the residual char morphology of Gte-VA-CF and Gte-FROH-CF composites after cone calorimetry tests. Neither material formed a visibly intumescent char layer, which is likely due to the tightly woven carbon fiber structure acting as a physical constraint, preventing the expansion of the char [180]. Specifically, the surface of Gte-VA-CF appears relatively smooth, indicating limited char formation and inadequate protection of the underlying fiber structure. In contrast, Gte-FROH-CF exhibits a uniform and continuous thin carbon layer covering the surface, suggesting that the incorporation of FROH enhances the charring ability of the epoxy matrix and promotes the formation of a denser protective barrier, thereby improving the condensed-phase flame-retardant performance [181].

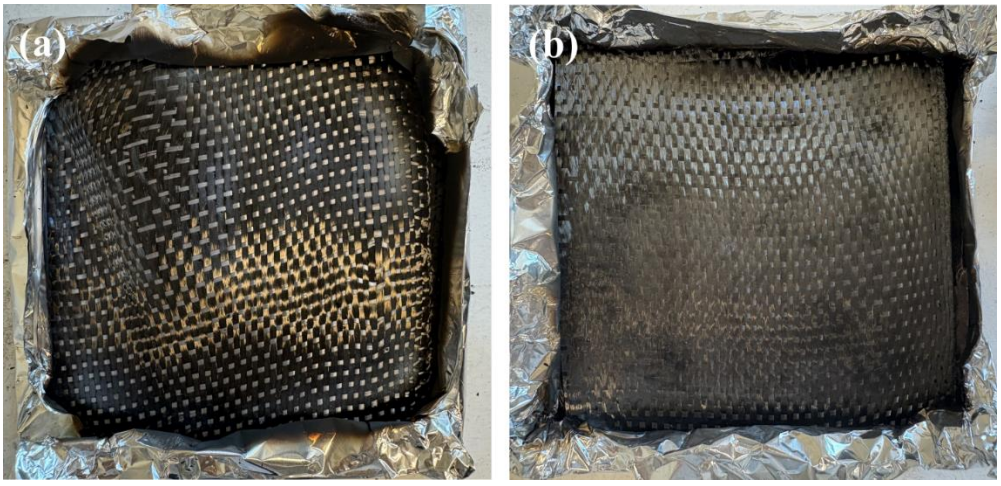

Figure 6-14 Photographs of the residual char after cone calorimeter test: (a) Gte-VA-CF and (b) Gte-FROH-CF

Figure 6-15 shows the SEM images of the residual char morphology on the surface of carbon fibers from Gte-VA-CF and Gte-FROH-CF composites after cone calorimetry tests. In Gte-VA-CF (**Figure 6-15 (a) and (b)**), the char layer appears loose and discontinuous, which fails to effectively block heat and oxygen transfer, leading to further degradation and combustion of the epoxy matrix. In contrast, Gte-FROH-CF (**Figure 6-15 (c) and (d)**) forms a more compact and continuous char layer that uniformly covers the surface of the carbon fibers, indicating superior condensed-phase flame retardant behavior. Due to their excellent thermal stability, carbon fibers do not decompose during combustion and serve as a robust structural scaffold that supports the residual char and

restricts the diffusion of heat and oxygen [182, 183]. The introduction of FROH significantly enhances the charring ability of the epoxy matrix. As the combustion progresses, the deposited char becomes denser, gradually filling the voids between carbon fibers. Together, the carbon fiber framework and the condensed char act as an effective physical barrier, preventing further combustion of the underlying material.

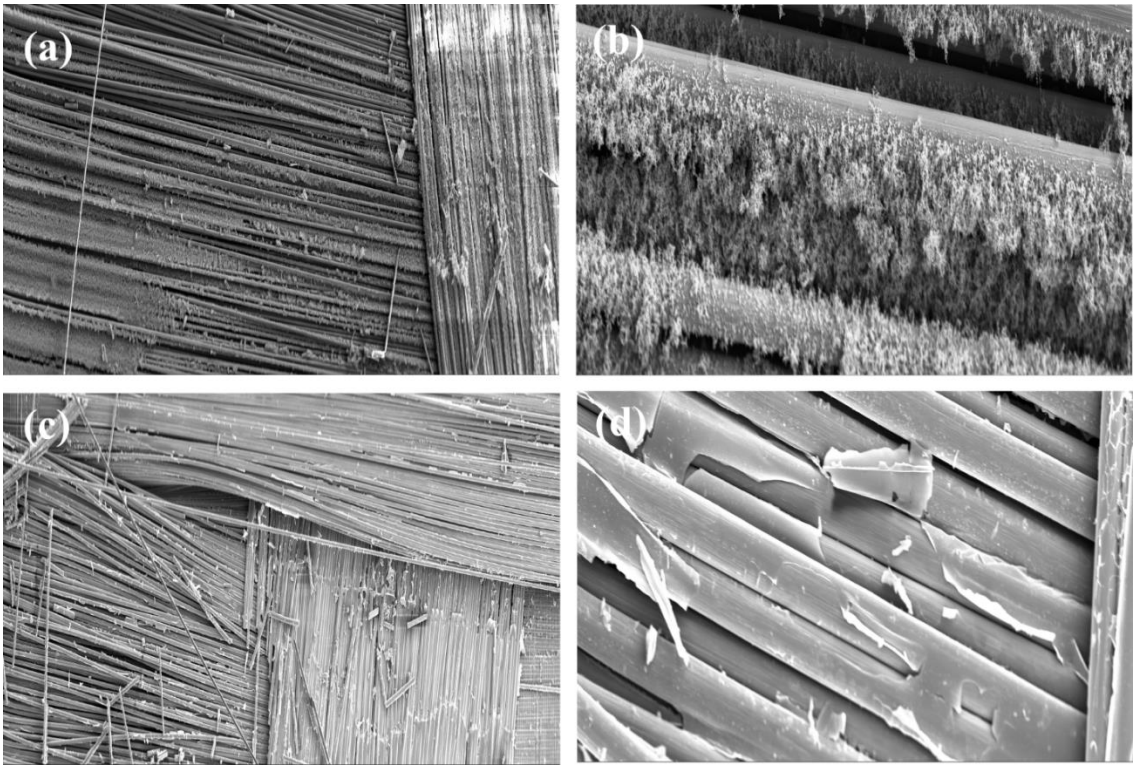

Figure 6-15 SEM images of the char residue of (a) Gte-VA-CF and (b) Gte-FROH-CF composites.

Figure 6-16 presents the element mapping of the char residue after combustion. Energy-dispersive X-ray spectroscopy (EDS) reveals the uniform distribution of carbon (C), oxygen (O), nitrogen (N), and phosphorus (P) in the residue. The presence of nitrogen and phosphorus, which are typical flame-retardant elements, confirms that a protective char layer enriched with N and P was formed during combustion, contributing to the enhanced condensed-phase flame-retardant performance of Gte-FROH-CF [184].

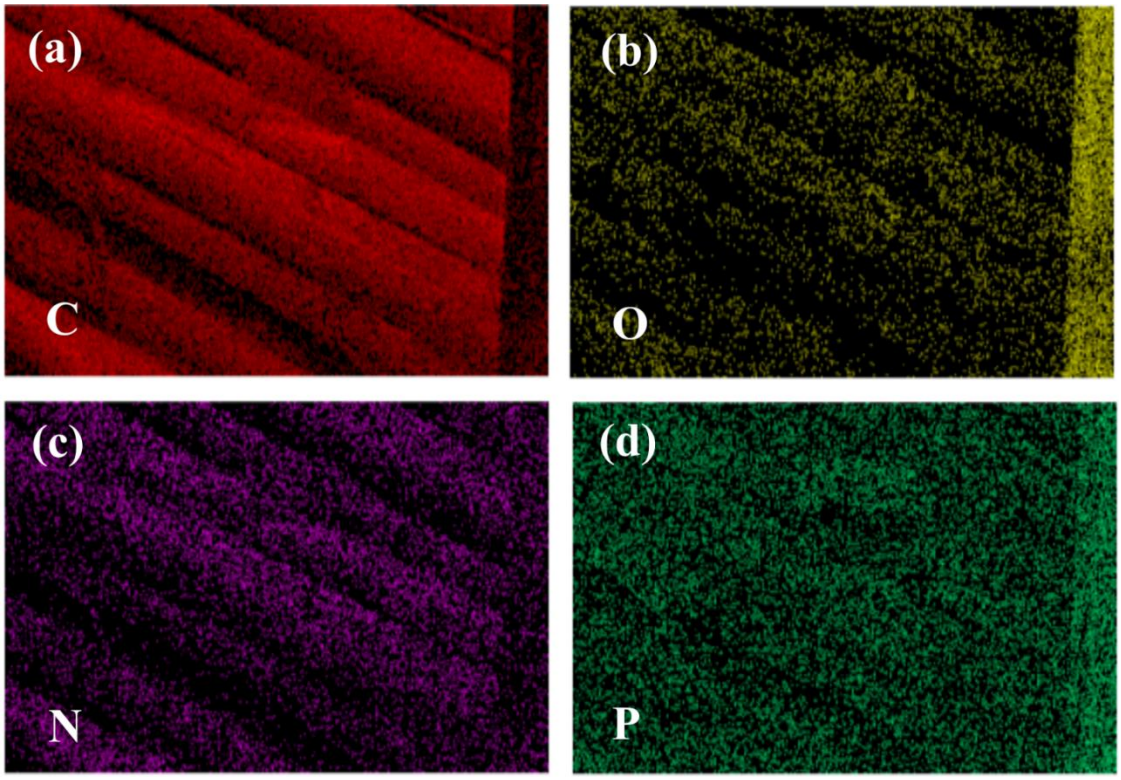

Figure 6-16 Elemental mapping images of the char residue of Gte-FROH-CF composite after combustion: (a) carbon (C), (b) oxygen (O), (c) nitrogen (N), and (d) phosphorus (P).

Based on the above analysis, the flame-retardant mechanism of the Gte-FROH-CF composite is illustrated in **Scheme 6-2**. During combustion, the carbon fibers absorb part of the released heat, which helps to slow down the internal heat transfer and suppress flame propagation. Simultaneously, the organic phosphorus groups in FROH decompose at elevated temperatures, releasing phosphorus-containing radicals (e.g., PO·, HPO·) that effectively quench highly reactive combustion radicals such as ·H and ·OH, thereby interrupting the chain reaction and inhibiting flame spread [185, 186]. Additionally, the thermal degradation of phosphorus components generates phosphoric and polyphosphoric acids (PA/PPA), which act as dehydration catalysts to promote the charring of the epoxy matrix. In the Gte-FROH-CF composite, the resulting char layer fills the voids between carbon fiber bundles, forming a compact barrier that impedes the transfer of heat and oxygen. This significantly reduces the heat release rate and smoke production, achieving a synergistic flame-retardant effect through both gas-phase and condensed-phase mechanisms [187].

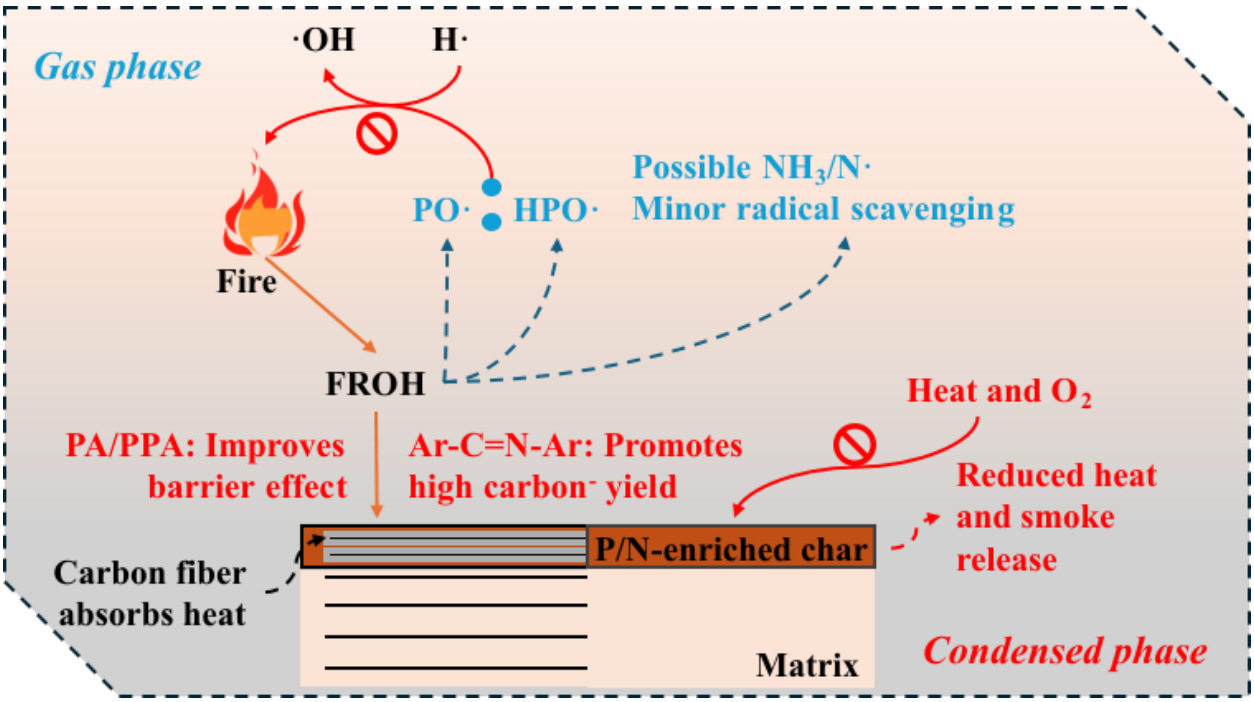

Scheme 6-2 Flame-retardant mechanism of Gte-FROH-CF composite via gas-phase radical inhibition and condensed-phase char formation.

Figure 6-17 shows the load–displacement curve of the 2 mm Gte-FROH-CF laminate under three-point bending. The sample exhibits an initial linear elastic deformation stage, reaching a maximum load of approximately 546.0 N, followed by a sharp load drop that indicates structural failure. Notably, the laminate retains a residual load-bearing capacity after the peak, suggesting a certain degree of toughness and damage tolerance.

As summarized in **Table 6-1**, calculated by eq 3, the average flexural strength of the Gte-FROH-CF composite reaches 1024.5 ± 50.0 MPa, demonstrating excellent mechanical performance. This high strength is mainly attributed to the outstanding reinforcing effect of carbon fibers and the strong interfacial adhesion between the fibers and the bio-based epoxy matrix. Moreover, the absence of catastrophic brittle fracture and the presence of post-failure deformation behavior may be related to the incorporation of flexible P–O bonds within the resin network [188].

Figure 6-17(b) compares the flexural strength of this work with other reported carbon fiber-reinforced epoxy composites. Remarkably, the Gte-FROH-CF composite achieves a flexural strength comparable to conventional high-performance CFRP systems, while additionally offering

intrinsic flame-retardant and recyclable properties. This combination highlights its promising potential for structural composite applications where sustainability and safety are also required.

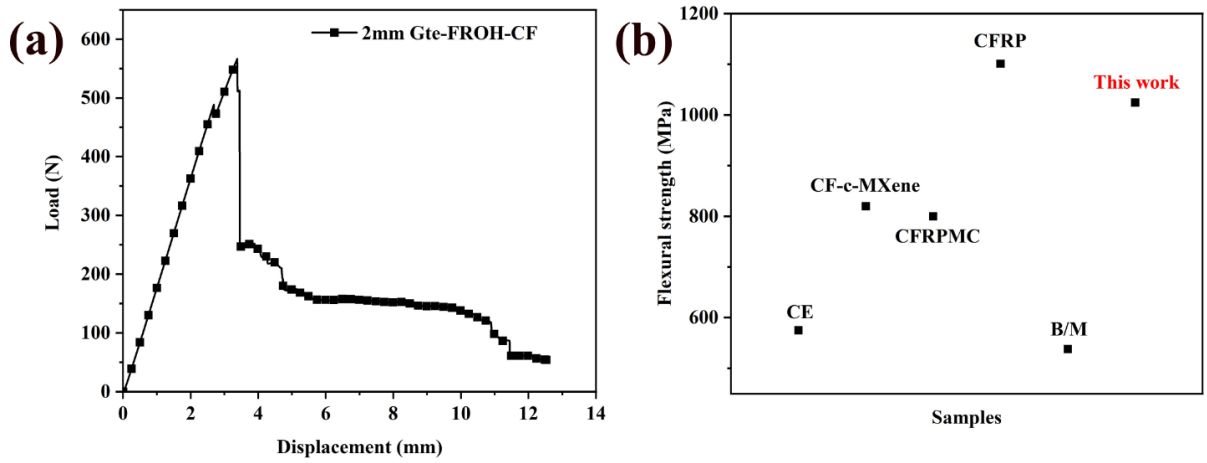

Figure 6-17 (a)Load–displacement curve of 2 mm Gte-FROH-CF laminate under three-point bending test, (b) Comparison of flexural strength with published work [189-193].

Figure 6-18 (a) illustrates the recyclability of the Gte-FROH-CF composite. The laminate was immersed in an ethylenediamine (EDA)-containing solvent system at 60 °C for 3 h. During this process, the resin matrix gradually swelled and degraded, leading to the release of carbon fibers from the polymer network. As shown in the images, the composite in the "Before" bottle remains intact, representing the original state, while the "After" bottle shows evident degradation, with carbon fiber bundles clearly separated from the matrix. This confirms that the dynamic imine bonds within the vitrimer matrix are cleavable under aminolysis, enabling controlled disassembly of the crosslinked network and non-destructive recovery of the carbon fibers.

Figure 6-18 (b) presents the SEM images of recovered carbon fibers. The fiber surfaces appear clean and smooth, indicating that the matrix was completely removed from the interface. To further compare the structural integrity of the fibers before and after recycling, Raman spectroscopy was performed, as shown in Figure **6-18 (c)**. The Raman spectra of virgin and recycled fibers exhibit nearly identical D and G bands, suggesting that the chemical structure of the carbon fibers remains unaffected by the recycling process.

Mechanical performance of the carbon fibers was also evaluated, as shown in **Figure 6-18 (d)**. The tensile strength and fracture strain of the recycled fibers were 2.52 GPa and 1.6%, respectively,

which are comparable to those of the virgin fibers. These results demonstrate that the recovered fibers retain excellent mechanical properties and can be reused in high-performance composite manufacturing.

In summary, the Gte-FROH-CF composite can be rapidly degraded in EDA solution, and the recovered carbon fibers exhibit similar surface morphology, chemical structure, and mechanical performance to their virgin counterparts.

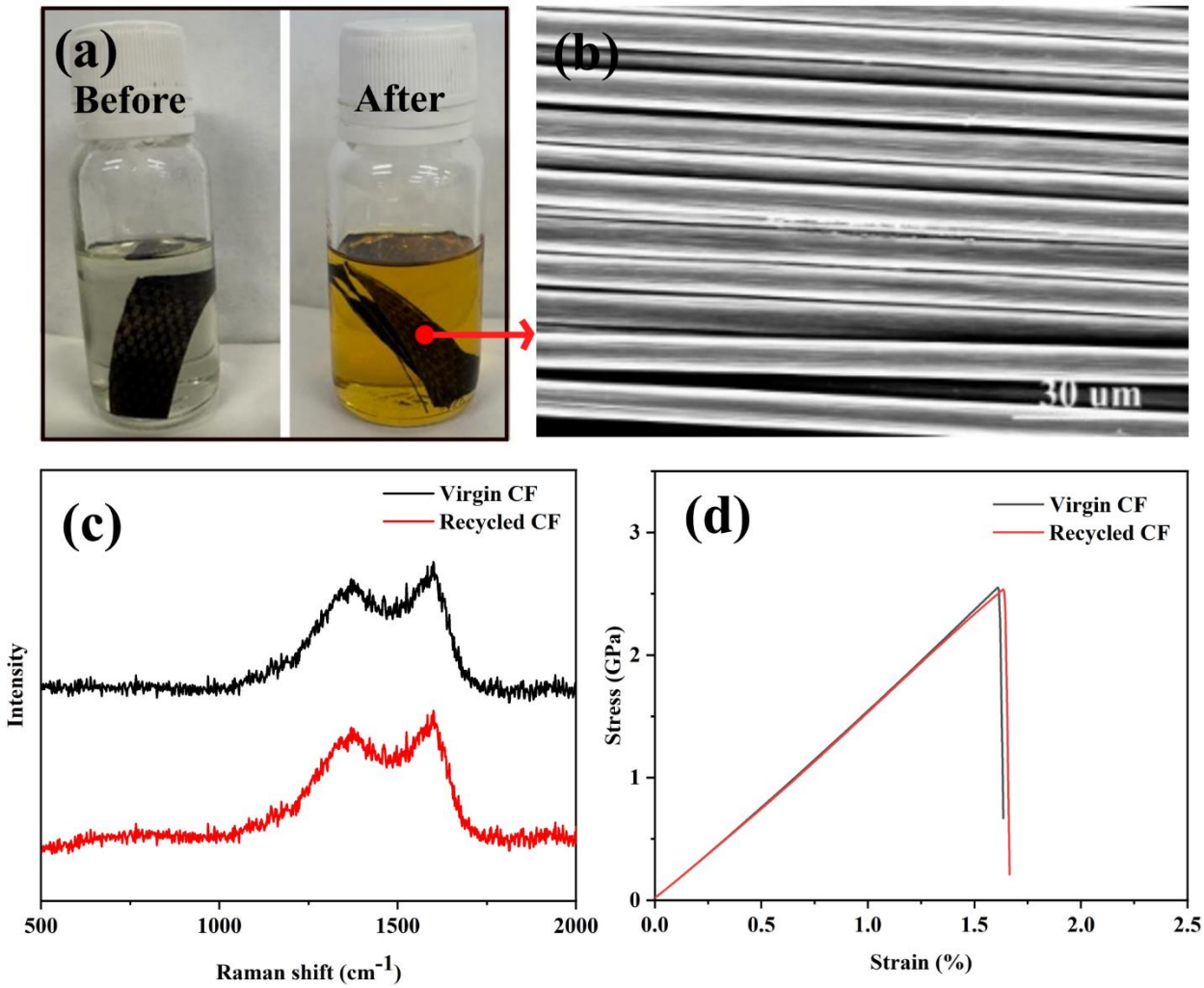

Figure 6-18 (a) Photographs showing the recycling process of the Gte-FROH-CF composite in EDA solution; (b) SEM image of the recovered carbon fibers; (c) Raman spectra of virgin and recycled carbon fibers; (d) Stress–strain curves of virgin and recycled single carbon fibers.

6.6 Summary

In this study, a CFRP was successfully developed based on a bio-based vitrimer epoxy system, in which a phosphorus-containing imine curing agent synthesized from vanillin, phosphorus oxychloride, and 4-aminophenol was introduced. This catalyst-free system forms a vitrimer network with excellent thermal processability, enabling the fabrication of continuous long-fiber prepregs via a melt-processing route suitable for efficient CFRP manufacturing. Performance evaluations demonstrated that the composite exhibits both excellent flame retardancy and mechanical strength. Specifically, the Gte-FROH-CF laminate achieved a UL-94 V-0 rating at a thickness of 2 mm, with a flexural strength as high as 1024.5 MPa, comparable to that of conventional high-performance thermoset CFRP. Moreover, owing to the presence of dynamic imine bonds in the vitrimer network, the composite shows outstanding recyclability. It can be rapidly degraded in EDA solution at 60 °C, allowing for complete matrix disassembly and non-destructive recovery of carbon fibers. The recovered fibers retain similar surface morphology, chemical structure, and tensile performance to the original ones, confirming their potential for reuse. Overall, this work proposes a promising strategy for designing bio-based vitrimer composites that combine flame retardancy, high strength, processability, and recyclability, offering a sustainable path forward for advanced structural composite development.

CHAPTER 7
Conclusions and Future Work

7.1 Conclusions

This dissertation aimed to develop recyclable, flame-retardant bio-based epoxy vitrimer systems and promote their sustainable application in continuous fiber-reinforced composites, following the research theme of "structure design–property optimization–practical application." Through systematic investigations across three studies, the main conclusions are summarized as follows:

(i) Construction of bio-based epoxy vitrimers with integrated flame retardancy and recyclability

A simple and efficient vitrimer system (GVD) was developed using glycerol triglycidyl ether (Gte), a vanillin-derived imine curing agent (VA), and DOPO as the phosphorus source. The introduction of only 5 wt% DOPO significantly enhanced the flame retardancy of the vitrimer: the cured GVD achieved a UL-94 V-0 rating, an LOI of 31%, and reductions of 38.2% in peak heat release rate (pHRR) and 26.3% in total heat release (THR) compared to the unmodified resin. The dynamic imine bonds endowed GVD with excellent thermal processability and recyclability, with the resin network fully degradable in ethanolamine solution at 60 °C within 2 hours, enabling efficient recovery of carbon fibers. These results demonstrate the multifunctional potential of bio-based epoxy vitrimers for sustainable, flame-retardant applications.

(ii) Optimization of vitrimer network structure for solvent-free melt processing

To address the limitations of solvent-based processing, a series of vitrimer networks (GTV) were designed by copolymerizing flexible aliphatic epoxy (Gte) with rigid aromatic epoxy (Tmte), cured by imine-containing agents. The optimized GTV-4 formulation achieved a glass transition temperature (T_g) of 91.1 °C, tensile strength of 73.4 MPa, and Young's modulus of 1069 MPa. The vitrimer exhibited excellent self-healing, shape memory, and recyclability. Importantly, the optimized vitrimer resin was successfully processed via melted impregnation without the use of solvents, overcoming key barriers to green manufacturing. The resulting carbon fiber-reinforced laminates maintained good mechanical integrity after multiple recycling cycles, with minimal loss of fiber morphology or composite performance.

(iii) Engineering-scale preparation of continuous fiber-reinforced vitrimer composites

To enable industrially viable continuous prepreg production, a novel phosphorus-containing imine curing agent with moderate reactivity was synthesized, allowing better control over vitrimer gel time and rheology. Combined with a bio-based epoxy resin, the vitrimer formulation supported semi-automated hot-melt prepregging. The resulting 2 mm-thick vitrimer-based CFRPs achieved excellent performance, with a UL-94 V-0 flame rating and a flexural strength of 1024.5 MPa, matching or exceeding conventional high-performance thermosets. This validated the feasibility of vitrimer resins for scalable, high-performance composite manufacturing.

7.2 Future work

Although this dissertation has successfully developed recyclable, flame-retardant bio-based epoxy vitrimer systems and systematically explored their structural design, performance optimization, and engineering application potential, several key scientific and technological challenges remain to be addressed. Future research may focus on the following directions:

(i) Systematic evaluation of the long-term service performance and environmental durability of composites

While continuous vitrimer prepregs have been successfully fabricated using a semi-automated system and their short-term mechanical performance has been validated, the storage stability of these prepregs and the evolution of mechanical properties over different storage periods remain to be clarified. Furthermore, the long-term performance and durability of vitrimer-based CFRPs under complex service environments (such as high temperature, humidity, and chemical exposure) require systematic investigation to establish lifetime prediction models and support reliable design for advanced engineering applications.

(ii) Development of multifunctional integrated composite designs

Building on the established flame retardancy and recyclability, future work could further introduce additional functional units (e.g., UV resistance, anti-aging, self-healing, or intelligent responsiveness) to develop multifunctional, integrated vitrimer composites. Such advancements would broaden application fields and meet the evolving demands for smart, high-performance, and sustainable materials.

(iii) Industrial scaling and standardization of continuous prepreg fabrication processes

The semi-automated hot-melt prepregging process developed in this work has demonstrated technical feasibility, but there remains room for optimization in industrial-scale production. Future improvements could focus on refining equipment design and process parameters, such as incorporating CNC-controlled systems for automatic adjustment of roller spacing, to enhance fabrication efficiency, product consistency, and controllability, thereby facilitating the standardization and scale-up of vitrimer-based CFRP.

(iv) Enhancement of closed-loop recycling systems and lifecycle assessment

Further optimization of recycling processes is needed to achieve efficient closed-loop recovery of fibers, resins, and degradation solvents, while improving the performance of recycled carbon fibers. In parallel, comprehensive lifecycle assessment frameworks should be established to promote truly sustainable recycling of vitrimer-based CFRP systems, aligning with carbon neutrality goals and the principles of green manufacturing.

References

[1] D. Feldman. Polymer history. Designed monomers and polymers. 11 (2008) 1-15. https://doi.org/10.1163/156855508X292383.

[2] M. Ciaccia and S. Di Stefano. Mechanisms of imine exchange reactions in organic solvents. Organic & biomolecular chemistry. 13 (2015) 646-654. https://doi.org/10.1039/C4OB02110J.

[3] R.-E. Parker and N. Isaacs. Mechanisms of epoxide reactions. Chemical reviews. 59 (1959) 737-799. https://doi.org/10.1021/cr50028a006.

[4] H. Q. Pham and M. J. Marks. Epoxy resins. Ullmann's encyclopedia of industrial chemistry. (2000) https://doi.org/10.1002/14356007.a09_547.pub2.

[5] M. A. Rashid, M. A. Islam, M. N. Hasan, M. N. N. Anu and M. H. Ikbal. A critical review of dynamic bonds containing curing agents for epoxy resin: Synthesis, challenges, and emerging applications. Polymer Degradation and Stability. (2024) 110980. https://doi.org/10.1016/j.polymdegradstab.2024.110980.

[6] S. Kumar, S. K. Samal, S. Mohanty and S. K. Nayak. Recent development of biobased epoxy resins: a review. Polymer-Plastics Technology and Engineering. 57 (2018) 133-155. https://doi.org/10.1080/03602559.2016.1253742.

[7] R. Bousoumah, V. Leso, I. Iavicoli, P. Huuskonen, S. Viegas, S. P. Porras, T. Santonen, N. Frery, A. Robert and S. Ndaw. Biomonitoring of occupational exposure to bisphenol A, bisphenol S and bisphenol F: A systematic review. Science of the Total Environment. 783 (2021) 146905. https://doi.org/10.1016/j.scitotenv.2021.146905.

[8] R. Auvergne, S. Caillol, G. David, B. Boutevin and J.-P. Pascault. Biobased thermosetting epoxy: present and future. Chemical reviews. 114 (2014) 1082-1115. https://doi.org/10.1021/cr3001274.

[9] D. J. Kalita, I. Tarnavchyk, B. J. Chisholm and D. C. Webster. Novel bio-based epoxy resins from eugenol as an alternative to BPA epoxy and high throughput screening of the cured coatings. Polymer. 233 (2021) 124191. https://doi.org/10.1016/j.polymer.2021.124191.

[10] C. Aouf, H. Nouailhas, M. Fache, S. Caillol, B. Boutevin and H. Fulcrand. Multi-functionalization of gallic acid. Synthesis of a novel bio-based epoxy resin. European Polymer Journal. 49 (2013) 1185-1195. https://doi.org/10.1016/j.eurpolymj.2012.11.025.

[11] E. Darroman, N. Durand, B. Boutevin and S. Caillol. Improved cardanol derived epoxy coatings. Progress in Organic Coatings. 91 (2016) 9-16. https://doi.org/10.1016/j.porgcoat.2015.11.012.

[12] S. Caillol, B. Boutevin and R. Auvergne. Eugenol, a developing asset in biobased epoxy resins. Polymer. 223 (2021) 123663. https://doi.org/10.1016/j.polymer.2021.123663.

[13] A. Jablonskis, A. Arshanitsa, A. Arnautov, G. Telysheva and D. Evtuguin. Evaluation of Ligno Boost™ softwood kraft lignin epoxidation as an approach for its application in cured epoxy resins. Industrial Crops and Products. 112 (2018) 225-235. https://doi.org/10.1016/j.indcrop.2017.12.003.

[14] F. Ng, G. Couture, C. Philippe, B. Boutevin and S. Caillol. Bio-based aromatic epoxy monomers for thermoset materials. Molecules. 22 (2017) 149. https ://doi.org/10.3390/molecules22010149.

[15] X.-L. Zhao, Y.-D. Li, Y. Weng and J.-B. Zeng. Biobased epoxy covalent adaptable networks for high-performance recoverable adhesives. Industrial Crops and Products. 192 (2023) 116016. https://doi.org/10.1016/j.indcrop.2022.116016.

[16] T. Aziz, F. Haq, A. Farid, L. Cheng, L. F. Chuah, A. Bokhari, M. Mubashir, D. Y. Y. Tang and P. L. Show. The epoxy resin system: function and role of curing agents. Carbon Letters. 34 (2024) 477-494. https://doi.org/10.1007/s42823-023-00547-7.

[17] L. Guo, K. J. Lamb and M. North. Recent developments in organocatalysed transformations of epoxides and carbon dioxide into cyclic carbonates. Green Chemistry. 23 (2021) 77-118. https://10.1039/D0GC03465G.

[18] Precedence Research. (2024). Epoxy resin market size, share, growth 2024 to 2034. Retrieved from https://www.precedenceresearch.com/epoxy-resin-market

[19] L. Klose, N. Meyer-Heydecke, S. Wongwattanarat, J. Chow, P. Pérez García, C. Carré, W. Streit, G. Antranikian, A. M. Romero and A. Liese. Towards sustainable recycling of epoxy-based polymers: approaches and challenges of epoxy biodegradation. Polymers. 15 (2023) 2653. https://doi.org/10.3390/polym15122653.

[20] B. J. Holliday and C. A. Mirkin. Strategies for the construction of supramolecular compounds through coordination chemistry. Angewandte Chemie International Edition. 40 (2001) 2022-2043. https://doi.org/10.1002/1521-3773(20010601)40:11<2022::AID-ANIE2022>3.0.CO;2-D.

[21] Y. Yang and M. W. Urban. Self-healing of polymers via supramolecular chemistry. Advanced Materials Interfaces. 5 (2018) 1800384. https://doi.org/10.1002/admi.201800384.

[22] B. Hosseinzadeh and M. Ahmadi. Coordination geometry in metallo-supramolecular polymer networks. Coordination Chemistry Reviews. 471 (2022) 214733. https://doi.org/10.1016/j.ccr.2022.214733.

[23] C. H. Li and J. L. Zuo. Self-healing polymers based on coordination bonds. Advanced Materials. 32 (2020) 1903762. https://doi.org/10.1002/adma.201903762.

[24] L. Yang, X. Tan, Z. Wang and X. Zhang. Supramolecular polymers: historical development, preparation, characterization, and functions. Chemical reviews. 115 (2015) 7196-7239. https://doi.org/10.1021/cr500633b.

[25] C. J. Kloxin, T. F. Scott, B. J. Adzima and C. N. Bowman. Covalent adaptable networks (CANs): a unique paradigm in cross-linked polymers. Macromolecules. 43 (2010) 2643-2653. https://doi.org/10.1021/ma902596s.

[26] A. Gandini. The furan/maleimide Diels–Alder reaction: A versatile click–unclick tool in macromolecular synthesis. Progress in Polymer Science. 38 (2013) 1-29. https://doi.org/10.1016/j.progpolymsci.2012.04.002.

[27] W. Denissen, J. M. Winne and F. E. Du Prez. Vitrimers: permanent organic networks with glass-like fluidity. Chemical science. 7 (2016) 30-38. https://10.1039/C5SC02223A.

[28] M. J. Webber and M. W. Tibbitt. Dynamic and reconfigurable materials from reversible network interactions. Nature Reviews Materials. 7 (2022) 541-556. https://doi.org/10.1038/s41578-021-00412-x.

[29] D. Montarnal, M. Capelot, F. Tournilhac and L. Leibler. Silica-like malleable materials from permanent organic networks. Science. 334 (2011) 965-968. 10.1126/science.1212648.

[30] M. Capelot, M. M. Unterlass, F. Tournilhac and L. Leibler. Catalytic control of the vitrimer glass transition. ACS Macro Letters. 1 (2012) 789-792. https://doi.org/10.1021/mz300239f.

[31] J. M. Winne, L. Leibler and F. E. Du Prez. Dynamic covalent chemistry in polymer networks: a mechanistic perspective. Polymer Chemistry. 10 (2019) 6091-6108. https://10.1039/C9PY01260E.

[32] W. Zou, J. Dong, Y. Luo, Q. Zhao and T. Xie. Dynamic covalent polymer networks: from old chemistry to modern day innovations. Advanced materials. 29 (2017) 1606100. https://doi.org/10.1002/adma.201606100.

[33] X. Feng and G. Li. Catalyst-free β-hydroxy phosphate ester exchange for robust fire-proof vitrimers. Chemical Engineering Journal. 417 (2021) 129132. https://doi.org/10.1016/j.cej.2021.129132.

[34] Y. Liu, S. Ma, Q. Li, S. Wang, K. Huang, X. Xu, B. Wang and J. Zhu. Dynamic transfer auto-catalysis of epoxy vitrimers enabled by the carboxylic acid/epoxy ratio based on facilely synthesized trifunctional monoesterified cyclic anhydrides. European Polymer Journal. 135 (2020) 109881. https://doi.org/10.1016/j.eurpolymj.2020.109881.

[35] J. Otera. Transesterification. Chemical reviews. 93 (1993) 1449-1470. https://doi.org/10.1021/cr00020a004.

[36] Z. Lei, H. Chen, S. Huang, L. J. Wayment, Q. Xu and W. Zhang. New advances in covalent network polymers via dynamic covalent chemistry. Chemical Reviews. 124 (2024) 7829-7906. https://doi.org/10.1021/acs.chemrev.3c00926.

[37] Y.-Y. Liu, J. He, Y.-D. Li, X.-L. Zhao and J.-B. Zeng. Biobased, reprocessable and weldable epoxy vitrimers from epoxidized soybean oil. Industrial Crops and Products. 153 (2020) 112576. https://doi.org/10.1016/j.indcrop.2020.112576.

[38] Y. Hu, S. Tong, L. Hu, M. Zhang, Q. Huang, Y. Sha, P. Jia and Y. Zhou. Molecularly engineered cardanol derived epoxy vitrimers based on dynamic disulfide and dynamic ester exchanges with desirable dynamic response, degradability, and recyclability. Chemical Engineering Journal. 477 (2023) 147284. https://doi.org/10.1016/j.cej.2023.147284.

[39] H. Liu, C. Liu, Y. Liu, Y. Jiang, X. Li and Y. Bai. Rapid repair and degradation: A study of high-performance recyclable vitrimer epoxy resin based on disulfide bonds. Polymer Testing. 137 (2024) 108528. https://doi.org/10.1016/j.polymertesting.2024.108528.

[40] M. E. Belowich and J. F. Stoddart. Dynamic imine chemistry. Chemical Society Reviews. 41 (2012) 2003-2024. https://doi.org/10.1039/C2CS15305J.

[41] W. Xie, S. Huang, S. Liu and J. Zhao. Imine-functionalized biomass-derived dynamic covalent thermosets enabled by heat-induced self-crosslinking and reversible structures. Chemical Engineering Journal. 404 (2021) 126598. https://doi.org/10.1016/j.cej.2020.126598.

[42] H. Memon, Y. Wei, L. Zhang, Q. Jiang and W. Liu. An imine-containing epoxy vitrimer with versatile recyclability and its application in fully recyclable carbon fiber reinforced composites. Composites Science and Technology. 199 (2020) 108314. https://doi.org/10.1016/j.compscitech.2020.108314.

[43] H. Memon, H. Liu, M. A. Rashid, L. Chen, Q. Jiang, L. Zhang, Y. Wei, W. Liu and Y. Qiu. Vanillin-based epoxy vitrimer with high performance and closed-loop recyclability. Macromolecules. 53 (2020) 621-630. https://doi.org/10.1021/acs.macromol.9b02006.

[44] R. Mustapha, A. R. Rahmat, R. Abdul Majid and S. N. H. Mustapha. Vegetable oil-based epoxy resins and their composites with bio-based hardener: A short review. Polymer-Plastics Technology and Materials. 58 (2019) 1311-1326. https://doi.org/10.1080/25740881.2018.1563119.

[45] F. Ferdosian, Y. Zhang, Z. Yuan, M. Anderson and C. C. Xu. Curing kinetics and mechanical properties of bio-based epoxy composites comprising lignin-based epoxy resins. European Polymer Journal. 82 (2016) 153-165. https://doi.org/10.1016/j.eurpolymj.2016.07.014.

[46] T.-Y. Gao, F.-D. Wang, Y. Xu, C.-X. Wei, S.-E. Zhu, W. Yang and H.-D. Lu. Luteolin-based epoxy resin with exceptional heat resistance, mechanical and flame retardant properties. Chemical Engineering Journal. 428 (2022) 131173. https://doi.org/10.1016/j.cej.2021.131173.

[47] S. Benyahya, C. Aouf, S. Caillol, B. Boutevin, J. P. Pascault and H. Fulcrand. Functionalized green tea tannins as phenolic prepolymers for bio-based epoxy resins. Industrial Crops and Products. 53 (2014) 296-307. https://doi.org/10.1016/j.indcrop.2013.12.045.

[48] L. Li, X. Chen, K. Jin and J. M. Torkelson. Vitrimers designed both to strongly suppress creep and to recover original cross-link density after reprocessing: quantitative theory and experiments. Macromolecules. 51 (2018) 5537-5546. https://doi.org/10.1021/acs.macromol.8b00922.

[49] W. Liu, T. Chen and R. Qiu. Soybean Oil-based Polymers and Their Composites. (2023) https://doi.org/10.1039/BK9781837671595-00042.

[50] S. K. Sahoo, V. Khandelwal and G. Manik. Development of completely bio‐based epoxy networks derived from epoxidized linseed and castor oil cured with citric acid. Polymers for Advanced Technologies. 29 (2018) 2080-2090. https://doi.org/10.1002/pat.4316.

[51] Y.-Y. Liu, G.-L. Liu, Y.-D. Li, Y. Weng and J.-B. Zeng. Biobased high-performance epoxy vitrimer with UV shielding for recyclable carbon fiber reinforced composites. ACS Sustainable Chemistry & Engineering. 9 (2021) 4638-4647. https://doi.org/10.1021/acssuschemeng.1c00231.

[52] S. Merighi, L. Mazzocchetti, T. Benelli and L. Giorgini. Evaluation of novel bio-based amino curing agent systems for epoxy resins: effect of tryptophan and guanine. Processes. 9 (2020) 42. https://doi.org/10.3390/pr9010042.

[53] M. Hayashi, R. Yano and A. Takasu. Synthesis of amorphous low T g polyesters with multiple COOH side groups and their utilization for elastomeric vitrimers based on post-polymerization cross-linking. Polymer Chemistry. 10 (2019) 2047-2056. https://10.1039/C9PY00293F.

[54] Y. Yang, Z. Pei, X. Zhang, L. Tao, Y. Wei and Y. Ji. Carbon nanotube–vitrimer composite for facile and efficient photo-welding of epoxy. Chemical Science. 5 (2014) 3486-3492. https://10.1039/C4SC00543K.

[55] S. Zhao and M. M. Abu-Omar. Recyclable and malleable epoxy thermoset bearing aromatic imine bonds. Macromolecules. 51 (2018) 9816-9824. https://doi.org/10.1021/acs.macromol.8b01976.

[56] A. Chao, I. Negulescu and D. Zhang. Dynamic covalent polymer networks based on degenerative imine bond exchange: tuning the malleability and self-healing properties by solvent. Macromolecules. 49 (2016) 6277-6284. https://doi.org/10.1021/acs.macromol.6b01443.

[57] Z. Zou, C. Zhu, Y. Li, X. Lei, W. Zhang and J. Xiao. Rehealable, fully recyclable, and malleable electronic skin enabled by dynamic covalent thermoset nanocomposite. Science advances. 4 (2018) eaaq0508. https://10.1126/sciadv.aaq0508.

[58] Q. Shi, C. Jin, Z. Chen, L. An and T. Wang. On the welding of vitrimers: chemistry, mechanics and applications. Advanced Functional Materials. 33 (2023) 2300288. https://doi.org/10.1002/adfm.202300288.

[59] A. Vashchuk and Y. Kobzar. Chemical welding of polymer networks. Materials Today Chemistry. 24 (2022) 100803. https://doi.org/10.1016/j.mtchem.2022.100803.

[60] Y. Yang, E. M. Terentjev, Y. Zhang, Q. Chen, Y. Zhao, Y. Wei and Y. Ji. Reprocessable thermoset soft actuators. Angewandte Chemie International Edition. 58 (2019) 17474-17479. https://doi.org/10.1002/anie.201911612.

[61] B. T. Michal, C. A. Jaye, E. J. Spencer and S. J. Rowan. Inherently photohealable and thermal shape-memory polydisulfide networks. ACS Macro Letters. 2 (2013) 694-699. https://doi.org/10.1021/mz400318m.

[62] M. Behl, M. Y. Razzaq and A. Lendlein. Multifunctional shape‐memory polymers. Advanced materials. 22 (2010) 3388-3410. https://doi.org/10.1002/adma.200904447.

[63] Z. Pei, Y. Yang, Q. Chen, Y. Wei and Y. Ji. Regional shape control of strategically assembled multishape memory vitrimers. Advanced Materials. 28 (2016) 156-160. https://10.1002/adma.201503789.

[64] D. Ozkan, M. S. Gok and A. C. Karaoglanli. Carbon fiber reinforced polymer (CFRP) composite materials, their characteristic properties, industrial application areas and their machinability. Engineering Design Applications III: Structures, Materials and Processes. (2020) 235-253. https://doi.org/10.1007/978-3-030-39062-4_20.

[65] D. K. Rajak, D. D. Pagar, P. L. Menezes and E. Linul. Fiber-reinforced polymer composites: Manufacturing, properties, and applications. Polymers. 11 (2019) 1667. https://doi.org/10.3390/polym11101667.

[66] J. Zhang, V. S. Chevali, H. Wang and C.-H. Wang. Current status of carbon fibre and carbon fibre composites recycling. Composites Part B: Engineering. 193 (2020) 108053. https://doi.org/10.1016/j.compositesb.2020.108053.

[67] E. Pakdel, S. Kashi, R. Varley and X. Wang. Recent progress in recycling carbon fibre reinforced composites and dry carbon fibre wastes. Resources, conservation and recycling. 166 (2021) 105340. https://doi.org/10.1016/j.resconrec.2020.105340.

[68] X. Qian, L. Song, Y. Bihe, B. Yu, Y. Shi, Y. Hu and R. K. Yuen. Organic/inorganic flame retardants containing phosphorus, nitrogen and silicon: Preparation and their performance on the flame retardancy of epoxy resins as a novel intumescent flame retardant system. Materials Chemistry and Physics. 143 (2014) 1243-1252. https://doi.org/10.1016/j.matchemphys.2013.11.029.

[69] M. Zhi, X. Yang, R. Fan, S. Yue, L. Zheng, Q. Liu and Y. He. A comprehensive review of reactive flame-retardant epoxy resin: fundamentals, recent developments, and perspectives. Polymer Degradation and Stability. 201 (2022) 109976. https://doi.org/10.1016/j.polymdegradstab.2022.109976.

[70] X. Li, Q. Bao, K. Chen, R. He, Y. Liu and Q. Wang. Reprocessable flame retardant silicone polyurethane based on dynamic phenylborate ester covalent and N–P–Si synergistic effect. ACS Sustainable Chemistry & Engineering. 10 (2022) 14174-14184. https://doi.org/10.1021/acssuschemeng.2c03717.

[71] S. Wang, X. Xing, X. Zhang, X. Wang and X. Jing. Room-temperature fully recyclable carbon fibre reinforced phenolic composites through dynamic covalent boronic ester bonds. Journal of Materials Chemistry A. 6 (2018) 10868-10878. https://doi.org/10.1039/C8TA01801D.

[72] J.-H. Chen, J.-H. Lu, X.-L. Pu, L. Chen and Y.-Z. Wang. Recyclable, malleable and intrinsically flame-retardant epoxy resin with catalytic transesterification. Chemosphere. 294 (2022) 133778. https://doi.org/10.1016/j.chemosphere.2022.133778.

[73] T. Liu, S. Zhang, C. Hao, C. Verdi, W. Liu, H. Liu and J. Zhang. Glycerol induced catalyst-free curing of epoxy and vitrimer preparation. Macromolecular Rapid Communications. 40 (2019) 1800889. https://doi.org/10.1002/marc.201800889.

[74] Y.-R. Zhang, S. Gu, Y.-Z. Wang and L. Chen. Intrinsically flame-retardant epoxy vitrimers with catalyst-free multi-reprocessability towards sustainable carbon fiber composites. Sustainable Materials and Technologies. 40 (2024) e00883. https://doi.org/10.1016/j.susmat.2024.e00883.

[75] Q.-R. Ren, S. Gu, J.-H. Liu, Y.-Z. Wang and L. Chen. Catalyst-free reprocessable, degradable and intrinsically flame-retardant epoxy vitrimer for carbon fiber reinforced composites. Polymer Degradation and Stability. 211 (2023) 110315. https://doi.org/10.1016/j.polymdegradstab.2023.110315.

[76] Y. Li, T. Liu, S. Zhang, L. Shao, M. Fei, H. Yu and J. Zhang. Catalyst-free vitrimer elastomers based on a dimer acid: robust mechanical performance, adaptability and hydrothermal recyclability. Green Chemistry. 22 (2020) 870-881. https://doi.org/10.1039/C9GC04080C.

[77] S. Yang, W. Liu, J. Guo, Z. Yang, Z. Qiao, C. Zhang, J. Li, J. Xu and N. Zhao. Direct and catalyst-free ester metathesis reaction for covalent adaptable networks. Journal of the American Chemical Society. 145 (2023) 20927-20935. https://doi.org/10.1021/jacs.3c06262.

[78] X. Li, J. Zhang, L. Zhang, A. R. de Luzuriaga, A. Rekondo and D.-Y. Wang. Recyclable flame-retardant epoxy composites based on disulfide bonds: Flammability and recyclability. Composites Communications. 25 (2021) 100754. https://doi.org/10.1016/j.coco.2021.100754.

[79] X. Liu, H. Wang, B. Zeng, X. Yi, W. Luo, G. Chen, Y. Xu, C. Yuan and L. Dai. Phosphorus-containing curing agents with dynamic bonds endowing epoxy resins with flame retardancy and remolding capability. Composites Part B: Engineering. 273 (2024) 111260. https://doi.org/10.1016/j.compositesb.2024.111260.

[80] R. Hajj, A. Duval, S. Dhers and L. Avérous. Network design to control polyimine vitrimer properties: physical versus chemical approach. Macromolecules. 53 (2020) 3796-3805. https://doi.org/10.1021/acs.macromol.0c00453.

[81] Y.-Y. Liu, J. He, Y.-D. Li, X.-L. Zhao and J.-B. Zeng. Biobased epoxy vitrimer from epoxidized soybean oil for reprocessable and recyclable carbon fiber reinforced composite. Composites Communications. 22 (2020) 100445. https://doi.org/10.1016/j.coco.2020.100445.

[82] W. Yang, H. Ding, W. Zhou, T. Liu, P. Xu, D. Puglia, J. M. Kenny and P. Ma. Design of inherent fire retarding and degradable bio-based epoxy vitrimer with excellent self-healing and mechanical reprocessability. Composites Science and Technology. 230 (2022) 109776. https://doi.org/10.1016/j.compscitech.2022.109776.

[83] J. Li, Z. Weng, Q. Cao, Y. Qi, B. Lu, S. Zhang, J. Wang and X. Jian. Synthesis of an aromatic amine derived from biomass and its use as a feedstock for versatile epoxy thermoset. Chemical Engineering Journal. 433 (2022) 134512. https://doi.org/10.1016/j.cej.2022.134512.

[84] M. Zhi, X. Yang, R. Fan, S. Yue, L. Zheng, Q. Liu and Y. He. Sustainable vanillin-based epoxy resin with excellent flame retardancy and mechanical properties. ACS Applied Polymer Materials. 5 (2023) 1312-1324. https://doi.org/10.1016/j.cogsc.2018.05.011.

[85] J. Peng, S. Xie, T. Liu, D. Wang, R. Ou, C. Guo, Q. Wang and Z. Liu. High-performance epoxy vitrimer with superior self-healing, shape-memory, flame retardancy, and antibacterial properties based on multifunctional curing agent. Composites Part B: Engineering. 242 (2022) 110109. https://doi.org/10.1016/j.compositesb.2022.110109.

[86] J. Zhang, H. Duan, J. Cao, J. Zou and H. Ma. A high-efficiency DOPO-based reactive flame retardant with bi-hydroxyl for low-flammability epoxy resin. Journal of Applied Polymer Science. 138 (2021) 50165. https://doi.org/10.1002/app.50165.

[87] P. Taynton, H. Ni, C. Zhu, K. Yu, S. Loob, Y. Jin, H. J. Qi and W. Zhang. Repairable woven carbon fiber composites with full recyclability enabled by malleable polyimine networks. Advanced Materials. 28 (2016) 2904-2909. https://10.1002/adma.201505245.

[88] X. Wang, S. Zhang and Y. Chen. Polyimine-Based Self-Healing Composites: A Review on Dynamic Covalent Thermosets for Sustainable and High-Performance Applications. Polymers. 17 (2025) 1607. https://doi.org/10.3390/polym17121607.

[89] J. H. Emon, M. A. Rashid, M. A. Islam, M. N. Hasan and M. K. Patoary. Review on the synthesis, recyclability, degradability, self-healability and potential applications of reversible

imine bond containing biobased epoxy thermosets. Reactions. 4 (2023) 737-765. https://doi.org/10.3390/reactions4040043.

[90] B. W. Liu, H. B. Zhao and Y. Z. Wang. Advanced flame-retardant methods for polymeric materials. Advanced Materials. 34 (2022) 2107905. https://doi.org/10.1002/adma.202107905.

[91] W. W. Klingler, A. Bifulco, C. Polisi, Z. Huang and S. Gaan. Recyclable inherently flame-retardant thermosets: Chemistry, properties and applications. Composites Part B: Engineering. 258 (2023) 110667. https://doi.org/10.1016/j.compositesb.2023.110667.

[92] M. Guerre, C. Taplan, J. M. Winne and F. E. Du Prez. Vitrimers: directing chemical reactivity to control material properties. Chemical science. 11 (2020) 4855-4870. https://10.1039/D0SC01069C.

[93] Y. Yang, D.-Y. Wang, R.-K. Jian, Z. Liu and G. Huang. Chemical structure construction of DOPO-containing compounds for flame retardancy of epoxy resin: A review. Progress in Organic Coatings. 175 (2023) 107316. https://doi.org/10.1016/j.porgcoat.2022.107316.

[94] S. Wang, S. Lou, P. Fan, L. Ma, J. Liu and T. Tang. A novel aromatic imine-containing DOPO-based reactive flame retardant towards enhanced flame-retardant and mechanical properties of epoxy resin. Polymer Degradation and Stability. 213 (2023) 110364. https://doi.org/10.1016/j.polymdegradstab.2023.110364.

[95] B. Xue, R. Tang, D. Xue, Y. Guan, Y. Sun, W. Zhao, J. Tan and X. Li. Sustainable alternative for bisphenol A epoxy resin high-performance and recyclable lignin-based epoxy vitrimers. Industrial Crops and Products. 168 (2021) 113583. https://doi.org/10.1016/j.indcrop.2021.113583.

[96] M. Fache, E. Darroman, V. Besse, R. Auvergne, S. Caillol and B. Boutevin. Vanillin, a promising biobased building-block for monomer synthesis. Green Chemistry. 16 (2014) 1987-1998. https://doi.org/10.1039/C3GC42613K.

[97] X. Zhang, Y. Eichen, Z. Miao, S. Zhang, Q. Cai, W. Liu, J. Zhao and Z. Wu. Novel Phosphazene-Based flame retardant polyimine vitrimers with Monomer-Recovery and high performances. Chemical Engineering Journal. 440 (2022) 135806. https://doi.org/10.1016/j.cej.2022.135806.

[98] B. Cai, L. Qian, Y. Qiu, J. Wang, W. Xi, Y. Chen and W. Tang. Group aggregation effect of polyphenolic phosphaphenanthrene macromolecule on enhancing fire safety and toughness of epoxy thermoset. Polymer Degradation and Stability. 205 (2022) 110154. https://doi.org/10.1016/j.polymdegradstab.2022.110154.

[99] P.-X. Tian, Y.-D. Li, Y. Weng, Z. Hu and J.-B. Zeng. Reprocessable, chemically recyclable, and flame-retardant biobased epoxy vitrimers. European Polymer Journal. 193 (2023) 112078. https://doi.org/10.1016/j.eurpolymj.2023.112078.

[100] L. Yan, Z. Xu, X. Wang, N. Deng and Z. Chu. Preparation of a novel mono-component intumescent flame retardant for enhancing the flame retardancy and smoke suppression properties of epoxy resin. Journal of Thermal Analysis and Calorimetry. 134 (2018) 1505-1519. https://doi.org/10.1007/s10973-018-7810-x.

[101] Z. Chi, Z. Guo, Z. Xu, M. Zhang, M. Li, L. Shang and Y. Ao. A DOPO-based phosphorus-nitrogen flame retardant bio-based epoxy resin from diphenolic acid: Synthesis, flame-retardant behavior and mechanism. Polymer Degradation and Stability. 176 (2020) 109151. https://doi.org/10.1016/j.polymdegradstab.2020.109151.

[102] X.-F. Liu, B.-W. Liu, X. Luo, D.-M. Guo, H.-Y. Zhong, L. Chen and Y.-Z. Wang. A novel phosphorus-containing semi-aromatic polyester toward flame retardancy and enhanced mechanical properties of epoxy resin. Chemical Engineering Journal. 380 (2020) 122471. https://doi.org/10.1016/j.cej.2019.122471.

[103] J. Hu, J. Shan, D. Wen, X. Liu, J. Zhao and Z. Tong. Flame retardant, mechanical properties and curing kinetics of DOPO-based epoxy resins. Polymer degradation and stability. 109 (2014) 218-225. https://doi.org/10.1016/j.polymdegradstab.2014.07.026.

[104] P. Wang and Z. Cai. Highly efficient flame-retardant epoxy resin with a novel DOPO-based triazole compound: Thermal stability, flame retardancy and mechanism. Polymer Degradation and Stability. 137 (2017) 138-150. https://doi.org/10.1016/j.polymdegradstab.2017.01.014.

[105] V. Varshney, S. S. Patnaik, A. K. Roy and B. L. Farmer. A molecular dynamics study of epoxy-based networks: cross-linking procedure and prediction of molecular and material properties. Macromolecules. 41 (2008) 6837-6842. https://doi.org/10.1021/ma801153e.

[106] Y. Zhang, B. Yu, B. Wang, K. M. Liew, L. Song, C. Wang and Y. Hu. Highly effective P–P synergy of a novel DOPO-based flame retardant for epoxy resin. Industrial & Engineering Chemistry Research. 56 (2017) 1245-1255. https://doi.org/10.1021/acs.iecr.6b04292.

[107] H. Duan, Y. Chen, S. Ji, R. Hu and H. Ma. A novel phosphorus/nitrogen-containing polycarboxylic acid endowing epoxy resin with excellent flame retardance and mechanical properties. Chemical Engineering Journal. 375 (2019) 121916. https://doi.org/10.1016/j.cej.2019.121916.

[108] P. Wang, H. Xiao, C. Duan, B. Wen and Z. Li. Sulfathiazole derivative with phosphaphenanthrene group: synthesis, characterization and its high flame-retardant activity on epoxy resin. Polymer Degradation and Stability. 173 (2020) 109078. https://doi.org/10.1016/j.polymdegradstab.2020.109078.

[109] R. Xie, Y. Yuan, P. Sun, Z. Liu, J. Ma, G. Yang, K. Wang, M. Li, L. Shang and Y. Ao. Design of epoxy resin with sustainability, high adhesion and excellent flame retardancy based on bio-based molecules. Journal of Materials Science. 57 (2022) 13078-13096. https://doi.org/10.1007/s10853-022-07399-y.

[110] Y. Xu, K. Odelius and M. Hakkarainen. Photocurable, thermally reprocessable, and chemically recyclable vanillin-based imine thermosets. ACS Sustainable Chemistry & Engineering. 8 (2020) 17272-17279. https://doi.org/10.1021/acssuschemeng.0c06248.

[111] X.-M. Ding, L. Chen, Y.-J. Xu, X.-H. Shi, X. Luo, X. Song and Y.-Z. Wang. Robust epoxy vitrimer with simultaneous ultrahigh impact property, fire safety, and multipath recyclability via rigid-flexible imine networks. ACS Sustainable Chemistry & Engineering. 11 (2023) 14445-14456. https://doi.org/10.1021/acssuschemeng.3c03189.

[112] X. Yang, Y. Ke, Q. Chen, L. Shen, J. Xue, R. L. Quirino, Z. Yan, Y. Luo and C. Zhang. Efficient transformation of renewable vanillin into reprocessable, acid-degradable and flame retardant polyimide vitrimers. Journal of Cleaner Production. 333 (2022) 130043. https://doi.org/10.1016/j.jclepro.2021.130043.

[113] T. K. Das, P. Ghosh and N. C. Das. Preparation, development, outcomes, and application versatility of carbon fiber-based polymer composites: a review. Advanced Composites and Hybrid Materials. 2 (2019) 214-233. https://doi.org/10.1007/s42114-018-0072-z.

[114] J. Zhang, G. Lin, U. Vaidya and H. Wang. Past, present and future prospective of global carbon fibre composite developments and applications. Composites Part B: Engineering. 250 (2023) 110463. https://doi.org/10.1016/j.compositesb.2022.110463.

[115] R. Wagmare, R. Harshe, J. Pednekar and T. U. Patro. Additive manufacturing of continuous fiber-reinforced polymer composites: Current trend and future directions. Progress in Additive Manufacturing. (2024) 1-28. https://doi.org/10.1007/s40964-024-00777-9.

[116] B. Jiang, Y. Huang, S. He, L. Xing and H. Wang. Quality analysis and control strategies for epoxy resin and prepreg. TrAC Trends in Analytical Chemistry. 74 (2015) 68-78. https://doi.org/10.1016/j.trac.2015.03.028.

[117] M.-X. Li, H.-L. Mo, S.-K. Lee, Y. Ren, W. Zhang and S.-W. Choi. Rapid Impregnating Resins for Fiber-Reinforced Composites Used in the Automobile Industry. Polymers. 15 (2023) 4192. https://doi.org/10.3390/polym15204192.

[118] A. R. Pouladvand, M. Mortezaei, H. Fattahi and I. A. Amraei. A novel custom-tailored epoxy prepreg formulation based on epoxy-amine dual-curable systems. Composites Part A: Applied Science and Manufacturing. 132 (2020) 105852. https://doi.org/10.1016/j.compositesa.2020.105852.

[119] X. Fernández-Francos, A.-O. Konuray, A. Belmonte, S. De la Flor, À. Serra and X. Ramis. Sequential curing of off-stoichiometric thiol–epoxy thermosets with a custom-tailored structure. Polymer chemistry. 7 (2016) 2280-2290. https://10.1039/C6PY00099A.

[120] M. Kim, H. Ko and S.-M. Park. Synergistic effects of amine-modified ammonium polyphosphate on curing behaviors and flame retardation properties of epoxy composites. Composites Part B: Engineering. 170 (2019) 19-30. https://doi.org/10.1016/j.compositesb.2019.04.016.

[121] D. Budelmann, C. Schmidt and D. Meiners. Tack of epoxy resin films for aerospace-grade prepregs: Influence of resin formulation, B-staging and toughening. Polymer Testing. 114 (2022) 107709. https://doi.org/10.1016/j.polymertesting.2022.107709.

[122] P. Van Velthem, W. Ballout, J. Horion, Y.-A. Janssens, V. Destoop, T. Pardoen and C. Bailly. Morphology and fracture properties of toughened highly crosslinked epoxy composites: A comparative study between high and low Tg tougheners. Composites Part B: Engineering. 101 (2016) 14-20. https://doi.org/10.1016/j.compositesb.2016.06.076.

[123] Z. Huang, Y. Wang, J. Zhu, J. Yu and Z. Hu. Surface engineering of nanosilica for vitrimer composites. Composites Science and Technology. 154 (2018) 18-27. https://doi.org/10.1016/j.compscitech.2017.11.006.

[124] A. M. Hubbard, Y. Ren, P. Papaioannou, A. Sarvestani, C. R. Picu, D. Konkolewicz, A. K. Roy, V. Varshney and D. Nepal. Vitrimer composites: understanding the role of filler in vitrimer applicability. ACS Applied Polymer Materials. 4 (2022) 6374-6385. https://doi.org/10.1021/acsapm.2c00770.

[125] L. E. Diodati, S. Liu, C. M. Rinaldi-Ramos and B. S. Sumerlin. Magnetic Nanoparticles Improve Flow Rate and Enable Self-Healing in Covalent Adaptable Networks. ACS Applied Materials & Interfaces. 15 (2023) 32957-32966. https://doi.org/10.1021/acsami.3c06329.

[126] J. Zhang, Z. Lei, S. Luo, Y. Jin, L. Qiu and W. Zhang. Malleable and recyclable conductive mwcnt-vitrimer composite for flexible electronics. ACS Applied Nano Materials. 3 (2020) 4845-4850. https://doi.org/10.1021/acsanm.0c00902.

[127] Y. Lei, A. Zhang and Y. Lin. Interpenetrating covalent adaptable networks with enhanced mechanical properties and facile reprocessability and recyclability. Polymer Chemistry. 12 (2021) 4052-4062. https://doi.org/10.1039/D1PY00623A.

[128] W. Zhang, L. Yin, M. Zhao, Z. Tan and G. Li. Rapid and non-destructive quality verification of epoxy resin product using ATR-FTIR spectroscopy coupled with chemometric methods. Microchemical Journal. 168 (2021) 106397. https://doi.org/10.1016/j.microc.2021.106397.

[129] Z. Chen, C. Jin, Z. Li, X. Li, L. Yang and T. Wang. Tough epoxy vitrimer with hybrid networks and its applications in reprocessable composites. Advanced Engineering Materials. 25 (2023) 2300031. https://doi.org/10.1002/adem.202300031.

[130] X. Zhou, M. Shen, F. Fu, Q. Li, H. Liu and Z. Song. High strength, self-healing and hydrophobic fully bio-based polybenzoxazine reinforced pine oleoresin-based vitrimer and its application in carbon fiber reinforced polymers. Chemical Engineering Journal. 484 (2024) 149585. https://doi.org/10.1016/j.cej.2024.149585.

[131] Y. Hu, S. Tong, Y. Sha, J. Yu, L. Hu, Q. Huang, P. Jia and Y. Zhou. Cardanol-based epoxy vitrimer/carbon fiber composites with integrated mechanical, self-healing, reprocessable, and welding properties and degradability. Chemical Engineering Journal. 471 (2023) 144633. https://doi.org/10.1016/j.cej.2023.144633.

[132] K. Tangthana-Umrung, Q. A. Poutrel and M. Gresil. Epoxy homopolymerization as a tool to tune the thermo-mechanical properties and fracture toughness of vitrimers. Macromolecules. 54 (2021) 8393-8406. https://doi.org/10.1021/acs.macromol.1c00861.

[133] M. Fei, W. Liu, L. Shao, Y. Cao, B. J. Bliss, B. Zhao and J. Zhang. Hemp fiber reinforced dual dynamic network vitrimer biocomposites with direct incorporation of amino silane. Chemical Engineering Journal. 480 (2024) 148091. https://doi.org/10.1016/j.cej.2023.148091.

[134] C. Huyan, D. Liu, C. Pan, D. Wang, Z. Guo, X. Zhang, S. Dai, B. B. Xu and F. Chen. Thermally recyclable and reprocessable glass fiber reinforced high performance thermosetting polyurethane vitrimer composites. Chemical Engineering Journal. 471 (2023) 144478. https://doi.org/10.1016/j.cej.2023.144478.

[135] H. Nabipour, X. Wang, B. Kandola, L. Song, Y. Kan, J. Chen and Y. Hu. A bio-based intrinsically flame-retardant epoxy vitrimer from furan derivatives and its application in recyclable carbon fiber composites. Polymer Degradation and Stability. 207 (2023) 110206. https://doi.org/10.1016/j.polymdegradstab.2022.110206.

[136] J. Liu, H. Feng, J. Dai, K. Yang, G. Chen, S. Wang, D. Jin and X. Liu. A Full-component recyclable Epoxy/BN thermal interface material with anisotropy high thermal conductivity and interface adaptability. Chemical Engineering Journal. 469 (2023) 143963. https://doi.org/10.1016/j.cej.2023.143963.

[137] N. Liu, H. Wang, B. Ma, B. Xu, L. Qu, D. Fang and Y. Yang. Enhancing cryogenic mechanical properties of epoxy resins toughened by biscitraconimide resin. Composites Science and Technology. 220 (2022) 109252. https://doi.org/10.1016/j.compscitech.2021.109252.

[138] G. Yang, S.-Y. Fu and J.-P. Yang. Preparation and mechanical properties of modified epoxy resins with flexible diamines. Polymer. 48 (2007) 302-310. https://doi.org/10.1016/j.polymer.2006.11.031.

[139] J. Zheng, Z. M. Png, S. H. Ng, G. X. Tham, E. Ye, S. S. Goh, X. J. Loh and Z. Li. Vitrimers: Current research trends and their emerging applications. Materials Today. 51 (2021) 586-625. https://doi.org/10.1016/j.mattod.2021.07.003.

[140] X.-L. Zhao, Z.-W. Zhang, Y.-D. Li, A.-K. Du, Y. Wu and J.-B. Zeng. Topological manipulation of fully biobased poly (epoxy imine): from thermoplastic elastomers to covalent adaptable networks and permanently cross-linked networks. ACS Sustainable Chemistry & Engineering. 11 (2023) 9846-9857. https://doi.org/10.1021/acssuschemeng.3c02667.

[141] S. Nie, Z. Zhao, J. Wang, S. Xia, H. Chen, H. Li, L. Ye and Z. Wang. Coral reefs-inspired strategy for hierarchical prussian blue derived nickel phyllosilicate architecture: Efficient flame retardancy and mechanical reinforcement of epoxy nanocomposites. Nano Materials Science. (2024) https://doi.org/10.1016/j.nanoms.2024.11.005.

[142] F. Zhao, W.-Q. Lian, Y.-D. Li, Y. Weng and J.-B. Zeng. Synthesis of epoxidized soybean oil-derived covalent adaptable networks through melt Schiff base condensation. Industrial Crops and Products. 187 (2022) 115499. https://doi.org/10.1016/j.indcrop.2022.115499.

[143] A. Liguori and M. Hakkarainen. Designed from Biobased Materials for Recycling: Imine-Based Covalent Adaptable Networks. Macromolecular rapid communications. 43 (2022) 2100816. https://doi.org/10.1002/marc.202100816.

[144] M. Asyraf, R. Ilyas, S. Sapuan, M. Harussani, H. Hariz, J. Aiman, D. M. Baitaba, M. Sanjay, M. Ishak and M. Norkhairunnisa. Advanced composite in aerospace applications: opportunities, challenges, and future perspective. Advanced Composites in Aerospace Engineering Applications. (2022) 471-498. https://doi.org/10.1007/978-3-030-88192-4_24.

[145] A. M. Pawlak, T. Górny, Ł. Dopierała and P. Paczos. The use of CFRP for structural reinforcement—literature review. Metals. 12 (2022) 1470. https://doi.org/10.3390/met12091470.

[146] S. Verma, B. Balasubramaniam and R. K. Gupta. Recycling, reclamation and re-manufacturing of carbon fibres. Current opinion in green and sustainable chemistry. 13 (2018) 86-90. https://doi.org/10.1016/j.cogsc.2018.05.011.

[147] S. Siengchin. A review on lightweight materials for defence applications: Present and future developments. Defence Technology. 24 (2023) 1-17. https://doi.org/10.1016/j.dt.2023.02.025.

[148] I. O. Oladele, T. F. Omotosho and A. A. Adediran. Polymer-based composites: an indispensable material for present and future applications. International Journal of Polymer Science. 2020 (2020) 8834518. https://doi.org/10.1155/2020/8834518.

[149] G. Pelin, M. Sonmez and C.-E. Pelin. The use of additive manufacturing techniques in the development of polymeric molds: a review. Polymers. 16 (2024) 1055. https://doi.org/10.3390/polym16081055.

[150] M. H. Hassan, A. Othman and S. Kamaruddin. A review on the manufacturing defects of complex-shaped laminate in aircraft composite structures. The International Journal of Advanced Manufacturing Technology. 91 (2017) 4081-4094. https://doi.org/10.1007/s00170-017-0096-5.

[151] Y. Somarathna, M. Herath, J. Epaarachchi and M. M. Islam. Formulation of Epoxy Prepregs, Synthesization Parameters, and Resin Impregnation Approaches—A Comprehensive Review. Polymers. 16 (2024) 3326. https://doi.org/10.3390/polym16233326.

[152] D. Budelmann, C. Schmidt and D. Meiners. Prepreg tack: A review of mechanisms, measurement, and manufacturing implication. Polymer composites. 41 (2020) 3440-3458. https://doi.org/10.1002/pc.25642.

[153] C. Zhang, G. Zhang, J. Xu, X. P. Shi and X. Wang. Review of curing deformation control methods for carbon fiber reinforced resin composites. Polymer Composites. 43 (2022) 3350-3370. https://doi.org/10.1002/pc.26648.

[154] M. Mehdikhani, L. Gorbatikh, I. Verpoest and S. V. Lomov. Voids in fiber-reinforced polymer composites: A review on their formation, characteristics, and effects on mechanical performance. Journal of Composite Materials. 53 (2019) 1579-1669. https://doi.org/10.1177/0021998318772152.

[155] W. Post, A. Susa, R. Blaauw, K. Molenveld and R. J. Knoop. A review on the potential and limitations of recyclable thermosets for structural applications. Polymer reviews. 60 (2020) 359-388. https://doi.org/10.1080/15583724.2019.1673406.

[156] E. Morici and N. T. Dintcheva. Recycling of thermoset materials and thermoset-based composites: challenge and opportunity. Polymers. 14 (2022) 4153. https://doi.org/10.3390/polym14194153.

[157] N. Zheng, Y. Xu, Q. Zhao and T. Xie. Dynamic covalent polymer networks: a molecular platform for designing functions beyond chemical recycling and self-healing. Chemical Reviews. 121 (2021) 1716-1745. https://doi.org/10.1021/acs.chemrev.0c00938.

[158] W. Li, Q. Chang, L. Xiao, K. Zhang, J. Huang, Y. Wang, J. Chen and X. Nie. Readily Recyclable, Auto-Catalyzed Tung Oil-Derived Vitrimers and Carbon Fiber-Reinforced Composites. Acs Applied Polymer Materials. 5 (2023) 4498-4508. https://doi.org/10.1021/acsapm.3c00614.

[159] D. Zhang, W. Cao, Z. Guo, H. Yan, Z. Fang, P. Chen and J. Li. Structure and properties of a flame retardant ternary vitrimer regulated by cyclic and long-chain dicarboxylic acids. Polymer Degradation and Stability. 207 (2023) 110234. https://doi.org/10.1016/j.polymdegradstab.2022.110234.

[160] T. Liu, C. Hao, L. Shao, W. Kuang, L. Cosimbescu, K. L. Simmons and J. Zhang. Carbon fiber reinforced epoxy vitrimer: robust mechanical performance and facile hydrothermal decomposition in pure water. Macromolecular rapid communications. 42 (2021) 2000458. https://doi.org/10.1002/marc.202000458.

[161] K. Dong, D. Zhao, Y. Pang, B. Liu, Q. Liu, T. Mu and C. Zhao. Multiple-reprocessable guaiacol-derived epoxy vitrimer with disulfide crosslinks and closed-loop recycling of carbon fiber-reinforced composites. Chemical Engineering Journal. 508 (2025) 160754. https://doi.org/10.1016/j.cej.2025.160754.

[162] H. Niu, Z. Xiao, P. Zhang, W. Guo, Y. Hu and X. Wang. Flame retardant, heat insulating and hydrophobic chitosan-derived aerogels for the clean-up of hazardous chemicals. Science of The Total Environment. 908 (2024) 168261. https://doi.org/10.1016/j.scitotenv.2023.168261.

[163] Q. Jiang, P. Li, Y. Liu and P. Zhu. Flame retardant cotton fabrics with anti-UV properties based on tea polyphenol-melamine-phenylphosphonic acid. Journal of colloid and interface science. 629 (2023) 392-403. https://doi.org/10.1016/j.jcis.2022.09.084.

[164] S. Wang, S. Ma, Q. Li, W. Yuan, B. Wang and J. Zhu. Robust, fire-safe, monomer-recovery, highly malleable thermosets from renewable bioresources. Macromolecules. 51 (2018) 8001-8012. https://doi.org/10.1021/acs.macromol.8b01601.

[165] M. A. R. Lubis, S. O. Handika, R. K. Sari, A. H. Iswanto, P. Antov, L. Kristak, S. H. Lee and A. Pizzi. Modification of ramie fiber via impregnation with low viscosity bio-polyurethane resins derived from lignin. Polymers. 14 (2022) 2165. https://doi.org/10.3390/polym14112165.

[166] S. Seth and S. Jhulki. Porous flexible frameworks: origins of flexibility and applications. Materials Horizons. 8 (2021) 700-727. https://doi.org/10.1039/D0MH01710H.

[167] H. Wang, Y. Yang, X. Yuan, W. L. Teo, Y. Wu, L. Tang and Y. Zhao. Structure–performance correlation guided applications of covalent organic frameworks. Materials Today. 53 (2022) 106-133. https://doi.org/10.1016/j.mattod.2022.02.001.

[168] K. Tanaka, M. Gon, S. Ito, J. Ochi and Y. Chujo. Recent progresses in the mechanistic studies of aggregation-induced emission-active boron complexes and clusters. Coordination Chemistry Reviews. 472 (2022) 214779. https://doi.org/10.1016/j.ccr.2022.214779.

[169] W.-J. Liu, H. Jiang and H.-Q. Yu. Development of biochar-based functional materials: toward a sustainable platform carbon material. Chemical reviews. 115 (2015) 12251-12285. https://doi.org/10.1021/acs.chemrev.5b00195.

[170] K. Deng, X. Feng, H. Yang and C. Yan. The rise of phosphate ester exchange in developing dynamic covalent networks: Advances and challenges. European Polymer Journal. 196 (2023) 112286. https://doi.org/10.1016/j.eurpolymj.2023.112286.

[171] S. Majumdar, H. Zhang, M. Soleimani, R. A. Van Benthem, J. P. Heuts and R. P. Sijbesma. Phosphate triester dynamic covalent networks. ACS Macro Letters. 9 (2020) 1753-1758. https://doi.org/10.1021/acsmacrolett.0c00636.

[172] X. Xu, S. Ma, J. Wu, J. Yang, B. Wang, S. Wang, Q. Li, J. Feng, S. You and J. Zhu. High-performance, command-degradable, antibacterial Schiff base epoxy thermosets: synthesis and

properties. Journal of Materials Chemistry A. 7 (2019) 15420-15431. https://doi.org/10.1039/C9TA05293C.

[173] Y. Tao, L. Fang, J. Zhou, C. Wang, J. Sun and Q. Fang. Gel–sol transition of vanillin-based polyimine vitrimers: imparting vitrimers with extra welding and self-healing abilities. ACS Applied Polymer Materials. 2 (2019) 295-303. https://doi.org/10.1021/acsapm.9b00809.

[174] S. Wang, S. Ma, Q. Li, X. Xu, B. Wang, W. Yuan, S. Zhou, S. You and J. Zhu. Facile in situ preparation of high-performance epoxy vitrimer from renewable resources and its application in nondestructive recyclable carbon fiber composite. Green chemistry. 21 (2019) 1484-1497. https://doi.org/10.1039/C8GC03477J.

[175] H. Geng, Y. Wang, Q. Yu, S. Gu, Y. Zhou, W. Xu, X. Zhang and D. Ye. Vanillin-based polyschiff vitrimers: reprocessability and chemical recyclability. ACS Sustainable Chemistry & Engineering. 6 (2018) 15463-15470. https://doi.org/10.1021/acssuschemeng.8b03925.

[176] L. Zhou, G. Zhang, Y. Feng, H. Zhang, J. Li and X. Shi. Design of a self-healing and flame-retardant cyclotriphosphazene-based epoxy vitrimer. Journal of materials science. 53 (2018) 7030-7047. https://doi.org/10.1007/s10853-018-2015-z.

[177] G. Ye, S. Huo, C. Wang, Y. Guo, Q. Yang, P. Song, H. Wang and Z. Liu. A transparent epoxy vitrimer with outstanding flame retardancy, toughness, and recyclability enabled by a hyperbranched P/N-derived polyester. Construction and Building Materials. 470 (2025) 140673. https://doi.org/10.1016/j.conbuildmat.2025.140673.

[178] Q. R. Ren, S. Gu, Y. Z. Wang and L. Chen. A phosphonate‐derived epoxy vitrimer with intrinsic flame retardancy and catalyst‐free reprocessability. Journal of Polymer Science. 62 (2024) 3195-3205. https://doi.org/10.1002/pol.20230211.

[179] F. Liu, L. Wang, L. Liu, K. Deng, H. Yuan, W. Zhou, Z. A. Omoniyi, H. Yang, X. Feng and C. Wan. A Simple and Catalyst-Free Strategy for Enhancing Flame Retardancy and Recyclability of Phosphonic/Carboxylic Mixed-Ester Epoxy Vitrimer. Polymer Degradation and Stability. (2025) 111512. https://doi.org/10.1016/j.polymdegradstab.2025.111512.

[180] D. Wang, Z. Zhang, X. Xu, Y. Qiu, G. Chang, K. Yuan, R. Xu and L. Meng. Cyclotriphosphazene based epoxy vitrimer with excellent recyclability and flame retardancy. Polymer Degradation and Stability. 238 (2025) 111346. https://doi.org/10.1016/j.polymdegradstab.2025.111346.

[181] F. Luo, S. Yang, X. Yang, Y. Feng, B. Lin, Y. Zou and H. Li. Catalyst-free sustainable epoxy vitrimers with fire safety offered by phosphorus-containing compounds. Polymer Degradation and Stability. 230 (2024) 111042. https://doi.org/10.1016/j.polymdegradstab.2024.111042.

[182] S. Jin, L. Qian, Y. Qiu, Y. Chen and F. Xin. High-efficiency flame retardant behavior of bi-DOPO compound with hydroxyl group on epoxy resin. Polymer Degradation and Stability. 166 (2019) 344-352. https://doi.org/10.1016/j.polymdegradstab.2019.06.024.

[183] S. Huo, P. Song, B. Yu, S. Ran, V. S. Chevali, L. Liu, Z. Fang and H. Wang. Phosphorus-containing flame retardant epoxy thermosets: Recent advances and future perspectives. Progress in Polymer Science. 114 (2021) 101366. https://doi.org/10.1016/j.progpolymsci.2021.101366.

[184] S. Yang, J. Wang, S. Huo, L. Cheng and M. Wang. Preparation and flame retardancy of an intumescent flame-retardant epoxy resin system constructed by multiple flame-retardant compositions containing phosphorus and nitrogen heterocycle. Polymer degradation and stability. 119 (2015) 251-259. https://doi.org/10.1016/j.polymdegradstab.2015.05.019.

[185] C. Yang, X. Xia, Y. Xiao, G. Wei, W. Li and Y. Lu. Degradable, intrinsically flame-retardant, low-water-absorbing vanillin-derived epoxy thermoset with a Schiff base structure. Polymer Degradation and Stability. 221 (2024) 110666. https://doi.org/10.1016/j.polymdegradstab.2024.110666.

[186] Y. Liu, Z. Yu, G. Lu, W. Chen, Z. Ye, Y. He, Z. Tang and J. Zhu. Versatile levulinic acid-derived dynamic covalent thermosets enabled by in situ generated imine and multiple hydrogen bonds. Chemical Engineering Journal. 451 (2023) 139053. https://doi.org/10.1016/j.cej.2022.139053.

[187] Y. Qi, Z. Weng, Y. Kou, L. Song, J. Li, J. Wang, S. Zhang, C. Liu and X. Jian. Synthesize and introduce bio-based aromatic s-triazine in epoxy resin: Enabling extremely high thermal stability, mechanical properties, and flame retardancy to achieve high-performance sustainable polymers. Chemical Engineering Journal. 406 (2021) 126881. https://doi.org/10.1016/j.cej.2020.126881.

[188] M. Li, X. Hao, M. Hu, Y. Huang, C. Tang, Y. Chen and L. Li. Synthesis of vanillin-based flame retardant epoxy coating on wood surface. Progress in Organic Coatings. 172 (2022) 107161. https://doi.org/10.1016/j.porgcoat.2022.107161.

[189] T. Yu, Z. Zhang, S. Song, Y. Bai and D. Wu. Tensile and flexural behaviors of additively manufactured continuous carbon fiber-reinforced polymer composites. Composite Structures. 225 (2019) 111147. https://doi.org/10.1016/j.compstruct.2019.111147.

[190] S. Hu, P. Han, C. Meng, Y. Yu, S. Han, H. Wang, G. Wei and Z. Gu. Comparative study of different bonding interactions on the interfacial adhesion and mechanical properties of MXene-decorated carbon fiber/epoxy resin composites. Composites Science and Technology. 245 (2024) 110352. https://doi.org/10.1016/j.compscitech.2023.110352.

[191] H. Yoshida, T. Ogasa and R. Hayashi. Statistical approach to the relationship between ILSS and void content of CFRP. Composites Science and Technology. 25 (1986) 3-18. https://doi.org/10.1016/0266-3538(86)90018-7.

[192] N. Ning, M. Wang, G. Zhou, Y. Qiu and Y. Wei. Effect of polymer nanoparticle morphology on fracture toughness enhancement of carbon fiber reinforced epoxy composites. Composites Part B: Engineering. 234 (2022) 109749. https://doi.org/10.1016/j.compositesb.2022.109749.

[193] L. Liu, C. Jia, J. He, F. Zhao, D. Fan, L. Xing, M. Wang, F. Wang, Z. Jiang and Y. Huang. Interfacial characterization, control and modification of carbon fiber reinforced polymer composites. Composites Science and Technology. 121 (2015) 56-72. https://doi.org/10.1016/j.compscitech.2015.08.002.

Abbreviations

2-AFD	2,2′-Diaminodiphenyl Disulfide
3D	Three- Dimensional
4-AFD	4,4′-Diaminodiphenyl Disulfide
APDS	4,4′-Diaminodiphenyl Disulfide
BPA	Bisphenol A
BPF	Bisphenol F
CAGR	Compound Annual Growth Rate
CANs	Covalent Adaptable Networks
C	Carbon
CCT	Cone Calorimeter Test
CFRP	Carbon Fiber-Reinforced Polymer
CFs	Carbon Fibers
CNT	Carbon Nanotube
DCBs	Dynamic Covalent Bonds
DDM	4,4′-Diaminodiphenylmethane
DGEBA	Diglycidyl Ether of Bisphenol A
DGEBF	Diglycidyl Ether Bisphenol F
DMSO	Dimethyl Sulfoxide
DOPO	9,10-Dihydro-9-Oxa-10-Phosphaphenanthrene-10-Oxide
DCM	Dichloromethane
DMeIm	1,2-Dimethylimidazole
DMF	N,N-Dimethylformamide
DTG	Derivative Thermogravimetry
DMA	Dynamic Mechanical Analysis
DPTA	3-Dithiodipropionic Acid
DSC	Differential Scanning Calorimetry
ECHA	European Chemicals Agency
EP	Epoxy Resin
E'	Storage Modulus
E_a	The Activation Energy
EDA	Ethylenediamine
EDX	Energy-Dispersive X-Ray Spectroscopy
EHC	Effective Heat Combustion
ESO	Epoxidized Soybean Oil
FGR	Fire Growth Rate
FPI	Fire Performance Index
FTIR	Fourier Transformation Infrared Spectroscopy
Gte	Glycerol Triglycidyl Ether
GV	A Pristine Epoxy Vitrimer
LOI	Limiting Oxygen Index
N	Nitrogen

NMR	Nuclear Magnetic Resonance
O	Oxygen
P	Phosphorus
PA	Phosphoric
PCO	Peak Co Production Rate
pHRR	Peak Heat Release Rate
$POCl_3$	Phosphoryl Chloride
PPA	Polyphosphoric Acids
$R_{690°C}$	Residual At 690 °C
SF	Shape Fixity
SMPs	Shape Memory Polymers
SPR	Smoke Production Rate
$T_{5\%}$	Initial Decomposition Temperature
tan δ	Loss Factor
TCO	Total Co Production
T_g	Glass Transition Temperature
TG-IR	Thermogravimetric Infrared Spectroscopy
TGA	Thermogravimetric Analyser
THF	Tetrahydrofuran
THR	Total Heat Release
T_{max}	Maximum Decomposition Temperature
Tmte	Tris(4-Hydroxyphenyl) Methane Triglycidyl Ether
TSP	Total Smoke Production
TTI	Time To Ignition
T_v	Topology Freezing Transition Temperature
UL-94	Vertical Burning Test

List of Schemes

List of Figures

List of Tables